学 位 申 請 論 文

伊 藤 誠

主 論 文

GRAVITATIONAL CLUSTERING OF GALAXIES:

COMPARISON BETWEEN THERMODYNAMIC THEORY

AND

N-BODY SIMULATIONS

Makoto Itoh

Department of Astronomy, Kyoto University

ABSTRACT

The thermodynamic theory of gravitational galaxy clustering gives a good description of the galaxy distribution for both N-body simulations and observations. However preliminary N-body simulations have been examined only for the present epoch. We now investigate how fast the distribution of galaxies reaches the state described by the thermodynamic theory and examine the dependence on the cosmological density Ω_0 and effects of an initial velocity dispersion using single-component N-body simulations. Moreover the thermodynamic theory assumes that all the galaxies have the same mass m. We also investigate the effects of mass spectra using N-body simulations with two mass components (m_1 and m_2).

Our N-body simulations of the single-component models show that homogeneous gravitational clustering in an expanding universe evolves slowly through a series of quasi-equilibrium states. This fundamental result, in agreement with previous theory, greatly simplifies the description of clustering, especially in the non-linear regime. Detailed comparisons of the thermodynamic theory with N-body experiments show that for a given initial distribution the rate and degree of relaxation toward the thermodynamic distribution are greater for larger values of Ω_0. This rate is modified if there is a large initial peculiar velocity dispersion, but the asymptotic state does not depend significantly on it. Initially cold or warm $\Omega_0 = 1$ models with a Poisson distribution relax very quickly to the thermodynamic form. They come into agreement with the theory after the universe expands by a factor of about 1.5. The three-dimensional volume and the two-dimensional projected distribution functions also agree well with each other.

Two-component models show that thermodynamic theory is applicable to two-component systems as long as the mass ratio of two components is in the range of $m_1 : m_2 = 1 : 1 \sim 1 : 10$. Our analyses show that the massive galaxies provide nuclei for clusters and speed up clustering in early stages, but these individual effects disappear and collective interactions dominate in late stages. The number of massive galaxies which are contained in clusters tends to increase as the mass ratio becomes larger. We describe the quantitative role that massive galaxies play in seeding clusters. The thermodynamic theory does not describe the distribution of galaxies for extreme mass ranges of $m_2/m_1 \gtrsim 15$.

1. INTRODUCTION

This thesis summarizes the portion of our studies on gravitational clustering of galaxies, which is in my charge. These studies are reported by Itoh, Inagaki and Saslaw (1988, 1990).

The quantitative description of the distribution of galaxies in the universe and its physical understanding are important problems of cosmology. One useful statistic is the two-point correlation function, $\xi(r)$. From observations, the two-point correlation function has the simple power law form (Totsuji and Kihara 1969; Peebles 1980; Davis and Peebles 1983)

$$\xi(r) = (r_0/r)^\gamma, \tag{1}$$

with $\gamma = 1.77$ and $r_0 = 5.4h^{-1}$ Mpc ($H_0 = 100h\,\mathrm{km\,s^{-1}Mpc^{-1}}$). This apparent simplicity has led many investigators to describe theoretical results and numerical simulations using $\xi(r)$. However, $\xi(r)$ contains very limited information. Extending this approach requires finding higher-order correlation functions. But this is not particularly effective, since they are difficult to calculate, uncertain to compute, and slow to converge. Moreover recent observational analyses give a considerable range of γ and r_0 (e.g., de Lapparent, Geller and Huchra 1988), and suggest that the two-point correlation function may not have the simple power law form of equation (1).

Fortunately, there is another easy and more effective statistical approach which is described by the probability distribution $f(N)$ for finding N galaxies in a volume of size V. Though $f(N)$ does not have such a simple form as $\xi(r)$, Saslaw and Hamilton (1984) theoretically derived a formula for the distribution of galaxies based on gravitational thermodynamics:

$$f(N) = \frac{\overline{N}(1-b)}{N!}\,[\,\overline{N}(1-b) + Nb\,]^{N-1}\,e^{-\overline{N}(1-b)-Nb}, \tag{2}$$

where $\overline{N} = \overline{n}V$, $\overline{n}$ is the average number density of galaxies, each having mass m, and b is the ratio of gravitational correlation energy, W, to the kinetic energy, K, of the peculiar motions of galaxies:

$$b = -\frac{W}{2K} = \frac{2\pi Gm^2\overline{n}}{3T}\int_0^\infty r\xi(r)dr. \tag{3}$$

Here T is the temperature in energy units.

Preliminary N-body experiments have been examined for the present epoch, where they showed good agreement between equation (2) and the simulated galaxy distribution (Saslaw

and Hamilton 1984; Saslaw 1985a). The observed galaxy distribution was subsequently found to agree very well with the predictions of equation (2) for a value of $b = 0.70 \pm 0.05$ (Crane and Saslaw, 1986). This is the value of b expected from the N-body simulations, and it suggests that much of the observed galaxy distribution is produced by gravitational clustering.

Although the thermodynamic distribution function gives a good description for both observed and experimental galaxy distributions, it also has some problems. First, the thermodynamic distribution function was derived for non-linear asymptotic equilibrium states. Neither the universe nor the N-body simulations have reached this state, or are likely to. Yet the result applies with high accuracy. Why? A possible explanation (Saslaw 1986) is that the system evolves through a series of quasi-equilibrium states, each of which satisfies equation (2) but with a value of b that increases slowly with time as clustering spreads to larger and larger scales. The time scale for b to change eventually exceeds the Hubble expansion time scale, and quasi-equilibrium conditions describe subsequent evolution. Second, the thermodynamic theory assumed that all galaxies have the same mass m. However, real galaxies have a range of masses. So it is important to investigate how different mass components affect the $f(N)$ statistics such as the form of $f(N)$, the value of b, etc.

In this thesis I report the results of a new series of N-body experiments designed to explore the time evolution of $f(N)$. Our first purpose is to determine how fast the distribution of galaxies reaches the state described by the thermodynamic theory. We find this can occur remarkably quickly. We also examine following important aspects of gravitational clustering as measured by $f(N)$:

1) its dependence on the cosmological density Ω_0,

2) the difference between the three-dimensional $f(N)$ and the two-dimensional projected $f(N)$, the latter being more easily related to observations,

and

3) effects of an initial velocity dispersion.

To investigate the effects of different mass components, we carried out simulations in which there are two mass components with less massive galaxies denoted m_1 and the more massive galaxies denoted m_2. Our main purpose is to examine several aspects of the effects of mass spectra on the $f(N)$ statistics:

1) the effects of mass spectra on the agreement with equation (2) and the fitted values of b,

2) the dependence of fitted values of b on the mass ratio ($m_1 : m_2 = 1 : 1 \sim 1 : 5$),

3) the number of galaxies of each mass contained in clusters

4) the distributions for extreme mass ratios; $m_1 : m_2 = 1 : 30$ and $1 : 100$,

and

5) the transitional behavior of the distributions for intermediate mass ratios; $m_1 : m_2 = 1 : 8$ and $1 : 15$.

We describe the N-body simulations in §2: their initial conditions, pictorial features of clustering and the evolution of their two-point correlation function. Section 3 describes the $f(N)$ statistics and Section 4 describes the evolution of b. Section 5 describes our procedure for identifying clusters from simulations and the effects of mass spectra. We examine the extreme cases in §6 where the two components have mass ratios $m_1 : m_2 = 1 : 30$ and $1 : 100$. This may help in understanding the distribution of dwarf galaxies. In §7 we discuss our conclusions.

2. N-BODY SIMULATIONS

2-1. Initial Conditions

2-1-1. Single-Component Models

Many initial conditions are possible, and may be related to conditions imagined in the early universe. Since our main aim here is to examine the physics of gravitational clustering, we make the system simple in order to make its physical interpretation easier. All 4000 particles (i.e. galaxies) in each run have the same mass. The initial distribution of galaxies is Poisson. We examine several initial velocity distributions. Most cases start cold, with no peculiar velocities relative to the Hubble expansion. Some cases start 'warm', with an initial Gaussian velocity dispersion $\langle v^2 \rangle^{1/2} = \bar{r} H_i$, where $\bar{r}$ is the average initial distance between particles and H_i is the initial Hubble constant. Other cases start 'hot' with $\langle v^2 \rangle^{1/2} = 3\bar{r} H_i$.

The values of the cosmological density parameters, in the standard Einstein-Friedmann models we adopt, are $\Omega_0 = 1, 0.1$, and 0.01 at $a/a_0 = 32$ where a is the cosmological expansion parameter with initial value a_0.

– 4 –

2-1-2. Two-Component Models

In order to investigate the effects of mass spectra and directly compare the results with the single-component models, we consider simple systems which have only two mass components. All 4000 particles are divided into $N_1 = 3500$ less massive galaxies and $N_2 = 500$ massive ones. We need a large enough number for N_2 so that we can calculate $f(N)$ for distributions of the massive and less massive galaxies separately. Several mass ratios of the less massive (m_1) and massive (m_2) galaxies are adopted. We set these ratios $m_1 : m_2 = 1 : 1$ (single-component models), $1 : 2, 1 : 3, 1 : 4$ and $1 : 5$ in order to examine how the mass ratio affects the rate of clustering, and $m_1 : m_2 = 1 : 30, 1 : 100$ for the extreme cases where massive galaxies dominate and determine the dynamics of the systems, and the less massive galaxies form a satellite system around the massive ones. We have also inspected the cases of intermediate mass ratios, i.e., $m_1 : m_2 = 1 : 8$ and $1 : 15$. For convenience, even if $m_1 : m_2 = 1 : 1$, we call the N_1 particles with mass m_1 the 'less massive' galaxies and the N_2 particles with m_2 as the 'massive' galaxies. The initial distribution of galaxies is Poisson and the initial velocity dispersion is cold. The value of the cosmological density parameter is $\Omega_0 = 1$ for all simulations.

The N-body simulations were done on the FACOM VP-200 and VP-400 at the Data Processing Center, Kyoto University using the COMOVEV code which was constructed by Dr. Sverre Aarseth (Aarseth and Inagaki 1986). This program solves the motion of particles in comoving coordinates in an expanding sphere of radius unity. A more detailed explanation of the integration method of this code is found in Aarseth (1985).

2-2. Pictorial Features of Clustering

2-2-1. Single-Component Models

Figure 1 shows, as an example, six projected distributions from an $\Omega_0 = 1$ cold run. The first is the initial state, the next three are at values of $a/a_0 = 2.80, 7.86$ and 15.62. These are all projected views of approximately 2000 galaxies in the same hemisphere, as seen by an observer at the center. The last two distributions, at $a/a_0 = 7.86$, are projections of this same hemisphere but confined first to the nearby galaxies with distances $0 < R < 0.5$ and finally to distant galaxies with $0.9 < R < 1.0$. The maximum comoving radius of the simulation is always scaled to $R = 1$. Clustering becomes noticeable first after one or two expansion time

scales, and then becomes non-linear very quickly.

All these pictures have interesting voids and filamentary structures formed simply by chance connections between different gravitationally clustering regions. It is easy to imagine a local observer of these pictures becoming quite enthralled with the view. Whether the view has any deeper significance, however, must be determined by objective statistical criteria. Any particular view of the universe is unlikely to be a fair example, since it does not embody the average properties.

2-2-2. Two-Component Models

Figure 2 shows projected positions of galaxies for $m_1 : m_2 = 1 : 5$ at $a/a_0 = 7.86$. At a glance, the massive galaxies appear to be concentrated in high density regions (i.e., clusters). This implies that these galaxies help seed the clusters and speed up the clustering. Clusters can, however, also form without being seeded. Note that the distribution of massive galaxies shows large voids and filamentary structures.

These impressions, however, are qualitative rather than quantitative. To quantify them, we will examine the number and proportion of massive galaxies contained in clusters and the rate of the clustering as a function of the mass ratio. A method for identifying clusters from the distribution of galaxies, and quantitative results are described in §5.

2-3. Two-Point Correlation Function

2-3-1. Single-Component Models

The two-point correlation function provides some very useful information about the galaxy distribution (e.g., Peebles 1980; Saslaw 1985b). Figure 3 shows $\xi(r)$ for a cold $\Omega_0 = 1$ example at $a/a_0 = 2.80$, 7.86, and 15.62; a cold $\Omega_0 = 0.1$ example at $a/a_0 = 2.80$, 15.62, and 31.06; and a cold $\Omega_0 = 0.01$ example at $a/a_0 = 2.80$, 15.62, and 31.06. For comparison we show a dashed power law of the form r^{-2}, which is the asymptotic thermodynamic prediction (Saslaw 1980, 1985b).

Figure 4 shows the growth of $\xi(r)$ for warm initial velocities with $\Omega_0 = 1$ (top raw), hot $\Omega_0 = 1$ (center raw), and hot $\Omega_0 = 0.1$ (bottom raw). From these figures we can see that $\xi(r)$ grows approximately self-similarly for this range of Ω_0. Growth is faster and the correlation length scale is larger for higher values of Ω_0. The values of the exponent and the scale length increase rapidly at first and then more slowly as the expansion inhibits larger

– 6 –

scale structure from forming. It is important to note that the fits to a power law are only approximate, because clustering develops at different rates on different scales. Higher initial velocity dispersion, for a given Ω_0, increase the time needed for substantial correlations to form.

2-3-2. Two-Component Models

Figure 5(a) shows correlation functions for all galaxies (ξ_T) in the case $m_1 : m_2 = 1 : 5$, $a/a_0 = 1.41 \sim 7.86$ and Figure 5(b) shows correlation functions of the less massive galaxies (ξ_{LM}) and the massive galaxies (ξ_M). ξ_{LM} has almost the same amplitude and exponent as ξ_T. On the other hand, ξ_M has larger amplitude than ξ_T in small scales but has similar amplitude to ξ_T and ξ_{LM} in large scales. This implies that the massive galaxies concentrate in clusters and is consistent with the pictorial impression.

Comparison between Figure 3 and Figure 5(a) shows that it is very difficult to see differences in the rate of clustering from the growth rate of the amplitude of $\xi(r)$ or from its exponents. This is because $\xi(r)$ does not always have a simple power law form through the entire range of r, unlike equation (1), and it is hard to determine an amplitude and exponent of $\xi(r)$ with high precision from simulations. As a result, $\xi(r)$ is not a sensitive unambiguous measure for representing the rate of clustering.

On the other hand, the $f(N)$ statistics contain much more information about clustering than does $\xi(r)$ [although the set of all correlation functions would contain even more information than $f(N)$] and the time evolution of the fitted values of b in equation (2) is a very sensitive measure and is able to describe the behavior of clustering. We therefore turn to it them the next two Sections.

3. $f(N)$ STATISTICS

3-1. Methods of $f(N)$ Statistics

3-1-1. Three-dimensional Fitting

There are two parameters, $\overline{N}$ and b, in the thermodynamic gravitational distribution of equation (2). Since these can be determined directly for the N-body simulation, the theory has no free parameters. To examine the degree of agreement between the theory from which equation (2) follows and the numerical experiments, we determine first how well the

experimental $f(N)$ fits equation (2) by using b as a free-fitting parameter, and second how well the resulting value of b_{fit} agrees with the value $b_{ab\ initio}$ calculated for the simulation from first principles. To calculate $b_{ab\ initio}$ we sum the gravitational forces between particles and subtract the mean field, taking the effect of the softening parameter into account (see Saslaw and Hamilton 1984). The thermal contribution to $b_{ab\ initio}$ follows by simply summing the squared peculiar velocities (with respect to the Hubble expansion) of the particles. The value of $\bar{n}$ is also determined directly from the sample volume of the experiment, as described in Appendix A.

It is important to examine the fits to $f(N)$ over the complete range of N, from the voids with $N = 0$ to very large volumes with $N \approx 100$. Each value of N emphasizes a different scale of the distribution. There are distributions that agree with observations or experiments for some values of N, but not for the entire range and these differences can be quite important. To examine the whole range, it is convenient to use two representations of $f(N)$. One is to fix N and to consider it as a function of V We denote this by $f_N(V)$. The other is to fix V and to consider it as a function of N. We call this $f_V(N)$. Since $\overline{N} = \bar{n}V$ we can also express this first representation as $f_N(\overline{N})$. The two forms have the normalizations

$$\int_0^\infty f_N(\overline{N})d\overline{N} = 1 \tag{4}$$

and

$$\sum_{N=0}^\infty f_V(N) = 1. \tag{5}$$

From the positions of the particles in an N-body simulation, we compute its $f_N(V)$ and $f_V(N)$ as follows. The radius of the boundary of the simulation in comoving coordinates is unity. First we generate 9500 spatial points randomly a sphere of radius $R = 0.8$ from the center of the system. To compute $f_N(V)$ we only use the points with $R \leq 0.6$ to avoid boundary effects. We then measure the distances from the randomly generated points to the first, second, third, etc. nearest particles. The set of distances to the $(N+1)$-th particle gives $f_N(V)$ for spherical volumes. Previous analyses (Saslaw 1985a) showed $f(N)$ to be essentially independent of the shape of the volume, so long as it is not pathological.

To compute $f_V(N)$ we count the numbers of particles contained in spheres of radii $r = 0.1, 0.2, 0.3$ and 0.4 centered on the randomly generated points. When computing

$f_V(N)$ for spheres of radii $r = 0.1, 0.2, 0.3,$ and 0.4, respectively, we use points within the radius $R = 0.8, 0.7, 0.6,$ and 0.6 from the center of the system. This maximum radius is 0.6 for $r = 0.4$ in order to include sufficient particles for a reasonably smooth fit.

3-1-2. Two-dimensional Fitting

Using simulations we also constructed two-dimensional $f(N)$ distributions by projecting the spatial distribution onto the celestial sphere of an observer at the center. This is useful for comparison with the observed galaxy distribution on our sky in the Zwicky catalogue for which $b_{fit} = 0.70 \pm 0.05$ (Crane and Saslaw 1986). For our two-dimensional analysis we first generated 4000 spatial points randomly on a sphere. Next we projected the particles onto the sphere, giving the view from the center. Then we measured the angles from the random spatial points to the first, second, third, etc. nearest projected particle position on the sphere. With a procedure similar to that for determining $f_N(V)$ we can calculate $f_N(\theta)$ as a function of the separation angle θ. To calculate $f_\theta(N)$ we count the number of particles projected into circles of radii $\theta = 0.1, 0.2, 0.3$ and 0.4 rad centered on the randomly generated points.

3-2. Fitting to the Thermodynamic $f(N)$

3-2-1. Single-Component Models

Figure 6 shows the evolving three-dimensional $f(N)$ distributions for simulations with $\Omega_0 = 1$ and cold initial velocities at three epochs: $a/a_0 = 2.80$ when relaxation to the thermodynamic distribution is already significant; $a/a_0 = 7.86$, approximately the present epoch as judged by the slope and amplitude of the two-point correlation function (See Appendix B for estimates of the present epoch); and $a/a_0 = 15.6$, about twice the present epoch. The dashed curves are best least-square fits to equation (2) using b as a fitting parameter. The fits to the thermodynamic distribution are very good. Fits to simulations with $\Omega_0 = 0.1$ and $\Omega_0 = 0.01$ are of similar or even better quality.

Figure 7 shows two-dimensional fitting, $f_N(\theta)$ and $f_\theta(N)$ for the simulations with $\Omega_0 = 1$ initially cold simulations at the present epoch $a/a_0 = 7.86$. Projection smooths out some of the local irregularities and the agreement, particularly of $f_\theta(N)$, with equation (2) is remarkable. Agreement at the other epochs is just as good.

3-2-2. Two-Component Models

Figure 8 shows three-dimensional fitting for $m_1 : m_2 = 1 : 5$ at $a/a_0 = 7.86$. The dashed curves are best fits to the solid experimental curves or histograms. Agreement between experimental and theoretical $f(N)$ is very good and the fitted values of b are almost the same as for the single-component models. At least in the range of mass ratio, $m_1 : m_2 = 1 : 1 \sim 1 : 5$, the mass spectrum does not affect the form of $f(N)$ expected from the gravitational thermodynamic theory and does not change the fitted values of b significantly. These results indicate that the thermodynamic $f(N)$ represents the distribution of particles accurately for multi-mass systems even though the thermodynamic theory of Saslaw and Hamilton (1984) assumes single-mass systems.

We also calculated $f(N)$ for each of the two mass components separately and fitted them to the thermodynamic $f(N)$. Figure 9 shows $f_N(V)$ and $f_V(N)$ of the less massive galaxies for $m_1 : m_2 = 1 : 5$ at $a/a_0 = 7.86$. Fitted values of b have slightly smaller values than those for all galaxies but the overall characteristics of the distributions are the same as those for all the galaxies. This is because the less massive galaxies are the dominant component: The mass of the less massive galaxies is about 60% of the total mass of galaxies for $m_1 : m_2 = 1 : 5$ and their number is 88% of the total number.

Figure 10 shows the results for just the massive galaxies for $m_1 : m_2 = 1 : 5$ at $a/a_0 = 7.86$. Although the fitted values of b are much smaller than those for the less massive galaxies, agreement between the theoretical and experimental distributions is very good. The reason why the fitted values of b for the massive galaxies are small is as follows:

Saslaw (1989) derived the relation between b for the whole system and b' for the distribution of particles selected randomly from the whole system by using the generating function of $f(N)$,

$$\frac{1}{(1 - b')^2} = \frac{1 - (1 - p)(2 - b)b}{(1 - b)^2}. \tag{6}$$

Here p is the probability that a galaxy is selected at random, in our case $p = N_2/N = 0.125$. For example, if $b = 0.8$ and $p = 0.125$, b' is expected to be 0.5. The case of $m_1 : m_2 = 1 : 1$ corresponds to this random selection and fitted values of b for the selected "massive" galaxies agree with the expected values of b' in equation (6) very well (see next Section, Figure 15(a)). For the other cases, however, the selection of the massive galaxies is biased by their own

masses. The values of b for the massive galaxies have slightly larger values than ones for a random selection because the massive galaxies are more clustered as discussed in §2.

From equation (6), we can also understand why the fitted values of b_{LM} for the less massive galaxies are smaller than b_T. If $p = N_1/N = 0.875$, equation (6) gives b' a slightly smaller value than b. For instance, $b' = 0.787$ when $b = 0.8$ and $p = 0.875$. We next consider the details of how b_M and b_{LM} are affected by differential clustering as the system evolves.

4. EVOLUTION OF b

4-1. Dependence on Ω_0

The most important property which determines the evolution of b from any particular initial state is the rate of expansion of the universe. This decides the maximum scale that gravitational clustering reaches before the expansion effectively 'freezes' development on larger scales with longer relaxation times. Section 3 showed that on the scales which are relaxed, the gravitational thermodynamic distribution of equation (2) is well satisfied. Therefore we fit equation (2) to the evolving simulation at intervals, to find how the best-fit value of b evolves with time, for both the three-dimensional and the projected distributions. We also calculate $b_{ab\ initio}$ at these times for comparison. The range of values at any given time for the values $N = 0, 1, 2, 3, 4$ and $r = 0.1, 0.2, 0.3$ and 0.4, all weighted equally for each realization, give the standard deviation indicated by the error bars.

Figure 11 shows the time evolution of all three values of b for initially cold $\Omega_0 = 1.0$, 0.1 and 0.01 single-component models. The two- and three-dimensional fits are made at the same time, but offset slightly in the graphs for clarity. Evidently in the case with most rapid clustering, $\Omega_0 = 1$, the fitted and ab initio values of b become nearly identical after about 1.5 initial expansion time scales. In the less relaxed $\Omega_0 = 0.1$ and 0.01 cases they differ substantially. However, in all cases the two- and three-dimensional values of b_{fit} agree within 0.05.

Although relaxation has not progressed sufficiently to bring $b_{ab\ initio}$ and b_{fit} at all close to agreement in the $\Omega_0 = 0.01$ models, the individual fits to equation (2) are even better than for $\Omega_0 = 1.0$; indeed they are almost perfect. The large values of $b_{ab\ initio}$ for low Ω_0 occur because the kinetic energy of peculiar velocities is low in these cases. Being relatively

unclustered, the velocities are dominated by the adiabatic cooling of the expansion of the universe. This is shown in Figure 12 which plots the evolution of W and K for the three values of Ω_0. Figures 13(a) show that three-dimensional peculiar velocity distributions of the initially cold $\Omega_0 = 1$ models at $a/a_0 = 2.80$ and 7.86, and the $\Omega_0 = 0.1$ and 0.01 models both at $a/a_0 = 31.06$. A Maxwell-Boltzmann distribution with the same dispersion is shown for comparison. In lower density universes the velocity dispersion is smaller and the most probable velocity is less. Figures 13(b) show the distributions of the radial velocities. Comparison with the Gaussian distribution having the same velocity dispersion shows that low-velocity particles are more abundant in the evolved distribution than they would be in a Gaussian distribution.

4-2. Effects of Initial Velocity Dispersion

The role of different initial states is also of great interest in gravitational clustering. Here we report what happens if the initial velocity dispersion is increased. Initial conditions which start warm, with a Gaussian velocity distribution having $\langle v^2 \rangle^{1/2} = \bar{r} H_i$, where $\bar{r}$ is the average distance between particles, evolve very similarly to the cold models of Figure 11. In the warm $\Omega_0 = 1$ models there is even better agreement between the 2 and 3-dimensional value of b_{fit}, and both agree with $b_{\text{ab initio}}$. The warm $\Omega_0 = 0.1$ models are not significantly different from the cold ones.

Hot initial conditions $\langle v^2 \rangle^{1/2} = 3\bar{r} H_i$, for $\Omega_0 = 1$ lead to the evolution shown in Figure 14. By comparison with Figure 11, the hot initial state leads to slower relaxation, larger dispersion in the values of b, and lower average values of b at the same expansion factor. Eventually, however, the excess peculiar motions die away and the system relaxes strongly to the same quasi-equilibrium state as the cold $\Omega_0 = 1$ model. The hot model must expand about twice as much as the cold model to reach this state. It is a feature of the hot cases that the kinetic energy decreases as a function of time.

For the hot $\Omega_0 = 0.1$ case, the time evolution of b is shown in Figure 14. Unlike the cold or warm cases, b_{fit} saturates at about $b_{\text{fit}} = 0.5$ and the dispersion of b_{fit} is quite large. The reason for this saturation is that clustering is weak at early times because the velocity dispersion is large, and subsequent clustering is suppressed by the rapid expansion of the universe.

4-3. Effects of Different Mass Components

Figure 15 shows the time evolution of the three-dimensional averaged fitted values of b for $m_1 : m_2 = 1 : 1 \sim 1 : 5$. Error bars give the standard deviations over the ten values of N and r Values of b_T are linked by a spline-interpolation and are indicated by a solid curve. The values of b' given by equation (6) using interpolated values are shown by dashed curves: the upper curve for $p = 0.875$ and lower one for $p = 0.125$. From Figure 15(a), fitted values of b_{LM} and b_M for $m_1 : m_2 = 1 : 1$ (corresponding to random selection) agree with the expected values of b' from equation (6) very well. However, b_M for $m_1 : m_2 \neq 1 : 1$ is much larger than the values for random selection, and its deviation from the dashed random selection curve becomes larger as the mass ratio becomes larger (Figure 15(b)$\sim$(e)). This shows that the massive galaxies cluster more rapidly and form the nuclei around which less massive galaxies cluster.

For $m_1 : m_2 = 1 : 1$, there are slight differences between b_M and b' at $a/a_0 = 2.0$ and $a/a_0 \gtrsim 10$. The reason for this is as follows: At the start, the positions of the galaxies are generated by the random number generator, however, the perfect random number generator does not exist. So there are some deviations from a Poisson distribution in the initial distribution, especially in the distribution of the relatively fewer massive galaxies. This deviation disappears rapidly due to the mixing processes of clustering and $b_1 - b' \simeq 0$ for $a/a_0 = 3 \sim 10$. In the later stages when $a/a_0 \gtrsim 10$, it is likely that a large fraction of the 'massive' galaxies are contained in the clusters or in the fields, so their selection will not be random. The values of b_{LM} for $m_1 : m_2 = 1 : 1$ in Figure 15(a) also agree with b' derived from equation (6). The departures of b_M and b_{LM} from the values of equation (6) therefore represent gravitational biasing of the sample.

In order to examine how different mass components modify the clustering, Figure 16 shows the evolution of $b_i - b'$ where b_i is an averaged fitted value of b for the massive galaxies in Figure 16(a) and for the less massive galaxies in Figure 16(b). The subscript i represents a mass ratio $i \equiv m_2/m_1$. Since the initial distribution is Poisson, $b_i = 0$ for $i = 1 \sim 5$ when $a/a_0 = 1$ ($f(N)$ in equation (2) with $b = 0$ gives the Poisson distribution). From Figure 16(a), as clustering proceeds, differences between b_i and b' for the massive galaxies grow rapidly until $a/a_0 \sim 6$ and have larger values for larger mass ratios. However, these

differences become small in the late stages of clustering for all cases.

This implies that in the early stages the massive galaxies speed up the clustering, but in late stages the distinction between different masses diminishes. In other words, although the mass of an individual galaxy is important at early stages, collective effects become more important at late stages and the effects of the mass spectrum are substantially reduced.

From Figure 16(b), the fitted values of b_i for the less massive galaxies are slightly smaller than b' in equation (6) with $p = 0.875$. Especially the difference $b_i - b'$ for $a/a_0 \lesssim 3$ is larger as the mass ratio is larger. This indicates that the less massive galaxies cluster more slowly than the massive ones during this stage. However, $b_i - b'$ approaches zero quickly in the late stages of clustering, and b_i converges to the value for random selection after $a/a_0 \sim 3$. This shows that the less massive galaxies are gathered together by the gravity of the more clustered massive galaxies and their subsequent clustering does not depend strongly on their smaller mass.

4-3. On Individual and Collective Interactions

Peculiar velocities may arise from interactions between individual galaxies, as well as from collective interactions between a galaxy and a cluster. The transition from individual interactions to collective effects in clustering can be seen from the time evolution of the velocity dispersions of the less massive and more massive galaxies in the two-component models. Figure 17 shows the time evolution of T_2/T_1, where T_j is the temperature of j-th component of galaxies in energy units defined by

$$T_j = \frac{2}{3N_j} \frac{1}{2} m_j \sum_{k=1}^{N_j} v_k^2, \qquad j = 1, 2 \tag{7}$$

with N_j and m_j the number and the mass of j-th component, respectively. If individual interactions dominate, the velocity distribution tends to relax toward a state of equipartition in which galaxies of different masses all have the same temperature, i.e., $\langle v^2 \rangle \propto m^{-1}$ If collective interactions dominate, the relaxation is towards a state where all mass components have the same velocity dispersion (e.g., Saslaw 1985b), i.e., $T_j \propto m_j$. In the early stages, the more massive galaxies cluster more rapidly and their velocity dispersion increases faster than the less massive galaxies, so the ratio of temperatures has a larger value than the ratio of masses. Next, the less massive galaxies cluster around the massive ones. Consequently

the less massive galaxies increase their velocity dispersion and the ratio of the temperatures begins to decrease. However, the ratio of the temperatures does not continue to decrease but converges to the value of the mass ratio. Thus equipartition is not established. Instead the two components of galaxies acquire the same velocity dispersions. This indicates that the collective effects dominate the later stages of clustering.

5. IDENTIFICATION OF CLUSTERS

As described in §2, the massive galaxies in the two-component models seem to be preferentially concentrated in high density clusters. To make this impression quantitative, we identify clusters in the simulations using the following procedure:

1) Calculate the local density at the i-th galaxy which is defined from j neighboring galaxies around the i-th galaxy (Casertano and Hut 1985)

$$\rho_j^{(i)} = \frac{m_i + \sum_{k=1}^{j-1} m_k + m_j/2}{V(r_{ij})},$$

where m_k is the mass of the k-th neighbor of the i-th galaxy and $V(r_{ij})$ is the volume of the sphere with radius r_{ij}, which is the distance between the i-th galaxy and the j-th galaxy. We adopt $j = 6$, because this number assures the small fluctuation and the localness of the density (Casertano and Hut 1985).

2) In order to search for galaxies in high density regions, first select one galaxy which has a high local density and regard its neighboring j galaxies as members of galaxies contained in a high density region. The criterion for 'high' local density is

$$\rho_j^{(i)} \geq \alpha \bar{\rho}$$

where α is numerical factor and $\bar{\rho}$ is the average mass density of galaxies. Next select galaxies from members which satisfy the criterion of 'high' local density and regard their neighboring j galaxies as new members. Repeat this procedure until new members do not appear.

3) Obtain groups of galaxies which are contained in high density regions by continuing the procedure 2) until there is no galaxy which satisfies the criterion of high local density.

4) Identify those groups containing more than 10 galaxies as clusters.

The number and population of clusters vary with the value of α. However, since our purpose is to investigate the dependence of the number of galaxies of each mass contained in clusters, we have no interest in determining the most adequate value of α to define clusters. Here we take $\alpha = 5 \times 10^2$, because the clusters identified with this value look reasonable.

Figure 18 shows the distribution of galaxies projected on the x-y plane and the clusters identified for $m_1 : m_2 = 1 : 1$ at $a/a_0 = 7.86$. Figure 19 shows the magnified features of one of the clusters and its surrounding galaxies. Figure 19 indicates the central concentration and filamentary structures of galaxies clearly. The ratios of the number of less massive and massive galaxies which are contained in the identified clusters ($N_{1\text{in}}$ and $N_{2\text{in}}$) to the total number of them (N_1 and N_2) are listed in Table 1. From Table 1, $N_{2\text{in}}/N_2$ becomes larger than $N_{1\text{in}}/N_1$ as the mass ratio (m_2/m_1) increases. This indicates that there is a higher probability that the massive galaxies are found in clusters (high density regions) and supports the impression of §2 that the massive galaxies are concentrated in clusters and speed up the clustering as seeds of the clusters.

From observations, the cluster-cluster correlation function of rich, though not of poor, clusters appears to have a larger amplitude than the galaxy-galaxy correlation function (e.g., Bahcall and Soneira 1983; Postman, Geller and Huchra 1986). Recently Coleman and Saslaw (1989) examined the $f(N)$ statistics for Abell clusters and found that their fitted value of b is about 0.3 ± 0.1. It would be very interesting to compare these observational results with the distribution of clusters in N-body simulations. Unfortunately the number of identified clusters in our simulations is too small to determine accurate statistical quantities from these simulations.

6. EVOLUTION OF THE SATELLITE SYSTEMS

In §3, the thermodynamic $f(N)$ was found to describe multi-mass systems with mass ratio $m_2/m_1 \lesssim 5$. This leads us to ask how well it may apply in extreme cases such as $m_1 : m_2 = 1 : 30$ or $1 : 100$. Figure 20 shows the projected positions for the case $m_1 : m_2 = 1 : 100$ at $a/a_0 = 7.86$. Its features are very different from those of Figure 2. Here the massive galaxies concentrate to form the compact cores of clusters with a great number of less massive galaxies gathered around them as satellite systems. These differences from

the less extreme mass ratio cases show up quantitatively in both the two-point correlation function and the $f(N)$ statistics.

The two-point correlation functions ξ_T for all galaxies are shown in Figure 21(a). They have larger amplitudes at large scales than ξ_T for $m_1 : m_2 = 1 : 5$, but at small scales, ξ_T has a rather smaller amplitude. Figure 21(b) shows two-point correlation functions for the less massive and massive galaxies. ξ_M has a power law form. However ξ_{LM} bends at $\xi_{LM} \sim 10$ and departs from a power law. The less massive galaxies are only several percent of the total mass and their mutual gravity is negligible. Therefore they cannot agglomerate by their self-gravity and ξ_{LM} does not grow on small scales. This is also why ξ_T has a small amplitude on small scales.

Figures 22, 23 and 24 show the resulting $f(N)$ statistics for the total, less massive and massive galaxies, respectively. The agreement between theoretical and experimental $f(N)$ distributions is not so good. In particular, the deviation from the thermodynamic distribution of $f_V(N)$ for $r = 0.3$ and $r = 0.4$ is very large and there are remarkable peaks of $f_V(N)$ at $N \sim 70$ for $r = 0.3$ for the total and less massive galaxies, and at $N \sim 120$ for $r = 0.4$. The massive galaxies have peaks at $N \sim 10$ for $r = 0.3$ and at $N \sim 15$ for $r = 0.4$. From Figure 20, there exist large clusters with these sizes and numbers of members. The typical size of clusters agrees with sampling volumes whose radius is $r = 0.3$ or 0.4. Thus these peaks in $f_V(N)$ indicate the typical number of galaxies which are contained in the sampling volumes with $r = 0.3$ or 0.4. Similar features are also found in the case of $m_1 : m_2 = 1 : 30$.

The basic reason why the thermodynamic distribution function does not closely reproduce the form of the experimental $f(N)$ for these extreme cases is because the number of galaxies in the sample volumes is not an accurate measure of the mass in the volume. So the assumption in the thermodynamic theory that mass is proportional to number is no longer correct for these cases. However $f(N)$ statistics are still useful for making the more complex structure of galaxy clustering evident in comparison with the thermodynamic $f(N)$. Thus the thermodynamic function of equation (2) can play the role of a *fiducial* distribution function even for these extreme cases.

It is interesting to ask at what value of m_2/m_1 the thermodynamic description of galaxy clustering breaks down. To examine the behavior of the clustering with intermediate mass

ratios, we did two further simulations with $m_1 : m_2 = 1 : 8$ and $1 : 15$. Since for the case of $m_1 : m_2 = 1 : 8$ the two components have almost the same total mass, it might be expected to give a marginal mass ratio which determines whether the thermodynamic distribution function can describe the experimental galaxy distribution. However, there is no obvious difference between the thermodynamic and experimental $f(N)$ distributions. On the other hand, the small peaks which deviate from the thermodynamic $f(N)$ are seen in the case of $m_1 : m_2 = 1 : 15$. Therefore we can safely conclude that the thermodynamic theory is not applicable to the cases of $m_2/m_1 \gtrsim 15$.

7. DISCUSSION

7-1. Single-Component Models

The most striking results of these experiments are 1) the rapidity with which the clustering relaxes to the thermodynamic $f(N)$ distribution and 2) the accuracy of the quasi-static approximation in which subsequent evolution occurs through a series of thermodynamic quasi-equilibrium states. We discuss these two results.

7-1-1. Relaxation

We can discern several measures of the type and degree of relaxation using these N-body simulations and the $f(N)$ statistic. The weakest form of relaxation is when the thermodynamic $f(N)$ distribution describes the simulations for all values of N, but with a value of b which depends strongly on N, or on scale length. This would normally indicate that relaxation has only occurred among several near neighbors, and not spread to larger scales. We would expect this to be the early form of relaxation from initial conditions dominated by a Poisson distribution or by any distribution with more power on small scales. The larger fluctuations on smaller scales would then have relaxation times that are short relative to the global expansion time scale.

If there is time and the relaxation spreads to very large scales, then it will be possible to fit the thermodynamic $f(N)$ distribution to all values of N with nearly the same value of b. Slight variations on larger scales may prevent b from being identical at all levels, but its dispersion should be small.

A further measure of relaxation, which is particularly informative about anisotropy,

is to compare the three-dimensional $f(N)$ distribution with the projected two-dimensional distribution for the same sample. Differences between the two fits and their values of b indicate the presence of oriented filamentary or cellular structure, including bubbles and froth.

Finally, the strongest degree of relaxation occurs when all these measures agree among themselves and with the value of $b_{\text{ab initio}}$ calculated directly from the positions and peculiar velocities of the particles. In this case, all the information available from the $f(N)$ distributions points to the system being in a relaxed quasi-equilibrium state. We call this case 'strong relaxation'

Our N-body simulations show that the degree of relaxation from an initial Poisson state depends mainly on the value of Ω_0 and on the initial velocity dispersion. Progress toward strong relaxation is most rapid if the initial state is either cold or warm and if $\Omega_0 \approx 1$. Figure 11 shows that strong relaxation occurs by $a/a_0 \approx 2.5$ in these cases, and it persists for the rest of the evolution. The time scale for strong relaxation in cold $\Omega_0 = 1$ models is therefore very nearly the same as the expansion time scale. Hot $\Omega_0 = 1$ cases in Figure 14 take about twice as long to relax strongly, and the dispersion of the values of b remains greater. Evidently the closer the system starts to the quasi-equilibrium state, the faster it relaxes to this state. This is opposite to the evolution of a violently relaxing system, and confirms that most of the initial relaxation occurs among near neighbors. Less dense universes, with $\Omega_0 \leq 0.1$ expand so rapidly that strong relaxation never occurs, whether they start hot or cold. If, someday, it becomes possible to determine $b_{\text{ab initio}}$ observationally , we will have a useful constraint on the value of Ω_0.

When the relaxation is weak, for $\Omega_0 < 1$, the fitted value of b is less than its ab initio value. Adiabatic cooling dominates the velocities of the weakly clustered galaxies and their contribution, growing as Ω_0 decreases, produces this discrepancy. If $\Omega_0 < 0.1$, relaxation is so feeble that the asymptotic value of b_{fit} is less than the observed value $b_{\text{obs}} = 0.70 \pm 0.05$. For example, with $\Omega_0 = 0.01$, we find b_{fit} tends toward the value 0.25 ± 0.1 after long times. So this may also be used for estimating the actual value of Ω_0, although it is not very sensitive when $\Omega_0 \geq 0.1$. Even for low values of Ω_0, the individual fits to the thermodynamic distribution function are very good, but the values of b for different volumes vary more than in the case of large Ω_0.

Relaxation from an initially nonzero velocity distribution differs from the growth of initially cold distributions such as those in Figure 13. In the initially cold distributions, the velocities never have a chance to become completely Maxwellian, although a Maxwellian is a reasonable zero-order approximation.

The velocity dispersion in the warm and hot models remains Maxwellian until about the time the system relaxes strongly. Then cooling of the unclustered galaxy velocities sets in. Figure 14 shows how this affects the evolution of b in the case of a hot $\Omega_0 = 1$ model, where the velocity distribution starts as a Maxwellian with a large dispersion at $a/a_0 = 1$, remains Maxwellian with a much reduced dispersion at $a/a_0 = 7.86$, when $b_{\rm fit} \approx b_{\rm ab\ initio}$, and becomes increasingly skewed and broad until the simulation was stopped at $a/a_0 = 31$. The warm $\Omega_0 = 1$ model behaves similarly, and begins to depart from the Maxwellian form at $a/a_0 \approx 2.8$. The corresponding $\Omega_0 = 0.1$ models begin to depart from Maxwellian distributions at slightly greater expansion factors, consistent with their relatively slower clustering.

Differences in the values of $b_{\rm fit}$ for $f_N(V)$ and $f_V(N)$ are a useful measure of the relaxation of different initial velocity distributions. Figure 25 shows these quantities for the projected counts in the cold, warm, and hot $\Omega_0 = 1$ simulations. The differences between $f_N(V)$ and $f_V(N)$ are somewhat larger for the projected counts than for the volume counts. The differences also increase as the initial velocity dispersion increases. In all these cases, the difference decreases as the universe expands, indicating the tendency toward relaxation. These differences also are reflected in the dispersion of each $b_{\rm fit}$ value in Figures 11 and 14. Values of b for $f_N(V)$ are almost always less than those for $f_V(N)$. This tendency is especially strong for the hot simulations. The reason is that on small scales the initial energy of peculiar motions is larger relative to the gravitational correlation energy and inhibits clustering on these small scales.

As the value of Ω_0 decreases, the differences between $b_{\rm fit}$ for $f_N(V)$ and $f_V(N)$ become larger for a given initial velocity dispersion, compared with the differences for the $\Omega_0 = 1$ cases. The observed values of $b_{\rm fit}$ for $f_N(V)$ and $f_V(N)$ are therefore inconsistent with various combinations of initial velocity dispersions and values of Ω_0 in these models. In particular, the cases of hot $\Omega_0 = 1$, hot $\Omega_0 = 0.1$, cold $\Omega_0 = 0.01$, warm $\Omega_0 = 0.01$ and hot $\Omega_0 = 0.01$ cannot represent the observations. Cold $\Omega_0 = 1$, warm $\Omega_0 = 1$, cold $\Omega_0 = 0.1$ and (marginally) warm

$\Omega_0 = 0.1$ models do agree with the observed range of $b_{\rm fit}$.

7-1-2. Quasi-equilibrium Evolution

Perhaps the most remarkable feature of these simulations is that, after a short relaxation period, they subsequently evolve through a series of quasi-equilibrium states. It is well known that gravitating systems have no rigorous 'equilibrium' state because an 'equilibrium' state should mean $b_{\rm ab\ initio} = b_{\rm fit}$ and no evolution. However it does not seem to have been appreciated that the evolution of gravitational galaxy clustering may occur through a sequence of 'quasi-equilibrium' states. A 'quasi-equilibrium' state is one which satisfies equation (2) with a value of $b < 1$ and in which $b_{\rm ab\ initio}$ may differ from $b_{\rm fit}$. In this state the clustering hierarchy has not grown to encompass all scales. Quasi-equilibrium evolution was hypothesized previously (Saslaw and Hamilton 1984; Saslaw 1985a,1986), and our present simulations provide the first strong evidence for it. The evidence is of two types. The first is the previously discussed goodness of fit to the thermodynamic distribution at any stage of the evolution after the initial relaxation. The second, which we take up now, is the time evolution of b.

In the cold models, for all three values of Ω_0, Figure 11 shows that the value of $b(t)$ increases rapidly, about as fast as the expansion time scale, until $a/a_0 \approx 5$. Subsequently $b(t)$ evolves more slowly, on a time scale longer than the expansion time scale. It appears to tend toward an asymptotic limit when the expansion factor a/a_0 is large. By the time that $a/a_0 = 15.6$ in the most relaxed ($\Omega_0 = 1$) model, the value of $b_{\rm ab\ initio} = 0.82$, the correlation energy is still growing slowly as $t^{0.2}$, and the kinetic peculiar energy increases as $t^{0.15}$

The qualitative form of $b_{\rm ab\ initio}(t)$ agrees with what one expects from the cosmic energy equation (Saslaw 1986). If the expansion factor $a \propto t^\alpha$ and the correlation energy $W \propto t^s$, then the asymptotic value of $b_{\rm ab\ initio} = (s + 2\alpha)/2(s + \alpha)$. With $\alpha = 2/3$ and $s = 0.2$, this gives $b_{\rm ab\ initio} = 0.88$, showing that the system has not completely relaxed at $a/a_0 = 15.6$. It may also be the case that s will decrease further at longer times (which we have not computed yet), and the asymptotic value of $b_{\rm ab\ initio}$ will be unity. The simulations with smaller Ω_0, computed for longer times, show this effect. After long times, for each Ω_0, the growth of correlation energy is much slower than either the linear approximation or the self-similar solution suggest. This is because the system has relaxed and no longer evolves strongly on the small scales which contain most of the correlation energy. On large scales, particularly

in the low Ω_0 models, subsequent evolution is prevented by the expansion, and so the state of clustering is 'frozen'

Models that are initially warm and hot, naturally behave quite differently. Instead of increasing, their kinetic energy starts to decrease due to the adiabatic expansion of the universe. The decrease continues until heating by clustering balances the adiabatic cooling. Then the kinetic energy increases again. The smaller Ω_0 is, and the hotter the system starts, the longer it cools. During this cooling phase, the dispersion of the values of b_{fit} is greater than for the initially cold models, indicating that the evolution is farther from equilibrium. Eventually the $\Omega_0 = 1$ and $\Omega_0 = 0.1$ models seem to reach approximately the same relaxed state, independent of their initial thermal energy. Expansion of the universe combines with gravitational clustering to remove the memory of most initial states of the system. After this occurs, the thermodynamic theory gives a very good fit to the $f(N)$ distribution of the simulations.

The basic physical assumptions of the thermodynamic theory are that the system is statistically homogeneous and that b is independent of scale. This assumptions are best satisfied in the initially cold or warm models with Ω_0 larger than about 0.1 which relax most rapidly and completely. These are also the models which best fit the theory.

7-2. Two-Component Models

From the two-component models, we obtain following conclusions:

1) The thermodynamic distribution function $f(N)$ agrees well with the experimental distribution for multi-mass systems as long as the mass ratio of the two components is in the range of $m_1 : m_2 = 1 : 1 \sim 1 : 10$. The existence of such mass spectra does not require modification of the form of $f(N)$ in equation (2) and does not change the fitted value of b significantly even though thermodynamic theory assumes that all galaxies have the same mass.

2) In the range of these mass ratios, the $f(N)$ statistic applies to each mass component separately. The fitted values of b for the massive galaxies are larger than those expected from random sampling, indicating differential clustering. Furthermore the time evolution of b and also of the temperature ratio T_2/T_1 of the two components indicates that two-body interactions are important only at early stages of clustering and collective effects dominate

the late stages of clustering.

3) The number of massive galaxies which are contained in clusters tends to increase as the mass ratio becomes larger; these massive galaxies play the role of seeds of clusters.

It might seem strange that although many massive galaxies concentrate in clusters even in late stages, the fitted values of b for the massive galaxies are very close to b' for random selection. This is because the radii of volumes sampled for $f_V(N)$ is much larger than the radii of the clusters (see Figure 18) and the irregularities of distributions of the massive galaxies are smoothed. Moreover the $f_N(V)$ representation is not very sensitive to small scale structures because the main portion of this function generally occurs for $r \gtrsim 0.1$ ($V = 4\pi r^3/3$), a scale much larger than the typical size of clusters.

It is therefore very interesting to ask whether small sample volumes can reveal the small scale structures. To explore this, we extended the small scale analyses to very small sampling volumes with radii $r = 0.01 \sim 0.08$. The values of $b_i(r) - b'(r)$ for massive galaxies in the complete sample range $0.01 \leq r \leq 0.4$ are shown in Figure 26. Here $b_i(r)$ is the fitted value of b for the sampling volumes of radius r and $b'(r)$ is the expected value from equation (6) regarding the fitted value of $b_i(r)$ for all the galaxies as b. From Figure 26(a), $b_i(r) - b'(r)$ at $a/a_0 = 7.86$ has larger values for scales of $r \lesssim 0.2$ as the mass ratio become larger. This shows that the massive galaxies are more clustered at this stage as shown in Figure 16(a). From Figure 26(b), however, the differences between $b_i(r)$ and $b'(r)$ for $r \gtrsim 0.1$ at $a/a_0 = 15.62$ become smaller, although the differences for the small scales do indeed become larger. This indicates that the massive galaxies concentrate in the clusters and give larger values to $b_i(r)$ on small scales. On the large scales, the large sampling volumes smooth small scale structures and the collective effects which do not significantly influence small scale structures are important. Therefore, $b_i(r) - b'(r)$ decreases as the radius r become larger. Thus we conclude that the $f_V(N)$ representation is especially useful for describing small scale structure.

4) The thermodynamic theory is not applicable to extreme cases of $m_2/m_1 \gtrsim 15$. However, $f(N)$ statistics can still reveal the structure of galaxy clustering by using the thermodynamic distribution function as a standard of comparison.

7-3. Observational implications

Although we have simulated models with relatively simple initial conditions, it seems possible to draw some tentative observational conclusions from them. When the simulations are scaled to a radius of about 40 Mpc, the average nearest neighbor distance is several megaparsecs. This is of the same order as the galaxy separation in the Zwicky Catalog, so it is reasonable to compare our results with the observations on this scale. (On larger observed scales where relaxation may not have developed as far, the value of b is expected to be smaller.)

The observations of $f(N)$ are consistent with Poisson initial conditions in $\Omega_0 > 0.1$ single-component models, but not with the other simulations. For example, in the hot $\Omega_0 = 1$ models the velocity dispersion has inhibited relaxation, and the fits for the number and the volume distributions give discordant values of b. Other initial conditions may also be quite consistent with the observations, especially since most homogeneous but non-Poisson initial states will be washed out by the strong gravitational relaxation (Suto, Itoh and Inagaki 1990).

The good agreement between observations which involve galaxies with a very wide range of masses, and these single-component models suggests that individual galaxy masses are fairly unimportant in the clustering process. This is confirmed by two-component models which show that most of the relaxation, after near neighbors form the first level of the clustering hierarchy, is a collective process. However these models with mass spectrum have only two mass components, so we intend to explore the effects of a continuous mass spectrum. It may be that collective interactions dominate more rapidly when the mass spectrum is continuous, producing somewhat less mass dependence of clustering than in two-component systems. This is would be consistent with an observed tendency for dwarf galaxies and bright galaxies to have generally similar distributions (Thuan, Gott and Schneider 1987; Binggelli, Terenghi and Sandage 1989; Eder, et al. 1989), as well as with the good agreement between equation (2) and the overall observed galaxy distribution (Crane and Saslaw 1986). This agreement might also imply that the mass range of galaxies is narrower than their luminosity range, especially if dark matter is significant (cf. Carignan and Freeman 1988). It is also likely that when the statistical $f(N)$ distributions are measured for galaxies of different types, they will show enhanced clustering of the more massive types, as predicted by these

two-component models. The amount of enhancement will depend on the mass spectrum, the initial conditions, and the influence of non-galactic dark matter if it is present in large amounts with a non-uniform distribution.

Gravitational clustering is probably the simplest explanation of the observed main features of the galaxy distribution. Other explanations, such as biased galaxy formation, are quite strongly constrained by the observed $f(N)$ distribution (Saslaw, Antia, and Chitre 1987). In such other explanations, the observed distribution is merely a passing scene, rather than a state to which matter relaxes.

ACKNOWLEDGMENT

APPENDIX A.

DETERMINATION OF $\bar{n}$

Determination of $\bar{n}$ is important when we look for the best-fit thermodynamic distribution. Though we should define $\bar{n}$ as the average number density averaged over the entire system, fluctuations will cause this to differ slightly from $\bar{n}$ in the region actually sampled. Therefore to determine $\bar{n}$ we first give a number j to each spatial point that is generated. If the number of the particles inside the sphere of radius r with the center on the j-th point is N_j, we define

$$\bar{n} = \frac{\sum N_j}{\sum V_j}, \tag{A1}$$

for the fitting of $f_V(N)$, where $V_j = 4\pi r^3/3$.

For the fitting of $f_N(V)$, equation (A1) does not give an accurate value of $\bar{n}$ because of the different average densities of the regions which are sampled. Therefore we adopted

$$\bar{n} = \frac{N(R < 0.6)}{V}, \tag{A2}$$

for fitting $f_N(V)$, where $N(R < 0.6)$ is the number of the particles inside the sphere of radius 0.6 from the center of the system and $V = 4\pi 0.6^3/3$.

APPENDIX B.

DETERMINATION OF THE PRESENT EPOCH IN THE SIMULATIONS

To determine the present epoch in the single-component models, we use the amplitude of the two-particle correlation function $\xi(r)$. We first assume that

$$\xi(r) = \left(\frac{r}{r_0}\right)^{-\gamma} \qquad \text{with} \qquad \gamma = 1.8 \quad \text{or} \quad 2.0 \tag{B1}$$

and find r_0 by a least square fit to the two-particle correlation function obtained from the simulations. The radius of the system is $40h^{-1}\mathrm{Mpc}$ according to Aarseth, Gott, and Turner (1979), where h is the present Hubble constant in the unit of $100h\,\mathrm{km\,s^{-1}Mpc^{-1}}$

Values of r_0 obtained from observations are not known very accurately: $r_0 = 4.23 \pm 0.26h^{-1}\mathrm{Mpc}$ according to Peebles (1980) and $r_0 = 5.4 \pm 0.3h^{-1}\mathrm{Mpc}$ according to Davis and Peebles (1983). Moreover the values of r_0 determined from the simulations depend on the range of the fitting, since the correlation functions are only approximately power laws. Thus

there are some ambiguities in the determination of the present epoch from the simulations. The range of values of a compatible with the present epoch are

$$a/a_0 = 5.6 \sim 7.9 \tag{B2}$$

for $\Omega_0 = 1$,

$$a/a_0 = 16 \sim 31 \tag{B3}$$

for $\Omega_0 = 0.1$. We could not determine the values of a/a_0 at the present epoch for $\Omega_0 = 0.01$ because the two-particle correlation functions obtained in the simulations are quite different from the observed one.

Two-dimensional fitted values of b for these epochs are

$$b_{fit} = 0.58 \pm 0.04 \qquad (\Omega_0 = 1, a/a_0 = 5.6)$$

$$b_{fit} = 0.67 \pm 0.04 \qquad (\Omega_0 = 1, a/a_0 = 7.9)$$

$$b_{fit} = 0.60 \pm 0.03 \qquad (\Omega_0 = 0.1, a/a_0 = 16)$$

$$b_{fit} = 0.62 \pm 0.03 \qquad (\Omega_0 = 0.1, a/a_0 = 22)$$

$$b_{fit} = 0.66 \pm 0.02 \qquad (\Omega_0 = 0.1, a/a_0 = 31).$$

The values of b_{fit} at $a/a_0 = 7.9$ for $\Omega_0 = 1$ and at $a/a_0 = 22$ and 31 for $\Omega_0 = 0.1$ are consistent with the observed value $b_{fit} = 0.70 \pm 0.05$ (Crane and Saslaw 1986).

REFERENCES

Aarseth, S.J. 1985, in *Multiple Time Scales*, ed. J.U.Brackbill and B.I.Cohen (New York: Academic Press), p.377.

Aarseth, S.J., Gott, J.R., and Turner, E.L. 1979, *Ap.J.*, **228**, 664.

Aarseth, S.J., and Inagaki, S. 1986, in *The Use of Supercomputers in stellar Dynamics*, ed. P.Hut and S.McMillan (Berlin: Springer-Verlag), p.203.

Bahcall, N.A., and Soneira, R.M. 1983, *Ap.J.*, **270**, 20.

Binggelli, B., Terenghi, M. and Sandage, A. 1989, preprint.

Carignan, C., and Freeman, K.C. 1988, *Ap.J. (Letters)*, **332**, L33.

Casertano, S., and Hut, P. 1985, *Ap.J.*, **298**, 80.

Coleman, P., and Saslaw, W.C. 1989, in preparation.

Crane, P., and Saslaw, W.C. 1986, *Ap.J.*, **301**, 1.

Davis, M., and Peebles, P.J.E. 1983, *Ap.J.*, **267**, 465.

Eder, J.A., Schombert, J.M., Dekel, A., and Oemler, A.Jr. 1989, *Ap.J.*, **340**, 29.

de Lapparent, V., Geller, M.J., and Huchra, J.P. 1988, *Ap.J.*, **332**, 44.

Itoh, M., Inagaki, S., and Saslaw, W.C. 1988, *Ap.J.*, **331**, 45.

Itoh, M., Inagaki, S., and Saslaw, W.C. 1990, *Ap.J.*, June 20.

Peebles, P.J.E. 1980, *The Large-Scale Structure of the Universe* (Princeton: Princeton University Press).

Postman, M., Geller, M.J., and Huchra, J.P 1986, *A.J.*, **91**, 1267.

Saslaw, W.C. 1980, *Ap.J.*, **235**, 299.

Saslaw, W.C. 1985a, *Ap.J.*, **297**, 49.

Saslaw, W.C. 1985b, *Gravitational Physics of Stellar and Galactic Systems* (Cambridge: Cambridge University Press).

Saslaw, W.C. 1986, *Ap.J.*, **304**, 11.

Saslaw, W.C. 1989, *Ap.J.*, **341**, 588.

Saslaw, W.C., Antia, H.M., and Chitre, S.M. 1987, *Ap.J.(Letters)*, **315**, L1.

Saslaw, W.C., and Hamilton, A.J.S. 1984, *Ap.J.*, **276**, 13.

Suto, Y., Itoh, M., and Inagaki, S. 1989, *Ap.J.*, February 20.

Thuan, T.X., Gott, J.R., and Schneider, S.E. 1987, *Ap.J.(Letters)*, **315**, L93.

Totsuji, H., and Kihara, T. 1969, *Pub.Astr.Soc.Japan.*, **21**, 221.

Table 1. The ratio of the number of massive and less massive galaxies which are contained in the identified clusters($N_{1\text{in}}$ and $N_{2\text{in}}$) to the total number of them(N_1 and N_2).

$m_1 : m_2$	1 : 1		1 : 2		1 : 3		1 : 4		1 : 5	
a/a_0	$\frac{N_{1\text{in}}}{N_1}$	$\frac{N_{2\text{in}}}{N_2}$	$\frac{N_{1\text{in}}}{N_1}$	$\frac{N_{2\text{in}}}{N_2}$	$\frac{N_{1\text{in}}}{N_1}$	$\frac{N_{2\text{in}}}{N_2}$	$\frac{N_{1\text{in}}}{N_1}$	$\frac{N_{2\text{in}}}{N_2}$	$\frac{N_{1\text{in}}}{N_1}$	$\frac{N_{2\text{in}}}{N_2}$
5.57	3.6%	4.4%	4.0%	7.6%	3.9%	8.2%	5.3%	11.6%	5.6%	11.2%
7.86	12.4%	13.8%	11.1%	18.2%	12.3%	21.2%	10.5%	22.8%	12.5%	28.4%
11.08	19.5%	20.6%	20.0%	30.6%	18.5%	32.4%	18.7%	41.2%	—	—
15.62	30.2%	31.8%	25.9%	40.2%	26.1%	47.8%	23.0%	52.2%	—	—

FIGURE CAPTIONS

Figure 1. Six projected distributions from an $\Omega_0 = 1$ cold run. The first is the initial state, the next three are at values of $a/a_0 = 2.80$, 7.86 and 15.62. These are all projected views of approximately 2000 galaxies in the same hemisphere, as seen by an observer at the center. The last two distributions, at $a/a_0 = 7.86$, are projections of this same hemisphere but confined first to the nearby galaxies with distances $0 < R < 0.5$ and in 1f to distant galaxies with $0.9 < R < 1.0$. The maximum comoving radius of the simulation is always scaled to $R = 1$.

Figure 2(a). Projected positions for all the galaxies with $m_1 : m_2 = 1 : 5$, $a/a_0 = 7.86$. (b) Projected positions for the less massive galaxies. (c) Projected positions for the massive galaxies.

Figure 3. Two-point correlation functions of cold $\Omega_0 = 1$, $\Omega_0 = 0.1$, and $\Omega_0 = 0.01$ simulations at three different expansion epochs a/a_0. For comparison we show a dotted power law of the form r^{-2}, which is the asymptotic thermodynamic prediction.

Figure 4. Two-point correlation functions for warm and hot initial velocities with $\Omega_0 = 1$ and $\Omega_0 = 0.1$.

Figure 5(a). Two-point correlation functions for all the galaxies with $m_1 : m_2 = 1 : 5$, $a/a_0 = 1.41 \sim 7.86$. (b) Two-point correlation functions for the less massive and massive galaxies.

Figure 6. $f(N)$ obtained by simulations for $\Omega_0 = 1$ and cold initial condition at the epoch of $a/a_0 = 2.8$, 7.86, and 15.6. The full curves are from the simulation and the dashed curves are the best-fit theoretical thermodynamic distribution with the resulting value of b given in the diagrams.

Figure 7. The projected distributions $f_N(\theta)$ and $f_\theta(N)$ for cold $\Omega_0 = 1.0$ simulations at $a/a_0 = 7.86$. The angle θ is measured in radians. Dashed lines show the best fit to the thermodynamic distribution with the resulting value of b given in the diagrams.

Figure 8(a). $f_N(V)$ for all the galaxies with $m_1 : m_2 = 1 : 5$, $a/a_0 = 7.86$. (b) $f_V(N)$ for all the galaxies with $m_1 : m_2 = 1 : 5$, $a/a_0 = 7.86$.

Figure 9(a). $f_N(V)$ for the less massive galaxies with $m_1 : m_2 = 1 : 5$, $a/a_0 = 7.86$. (b) $f_V(N)$ for the less massive galaxies with $m_1 : m_2 = 1 : 5$, $a/a_0 = 7.86$.

Figure 10(a). $f_N(V)$ for the massive galaxies with $m_1 : m_2 = 1 : 5$, $a/a_0 = 7.86$. (b) $f_V(N)$ for the massive galaxies with $m_1 : m_2 = 1 : 5$, $a/a_0 = 7.86$.

Figure 11. The time evolution of b. The crosses show $b_{ab\ initio}$, which is calculated from equation (3). The circles show the best-fit values for three-dimensional fitting and the filled squares show the best-fit values for two-dimensional fitting. These are for the initially cold $\Omega_0 = 1$, $\Omega_0 = 0.1$, and $\Omega_0 = 0.01$ experiments. The error bars show the dispersion of b.

Figure 12. The time evolution of the gravitational correlation energy W, and the peculiar kinetic energy K for the initially cold cases of $\Omega_0 = 1$, 0.1 and 0.01.

Figure 13(a). The distribution of three-dimensional peculiar velocity for the initially cold cases with $\Omega_0 = 1$ at the epoch of $a/a_0 = 2.8$, $\Omega_0 = 1$ at the epoch of $a/a_0 = 7.86$, $\Omega_0 = 0.1$ at the epoch of $a/a_0 = 31.06$ and $\Omega_0 = 0.01$ at the epoch of $a/a_0 = 31.06$. Dashed curves are the Maxwell-Boltzmann distributions with the same velocity dispersions as the simulations. (b) The distribution of radial peculiar velocity for the initially cold cases with $\Omega_0 = 1$ at the epoch of $a/a_0 = 7.86$, $\Omega_0 = 0.1$ at $a/a_0 = 31.06$ and $\Omega_0 = 0.01$ at $a/a_0 = 31.06$. Dashed curves are the Gaussian distributions with the same velocity dispersions.

Figure 14. The time evolution of b for systems with the hot initial condition for the cases $\Omega_0 = 1$ and $\Omega_0 = 0.1$.

Figure 15(a). Time evolution of b for $m_1 : m_2 = 1 : 1$. (b) The same for $m_1 : m_2 = 1 : 2$. (c) The same for $m_1 : m_2 = 1 : 3$. (d) The same for $m_1 : m_2 = 1 : 4$. (e) The same for $m_1 : m_2 = 1 : 5$.

Figure 16(a). Time evolution of $b_i - b'$ for the massive galaxies, where $i \equiv m_2/m_1$. (b) The same for the less massive galaxies.

Figure 17. Time evolution of T_2/T_1.

Figure 18. The distribution for galaxies and identified clusters indicated by small circles with $m_1 : m_2 = 1 : 1$, $a/a_0 = 7.86$.

Figure 19. The distribution for galaxies of one cluster with $m_1 : m_2 = 1 : 1$, $a/a_0 = 7.86$.

Figure 20(a). Projected positions for all the galaxies with $m_1 : m_2 = 1 : 100$, $a/a_0 = 7.86$. (b) Projected positions for the less massive galaxies. (c) Projected positions for the massive

galaxies.

Figure 21(a). Two-point correlation functions for all the galaxies with $m_1 : m_2 = 1 : 100$, $a/a_0 = 1.41 \sim 7.86$. (b) Two-point correlation functions for the less massive and massive galaxies.

Figure 22(a). $f_N(V)$ for all the galaxies with $m_1 : m_2 = 1 : 100$, $a/a_0 = 7.86$. (b) $f_V(N)$ for all the galaxies with $m_1 : m_2 = 1 : 100$, $a/a_0 = 7.86$.

Figure 23(a). $f_N(V)$ for the less massive galaxies with $m_1 : m_2 = 1 : 100$, $a/a_0 = 7.86$. (b) $f_V(N)$ for the less massive galaxies with $m_1 : m_2 = 1 : 100$, $a/a_0 = 7.86$.

Figure 24(a). $f_N(V)$ for the massive galaxies with $m_1 : m_2 = 1 : 100$, $a/a_0 = 7.86$. (b) $f_V(N)$ for the massive galaxies with $m_1 : m_2 = 1 : 100$, $a/a_0 = 7.86$.

Figure 25. Values of b_{fit} for $f_N(V)$ and $f_V(N)$ for projected distributions in cold, warm, and hot $\Omega_0 = 1$ simulations.

Figure 26(a). The scale dependence of $b_i(r) - b'(r)$ for the massive galaxies at $a/a_0 = 7.86$. (b) The same at $a/a_0 = 15.62$.
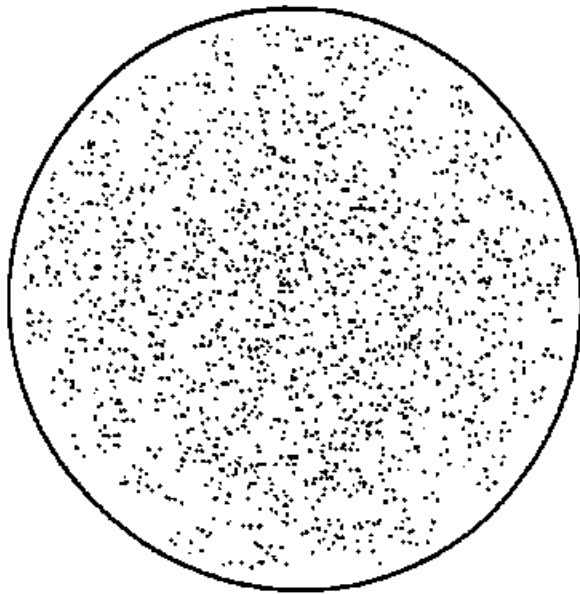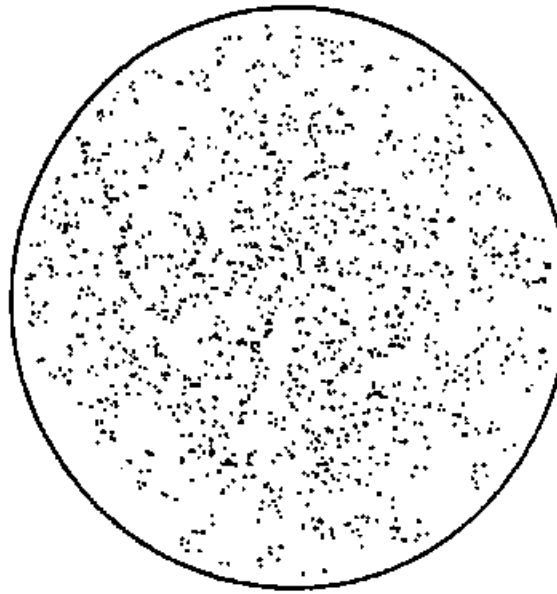
$a/a_0 = 1.00 \quad 0.0 < R < 1.0$ $a/a_0 = 2.80 \quad 0.0 < R < 1.0$ $a/a_0 = 7.86 \quad 0.0 < R < 1.0$
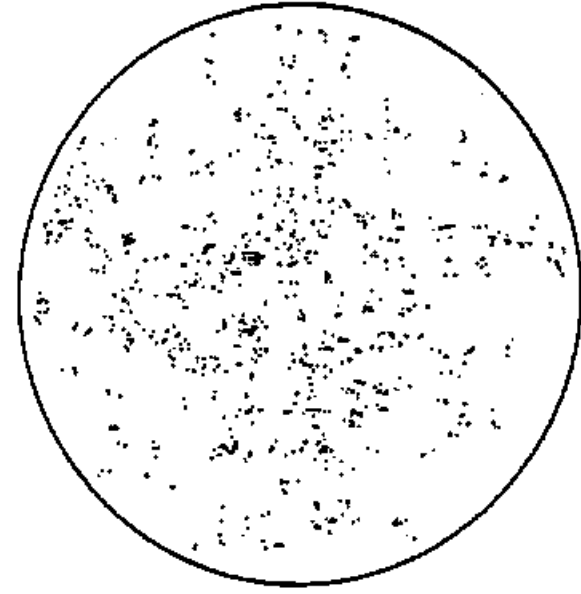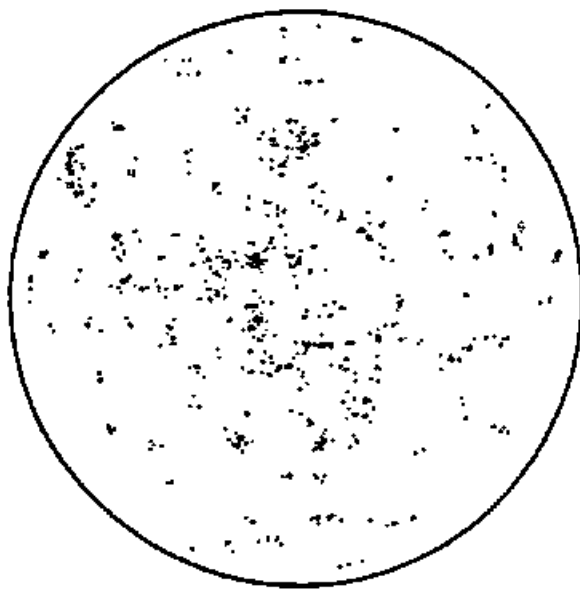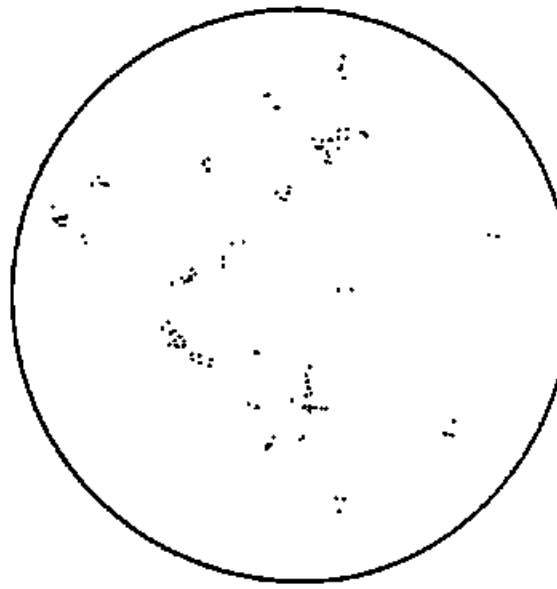
$a/a_0 = 15.62 \quad 0.0 < R < 1.0$ $a/a_0 = 7.86 \quad 0.0 < R < 0.5$ $a/a_0 = 7.86 \quad 0.9 < R < 1.0$
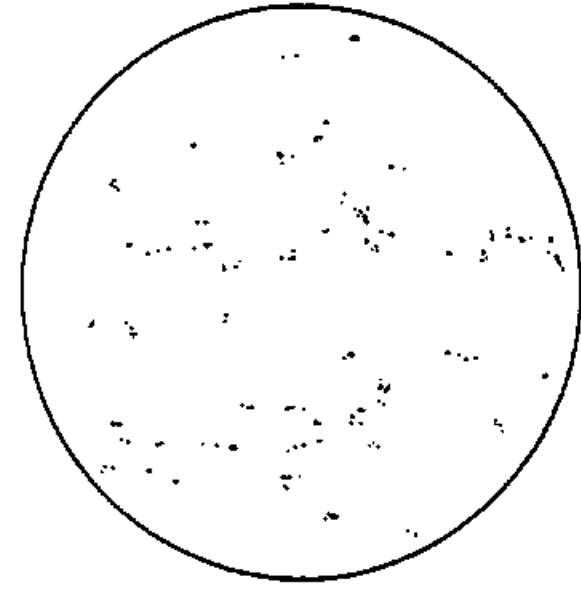
Figure 1
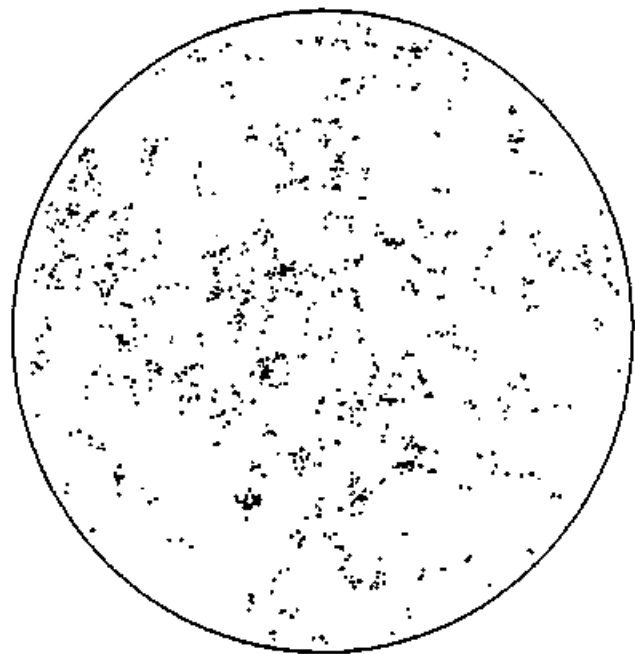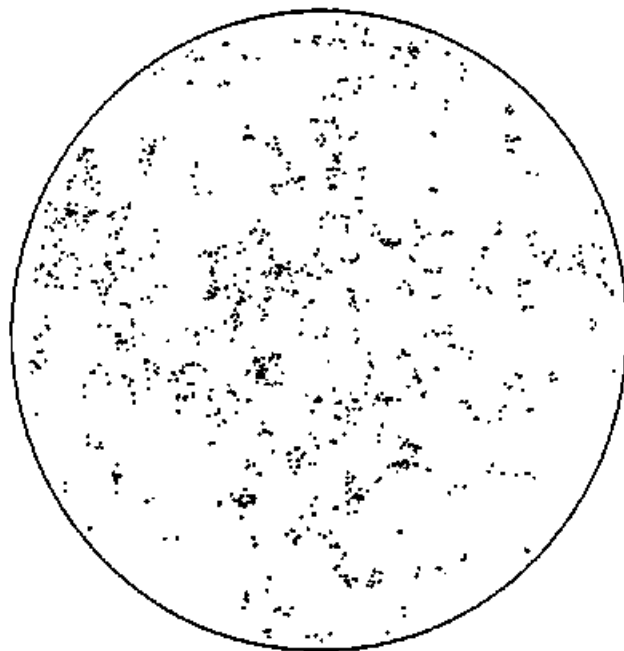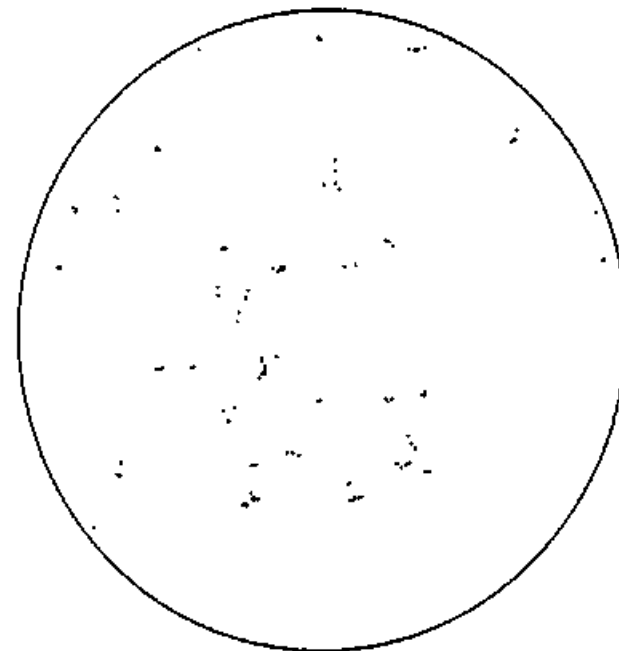
Figure 2(a)   Figure 2(b)   Figure 2(c)
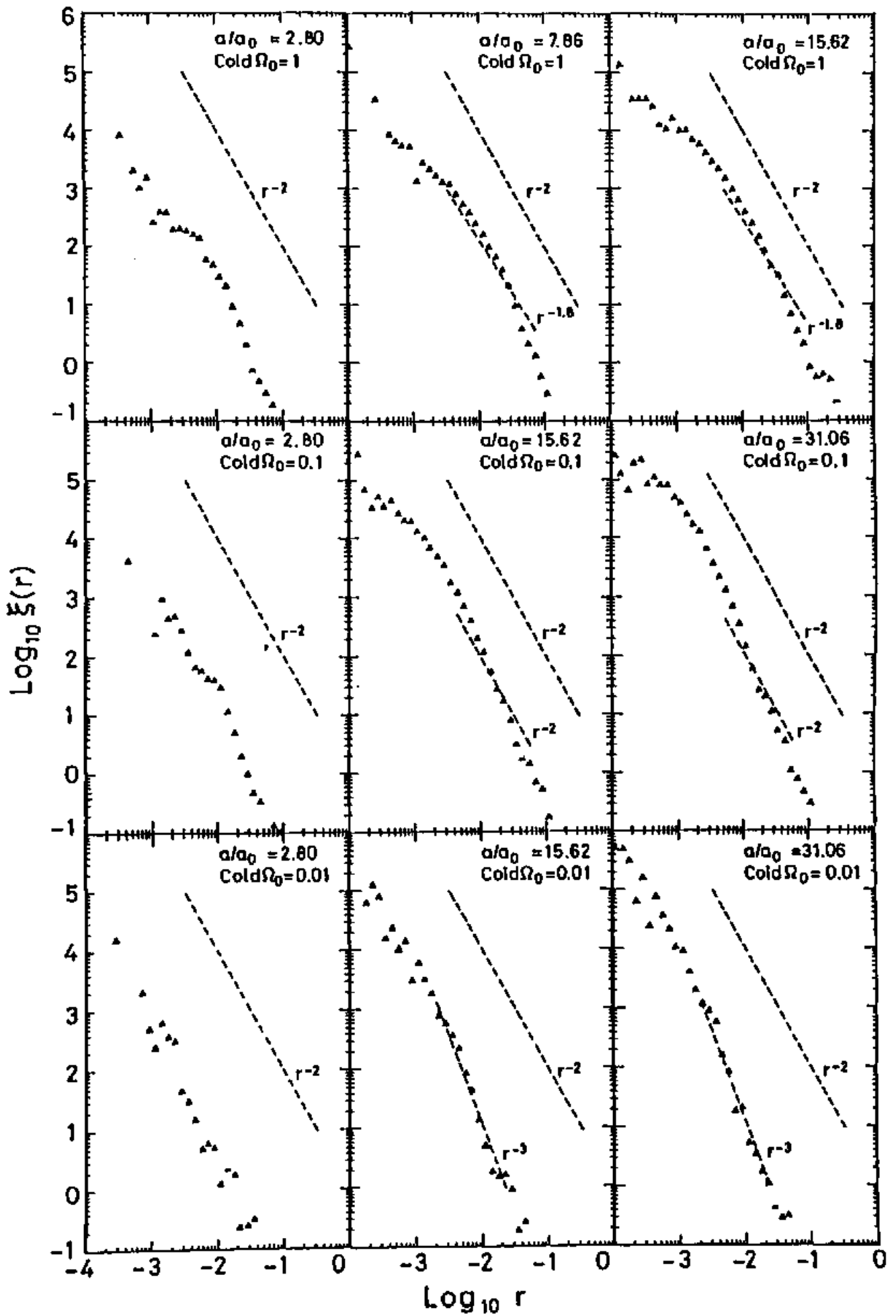
Figure 3
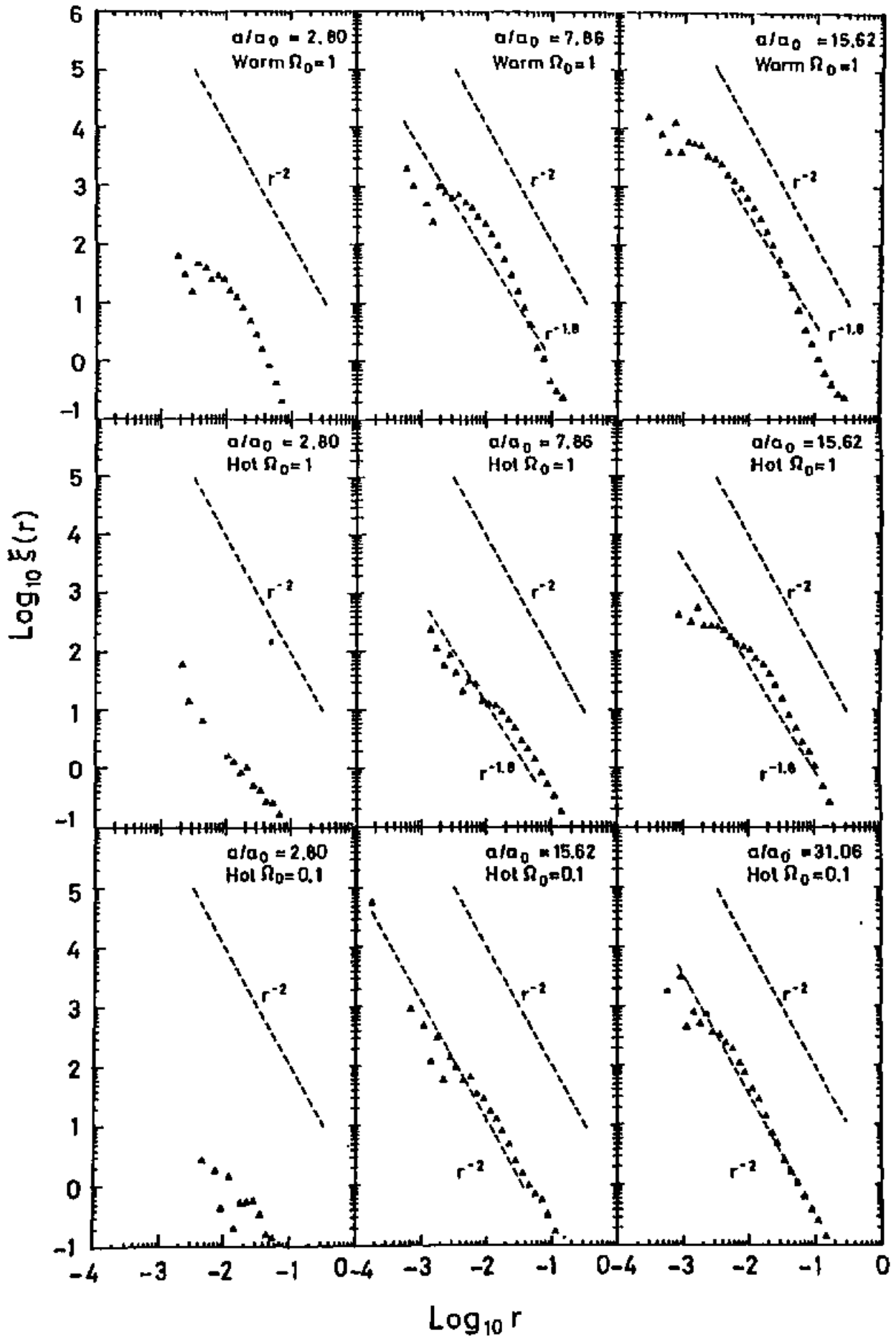
Figure 4
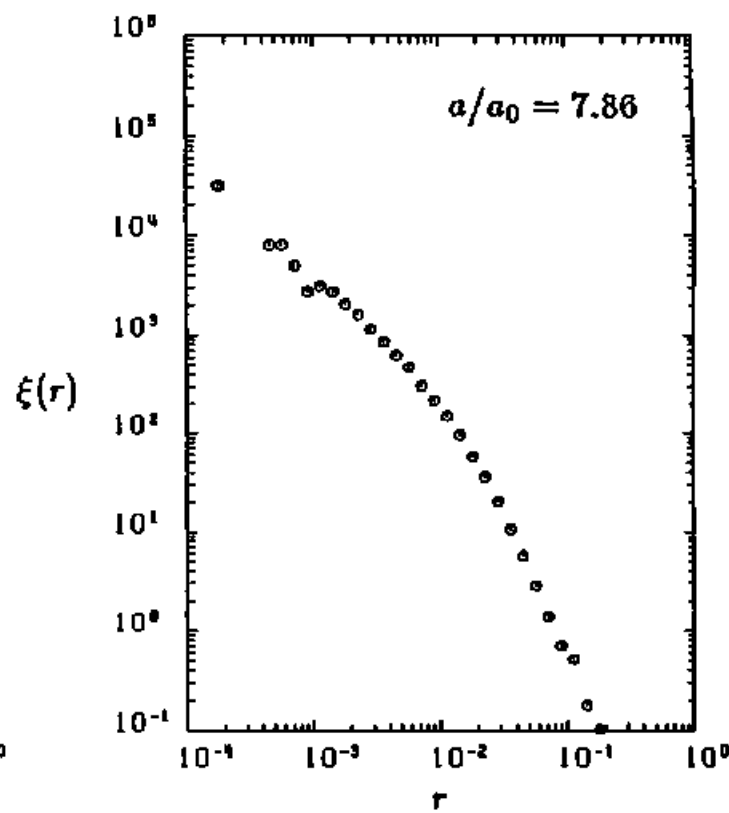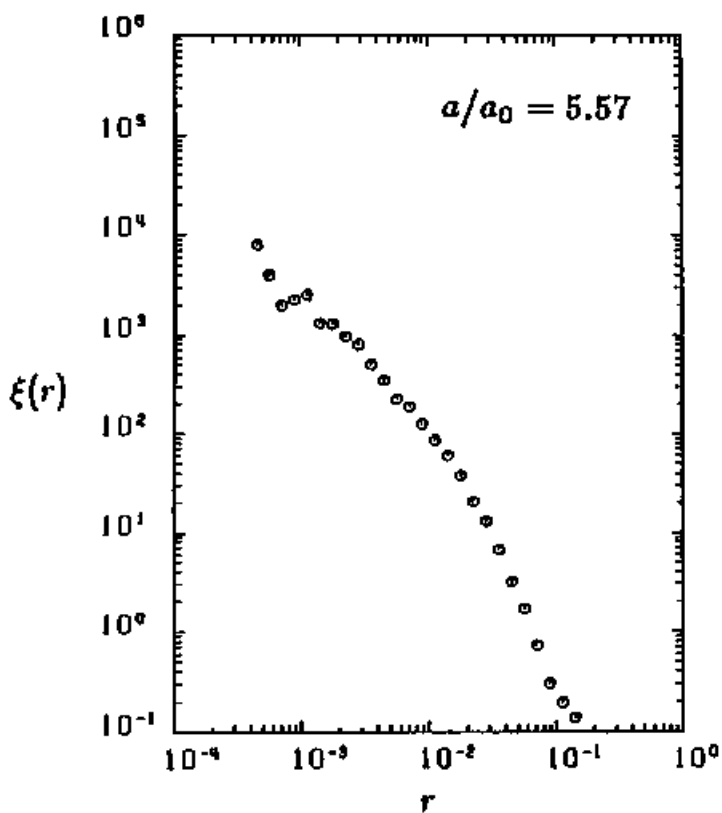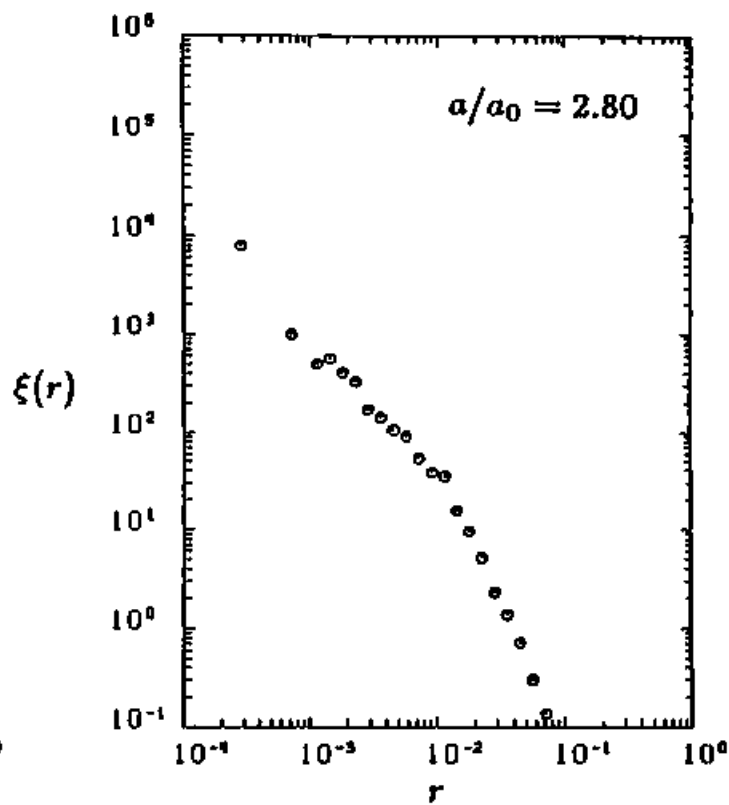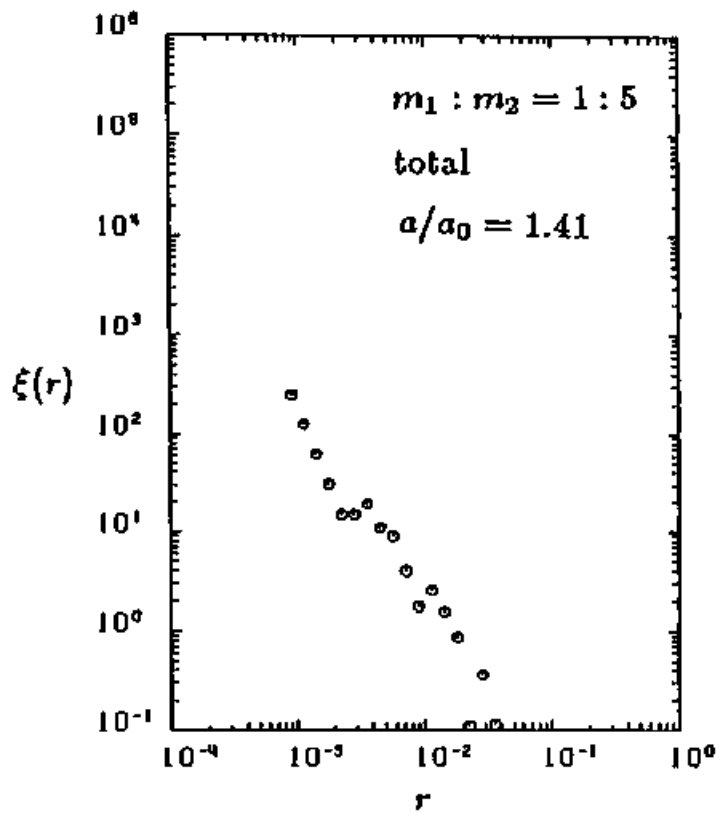
Figure 5(a)
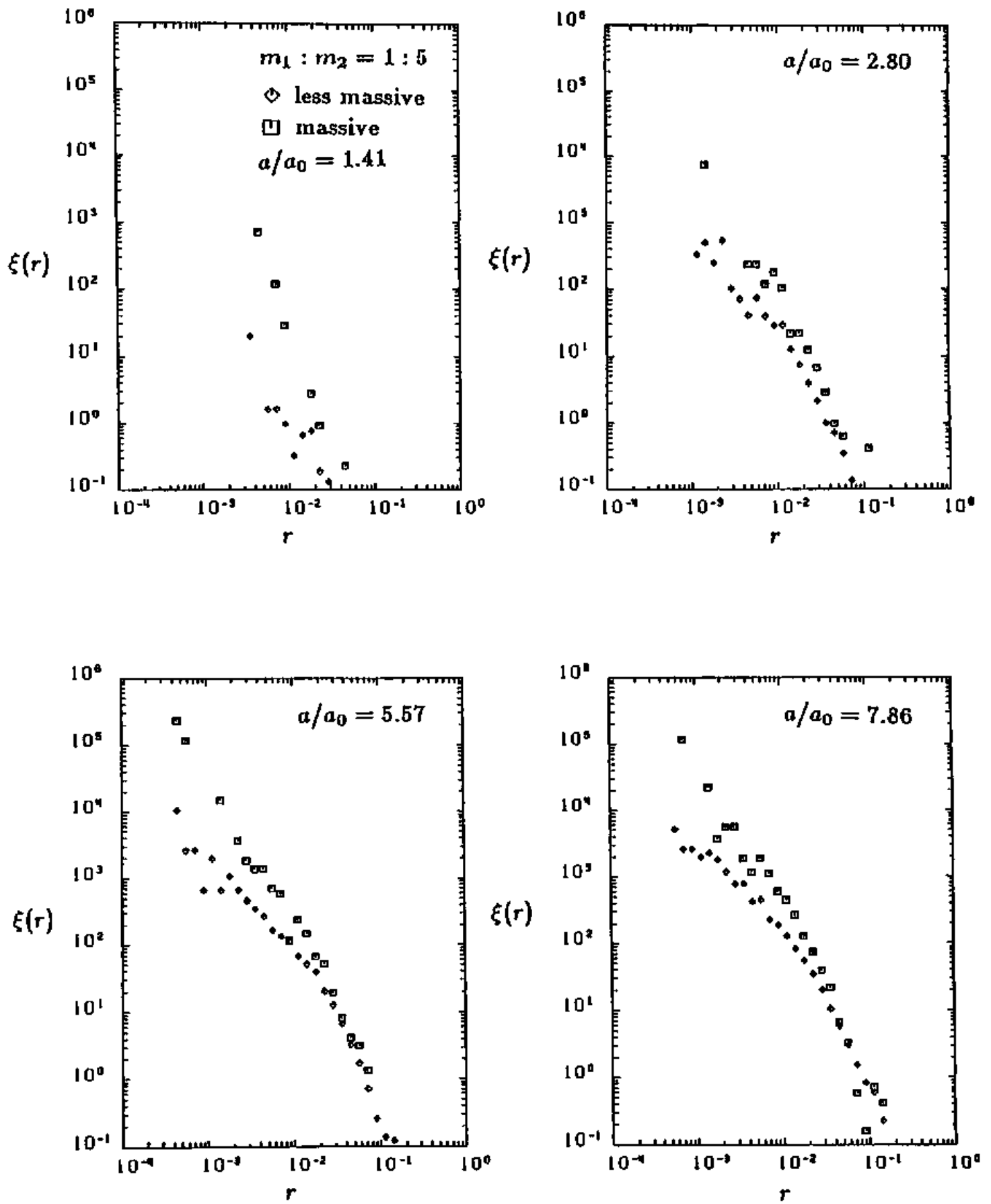
Figure 5(b)
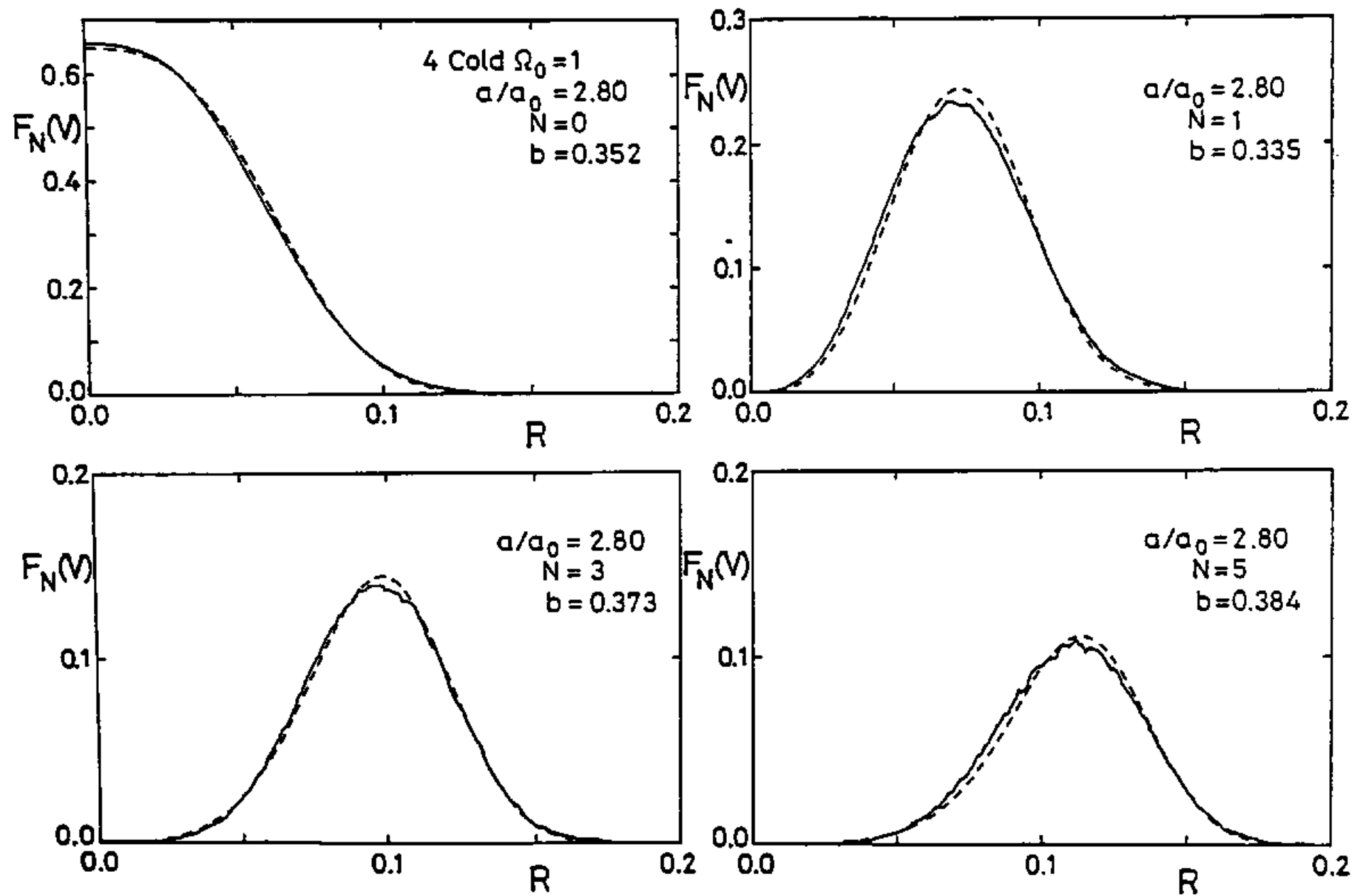
Figure 6
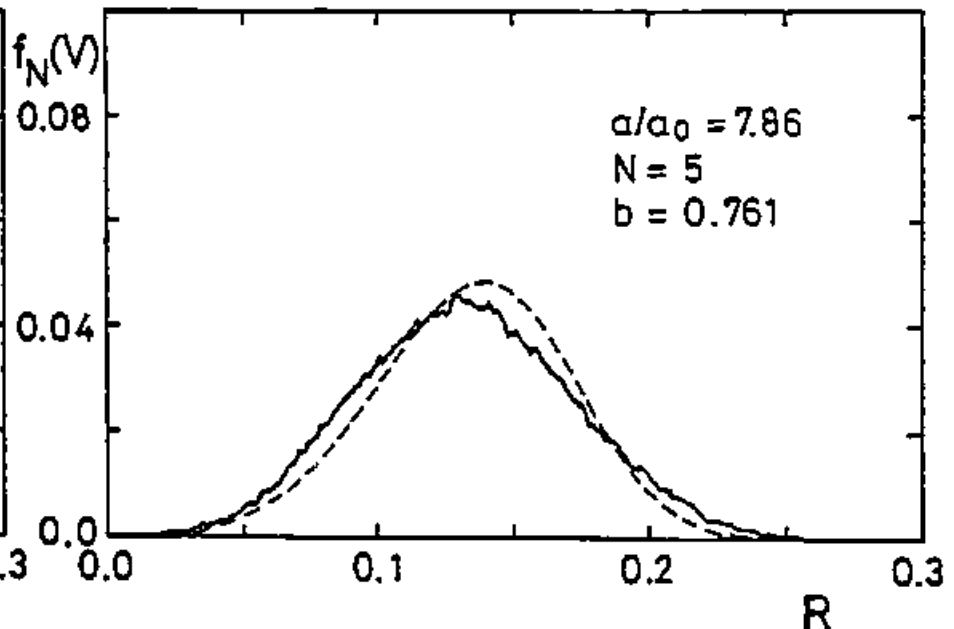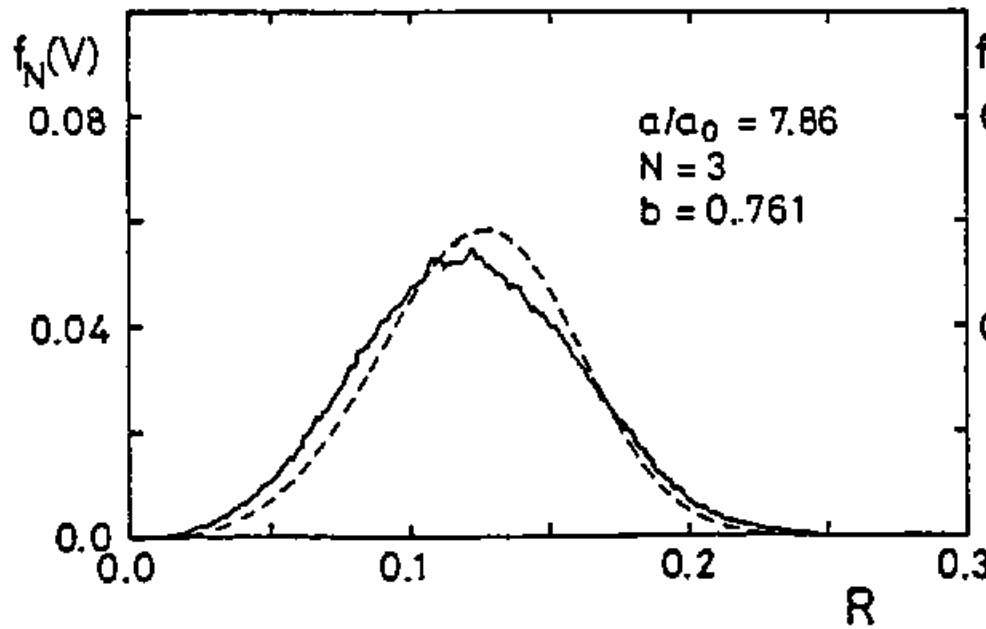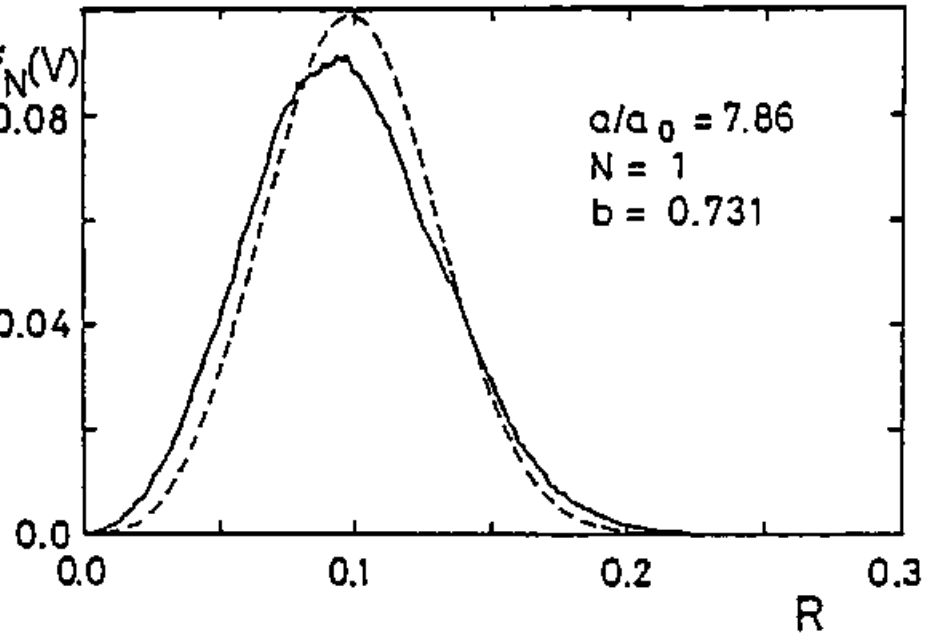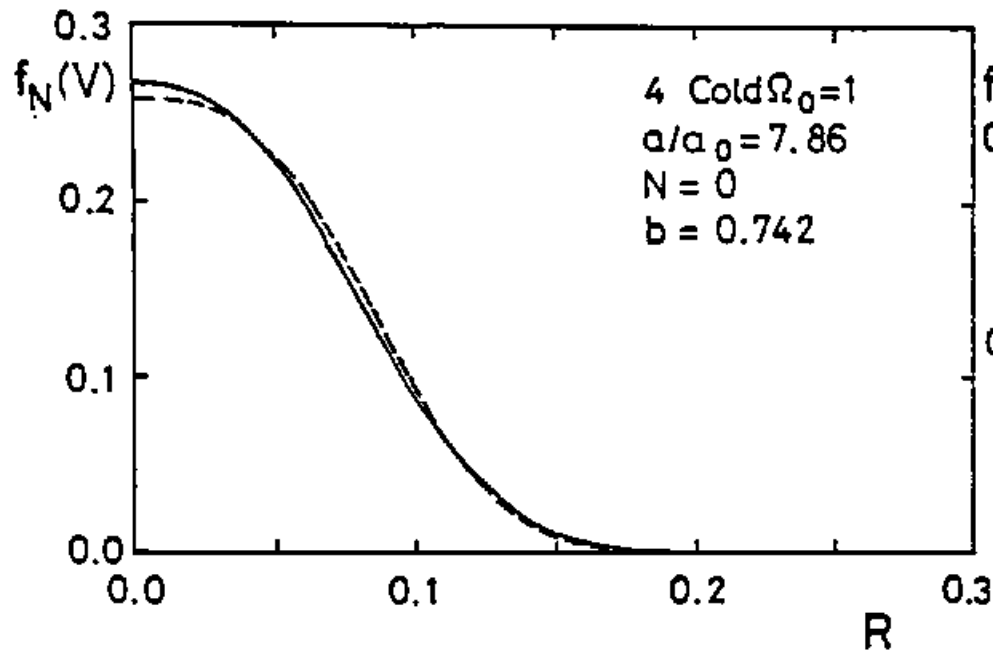
Figure 6–Continued
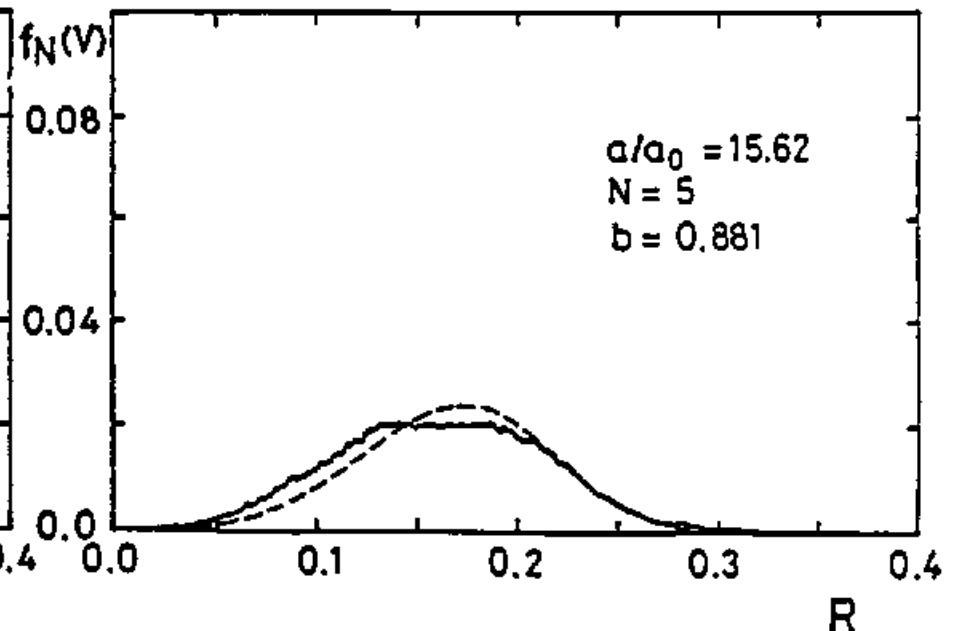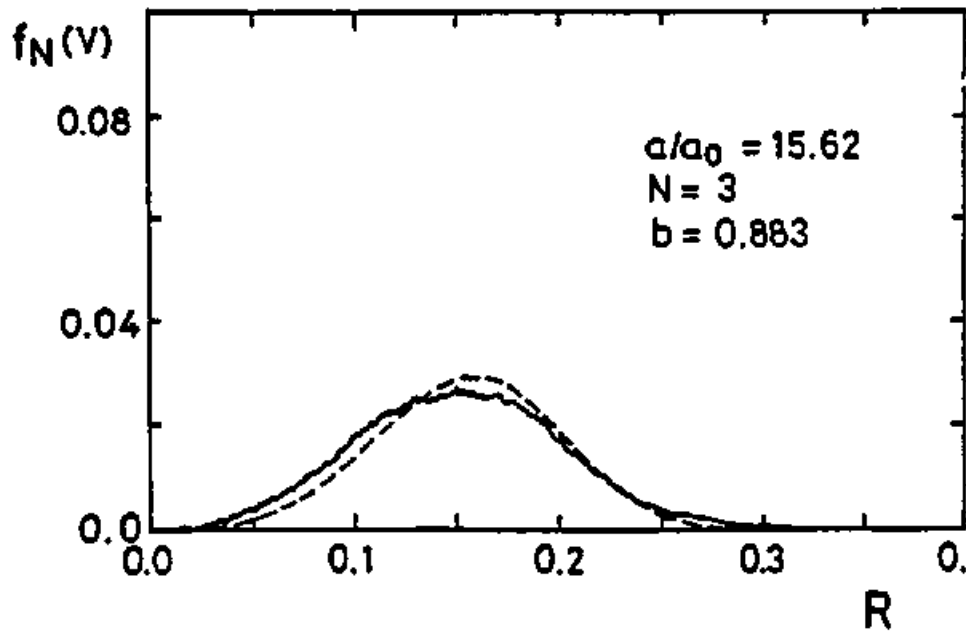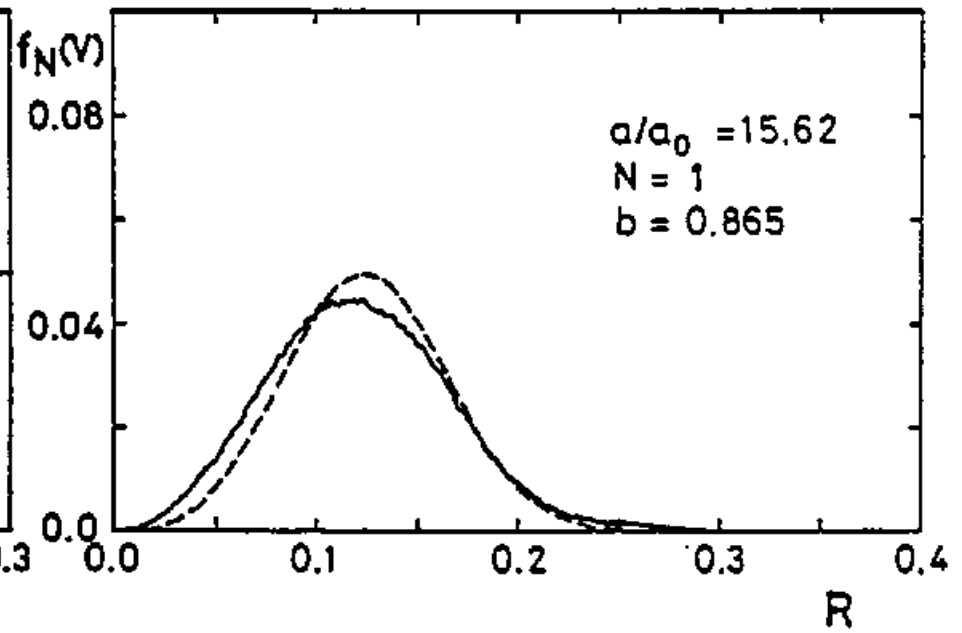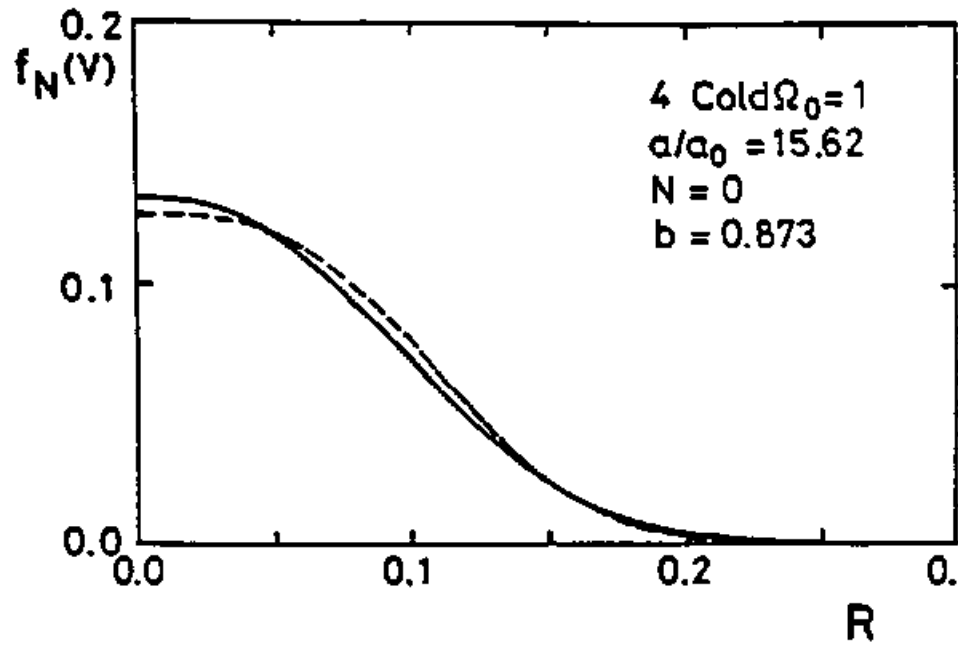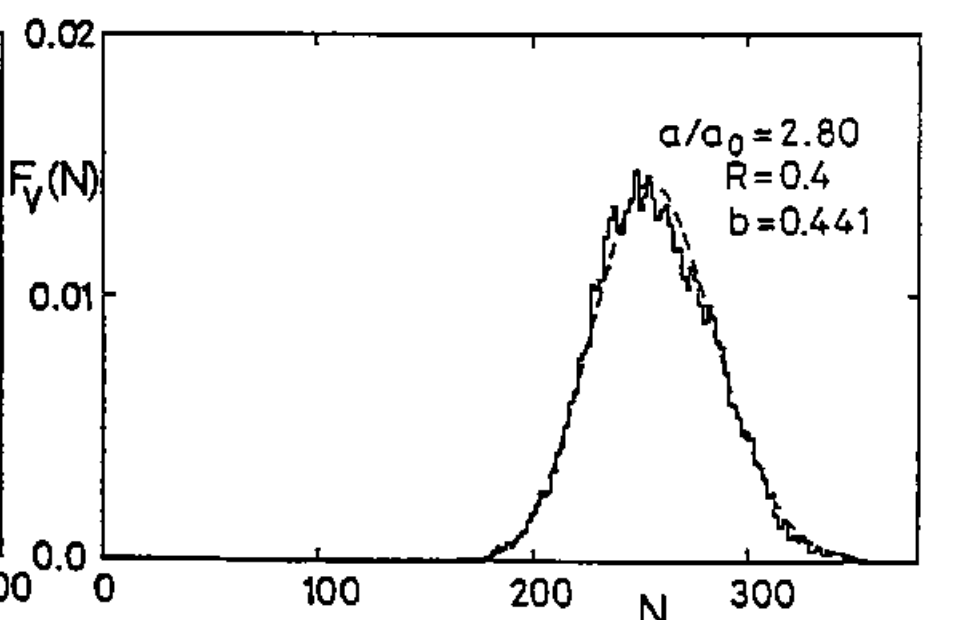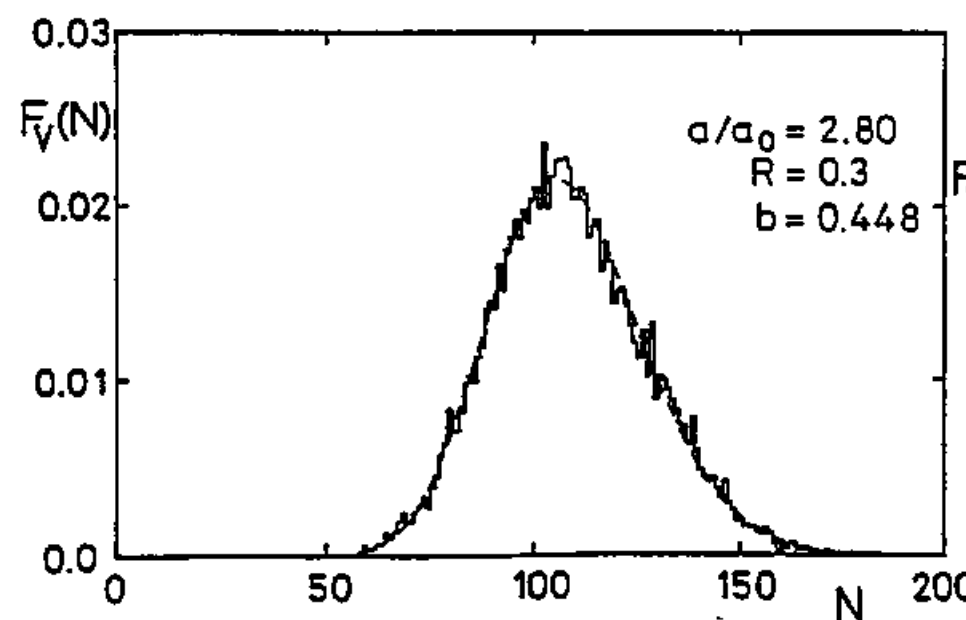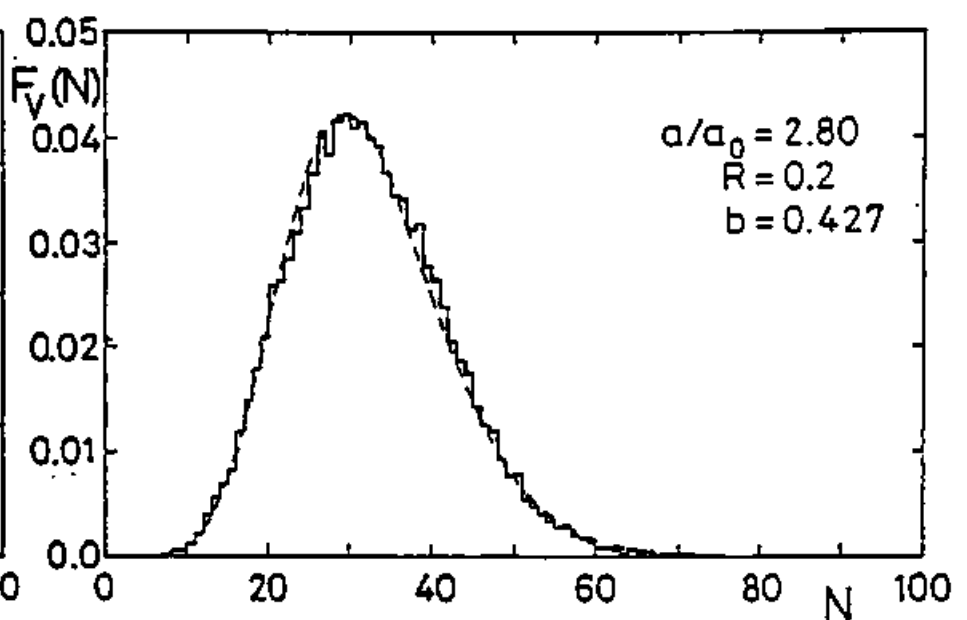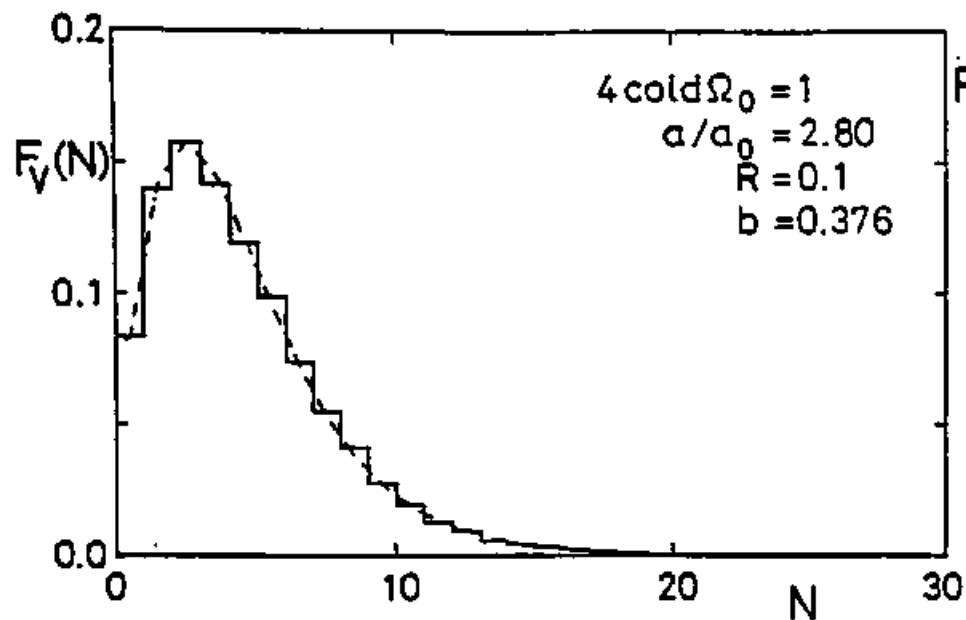
Figure 6–Continued
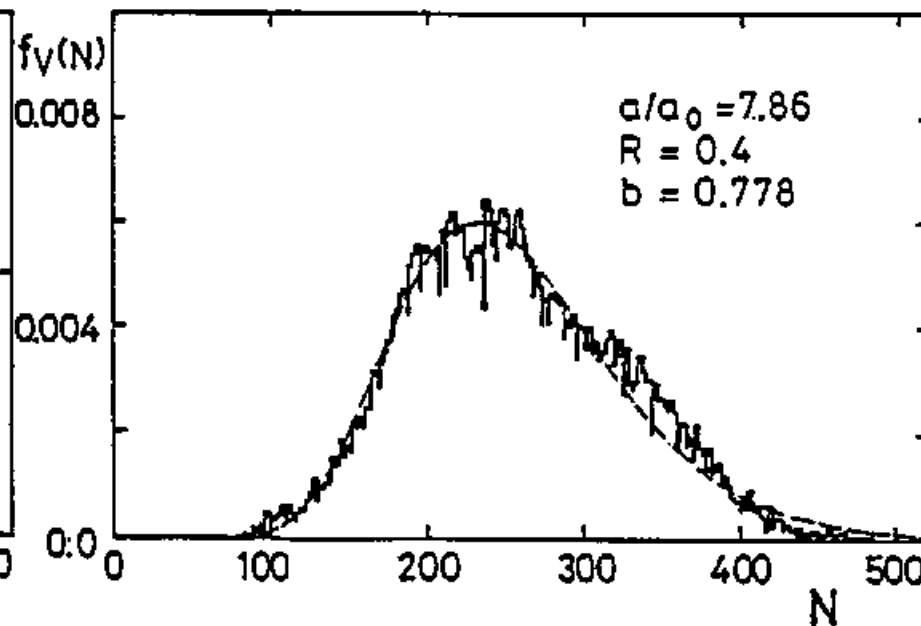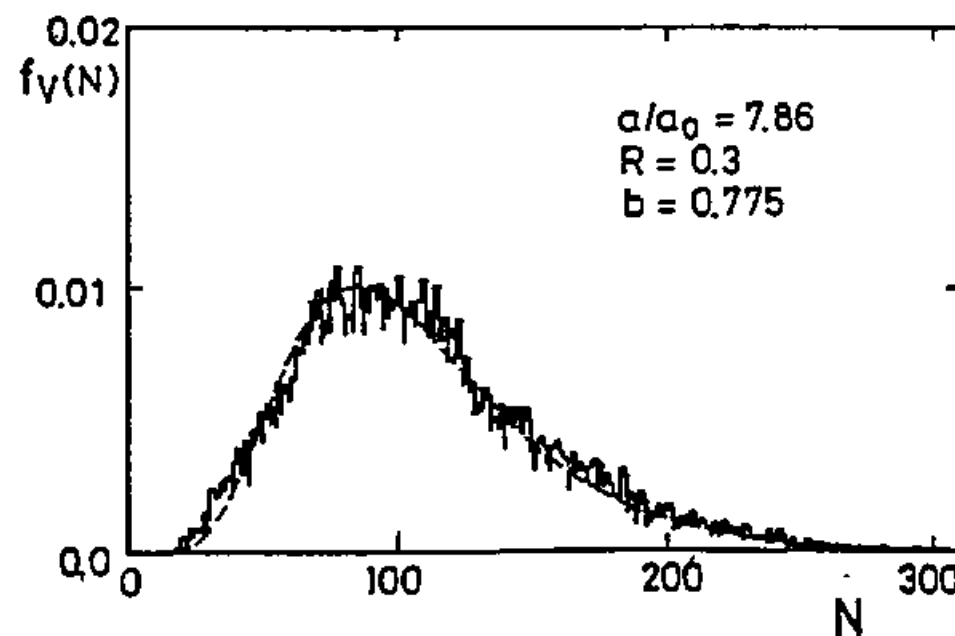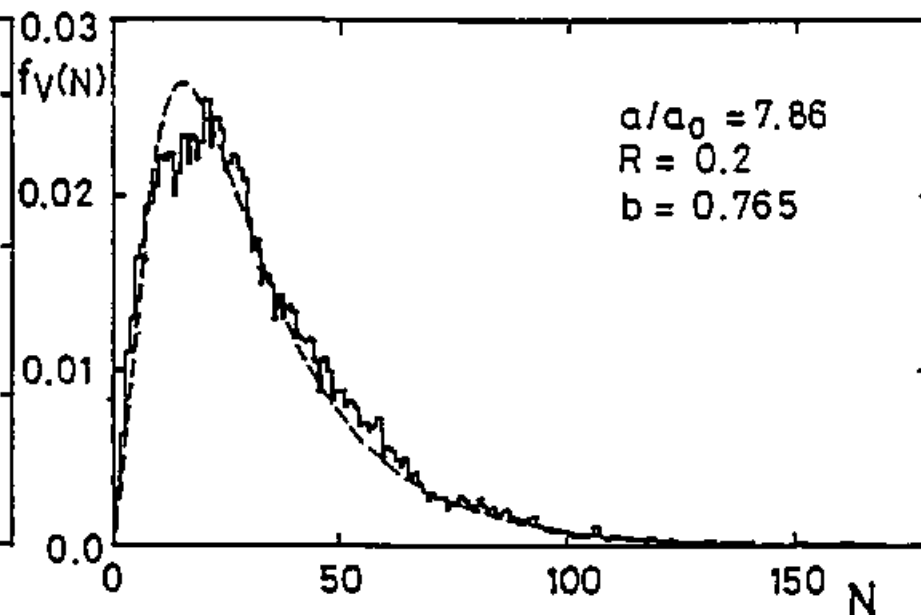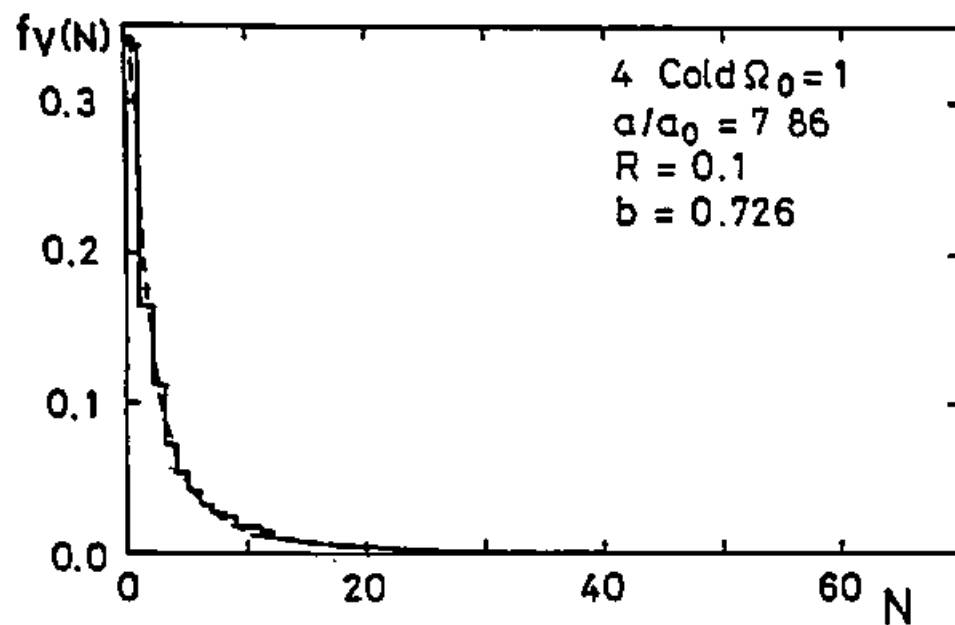
Figure 6–Continued
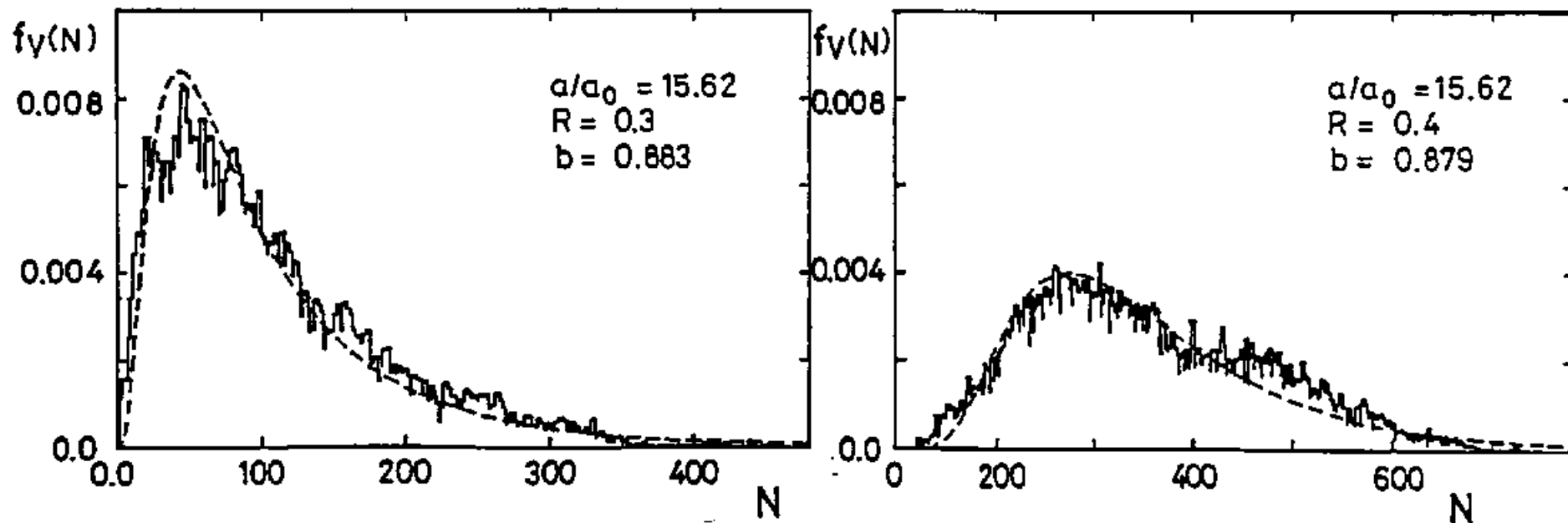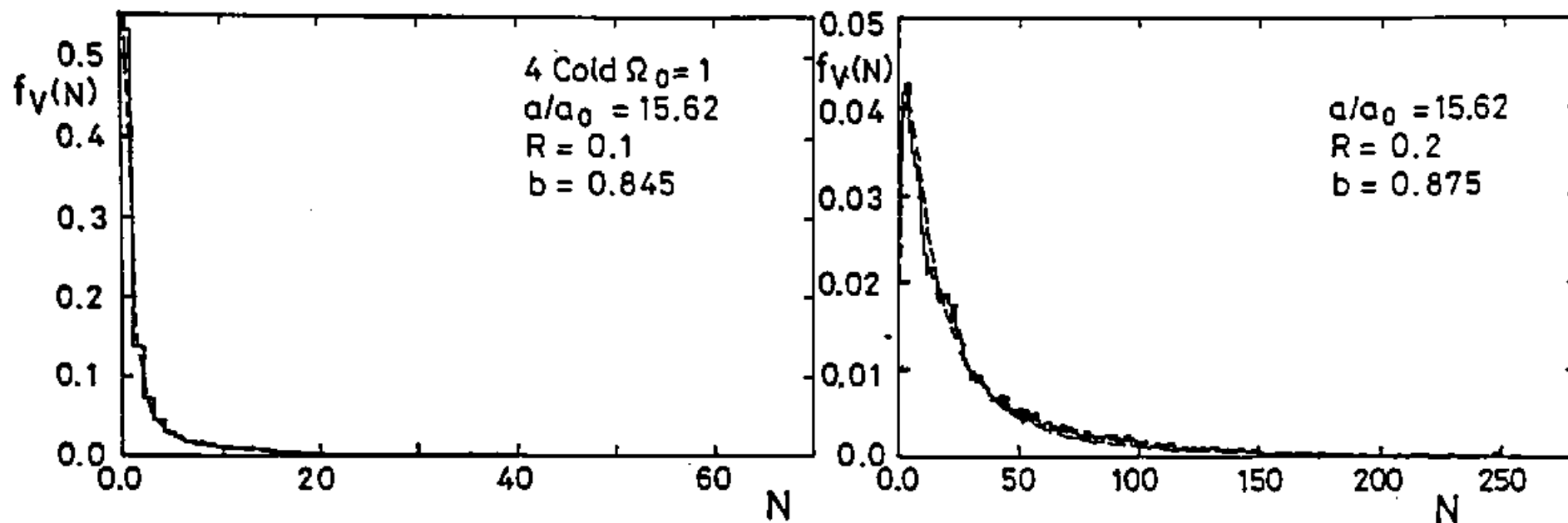
Figure 6–Continued
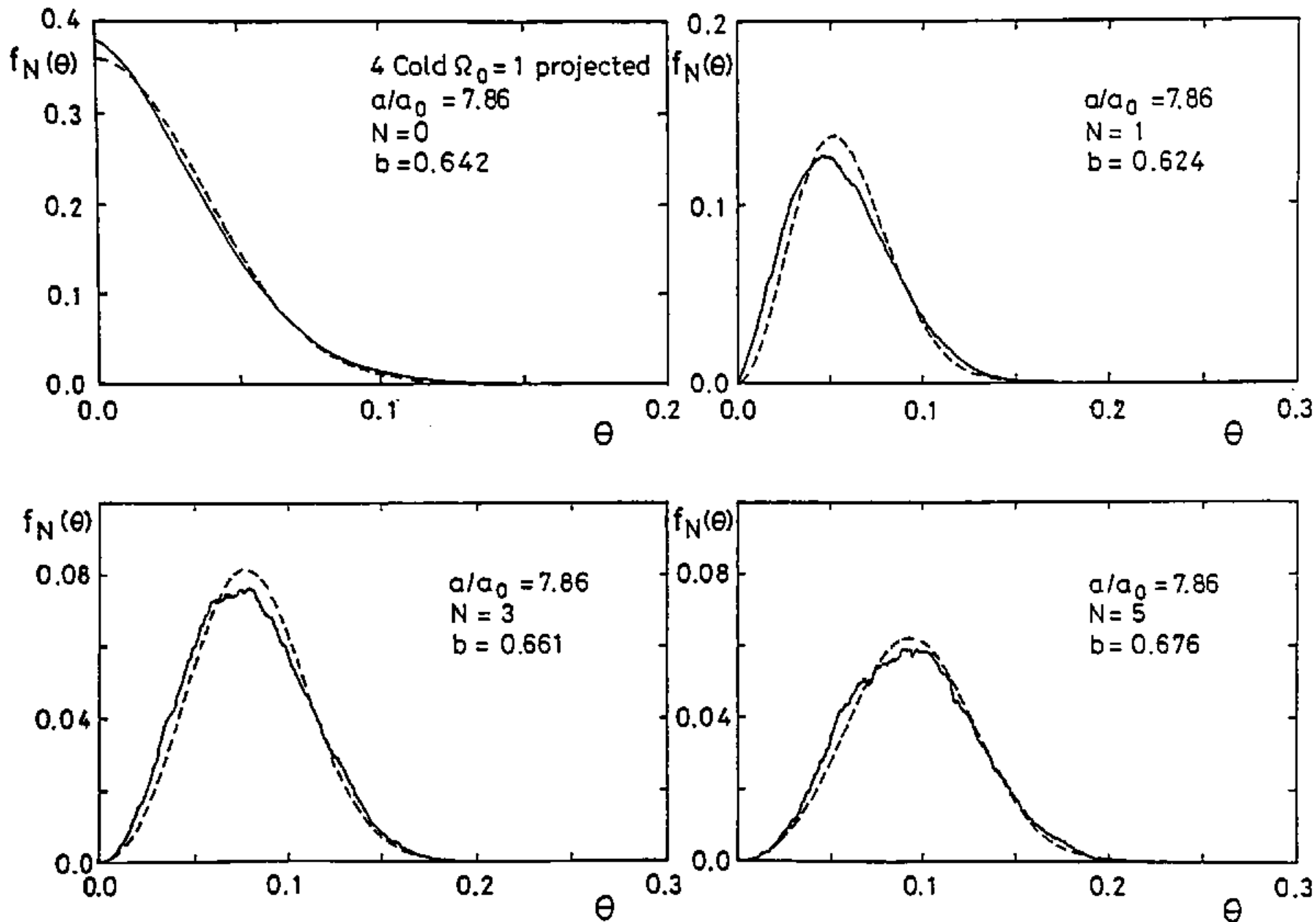
Figure 6–Continued

Figure 7
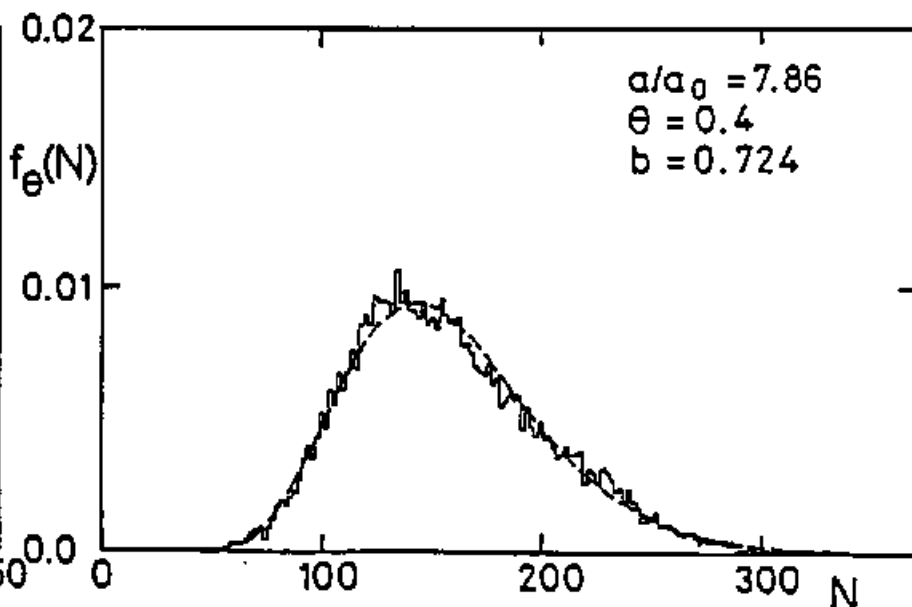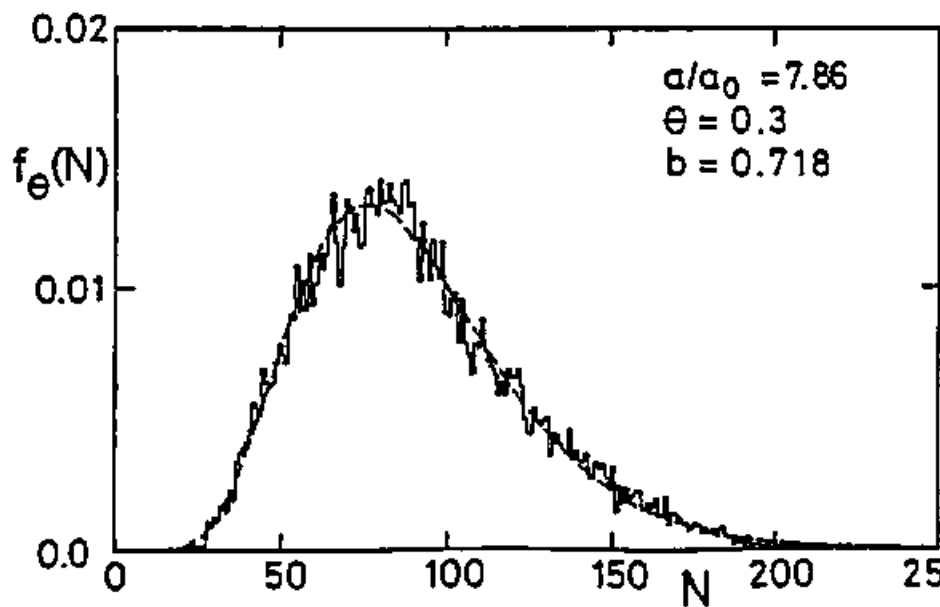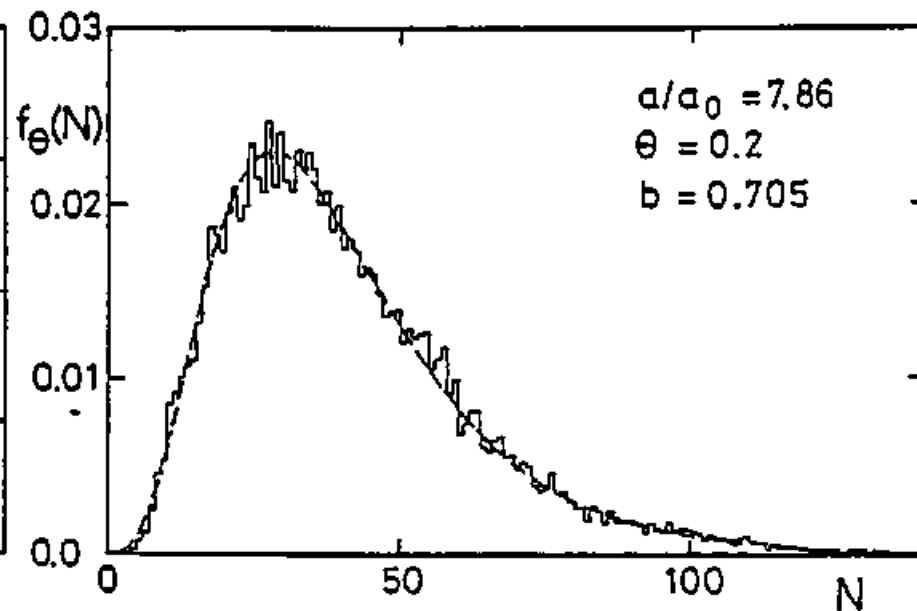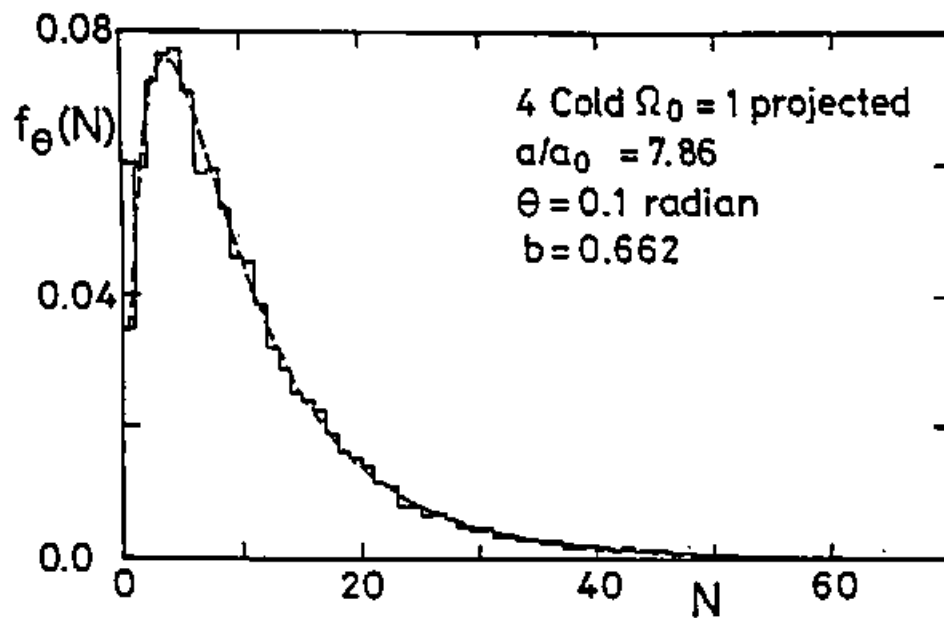
Figure 7–Continued
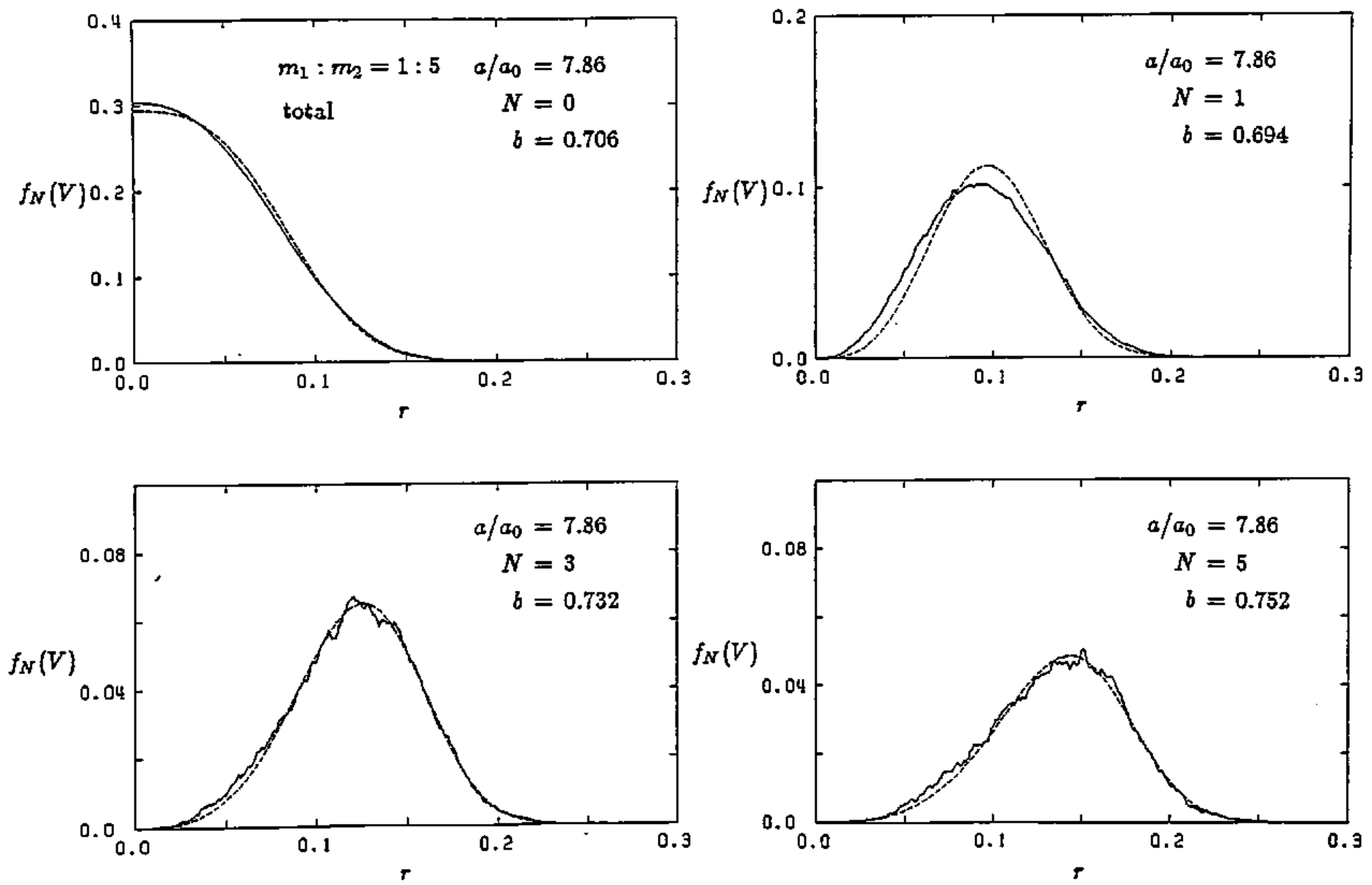
Figure 8(a)
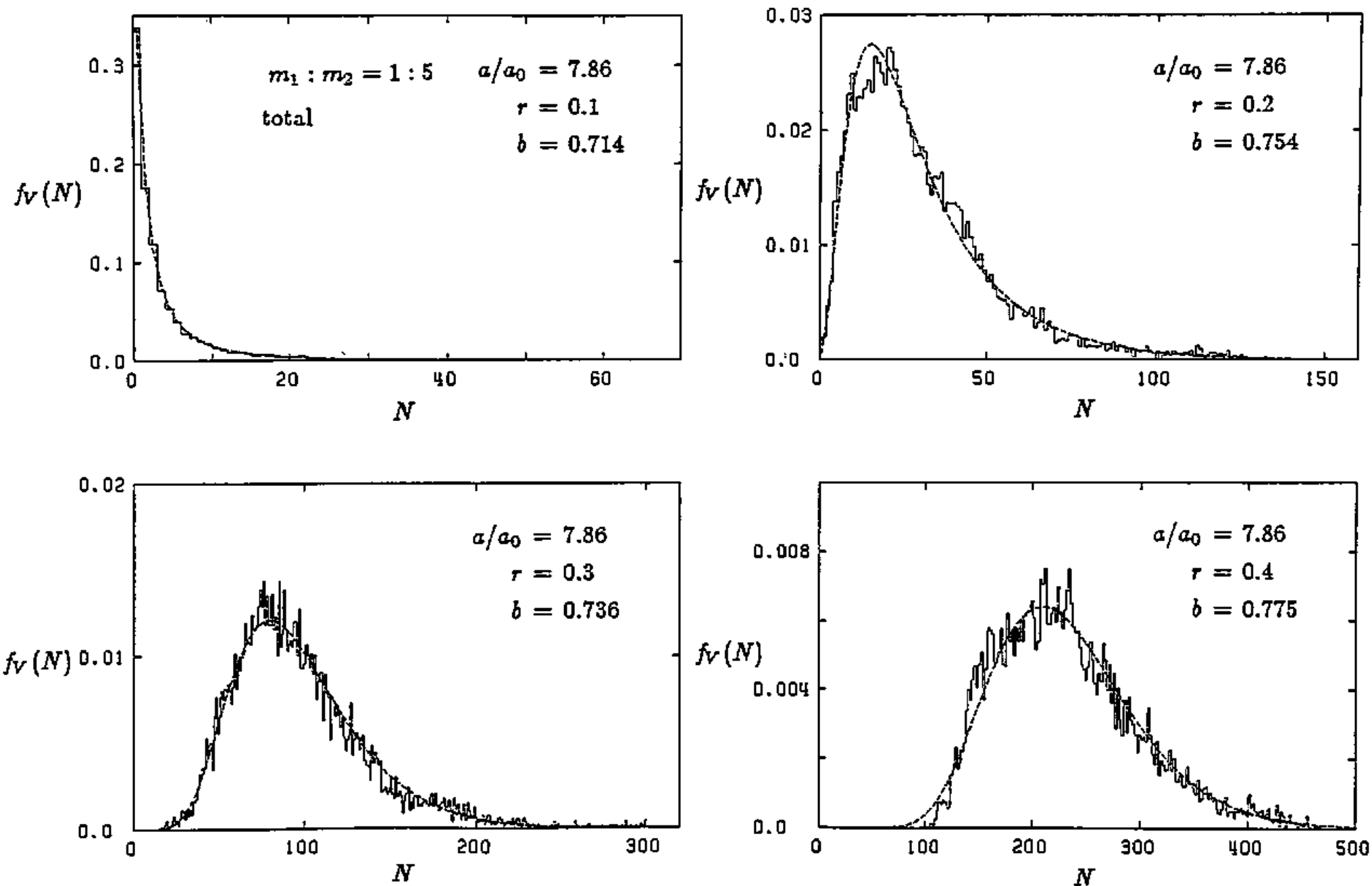
Figure 8(b)
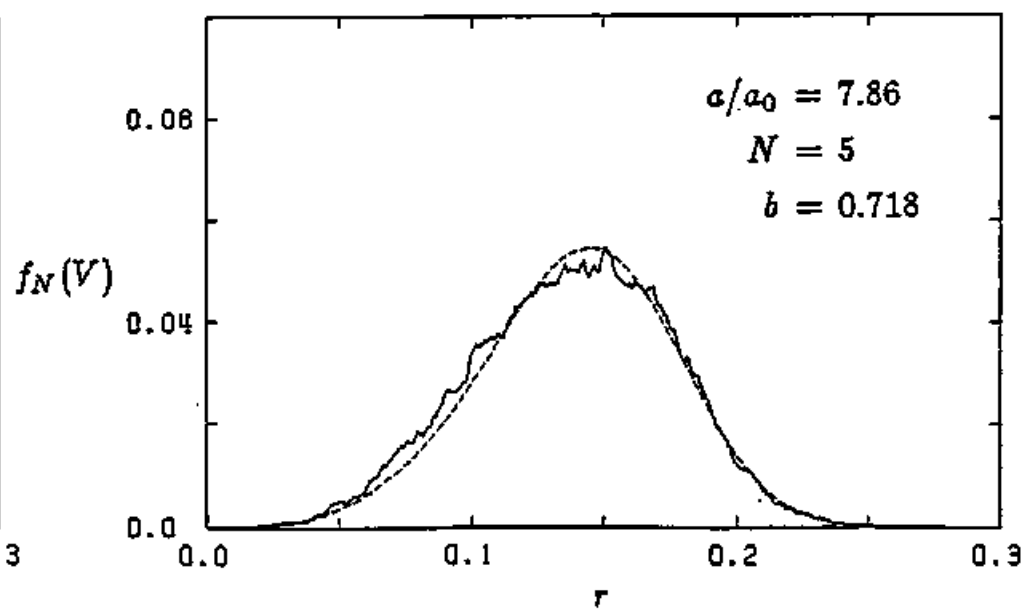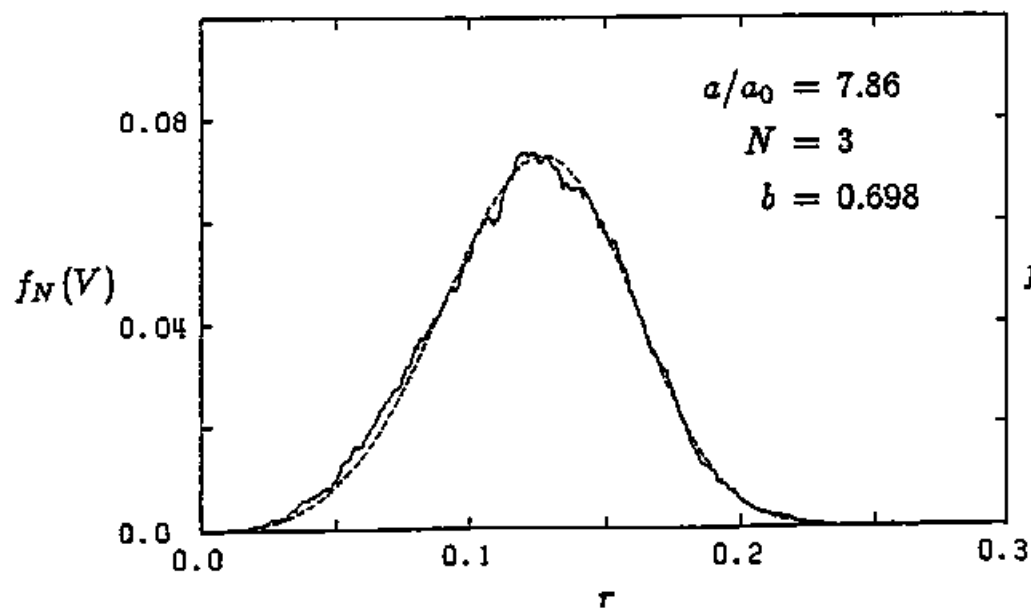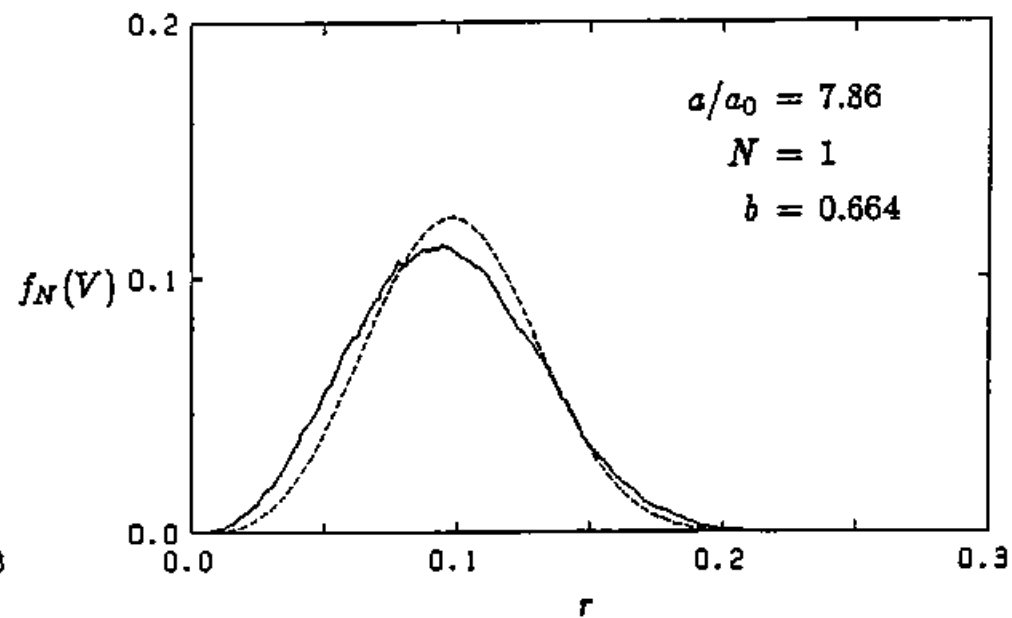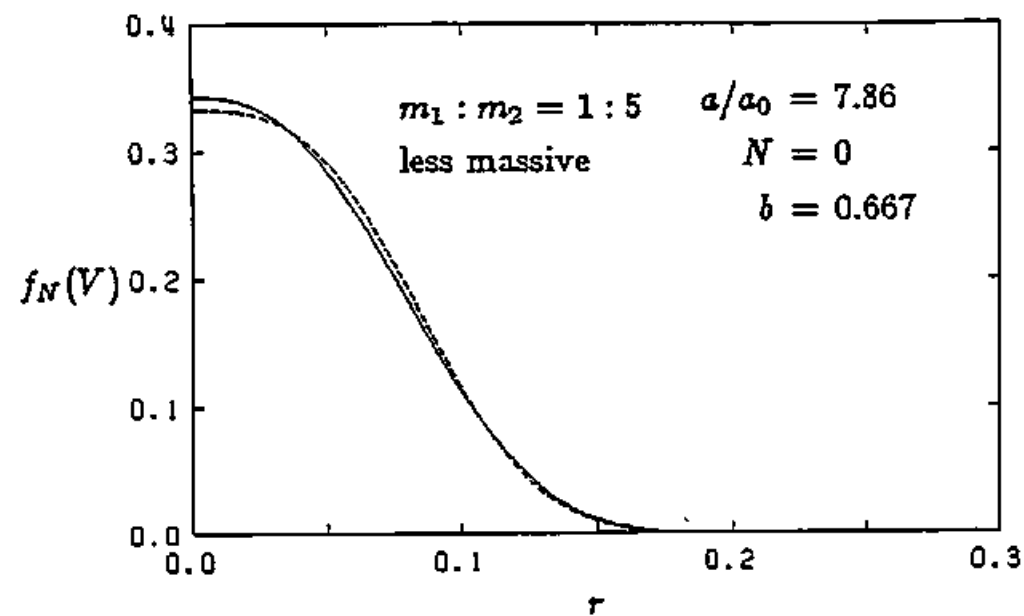
Figure 9(a)
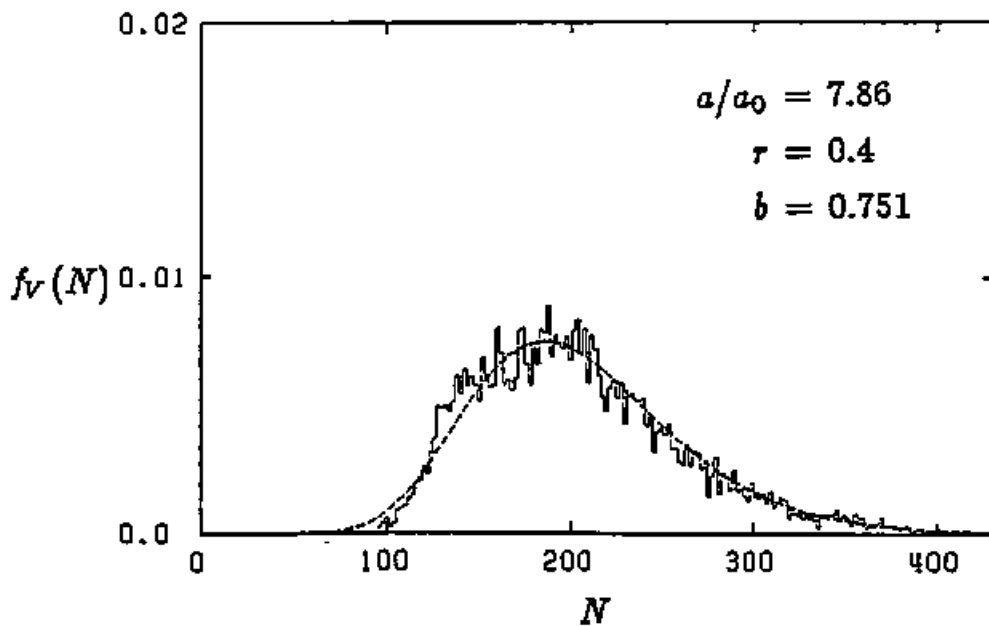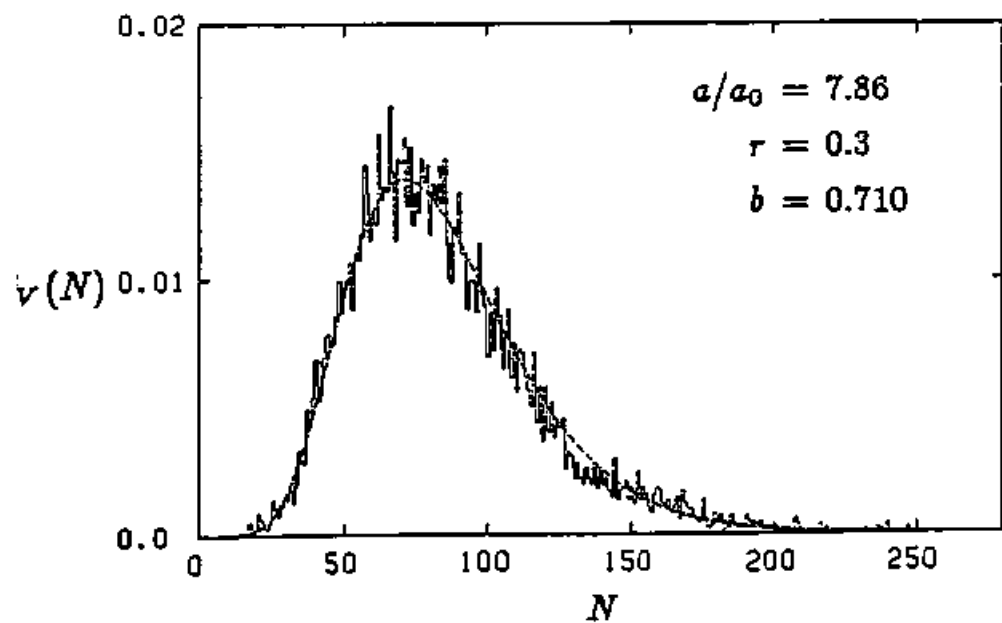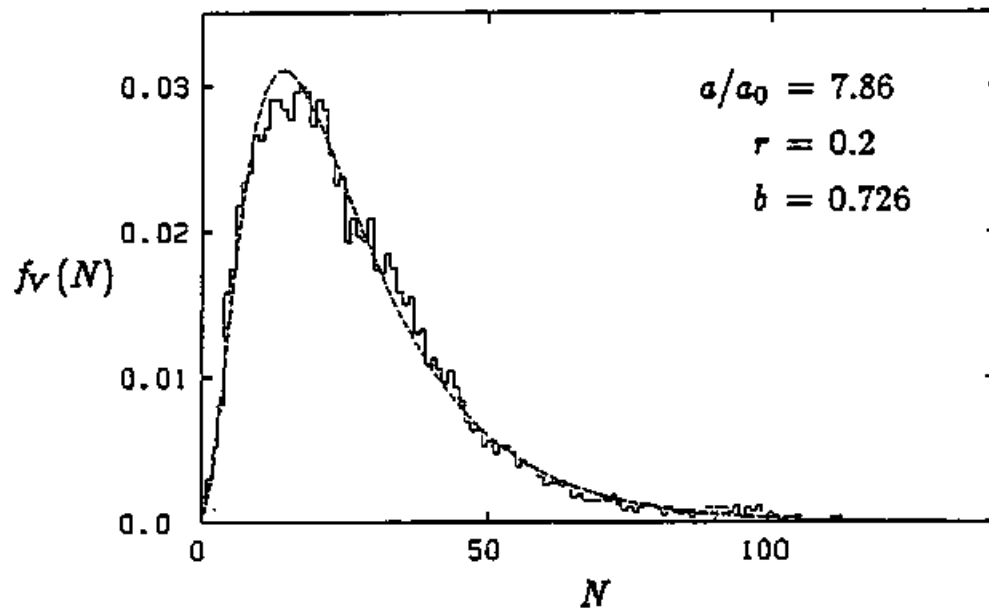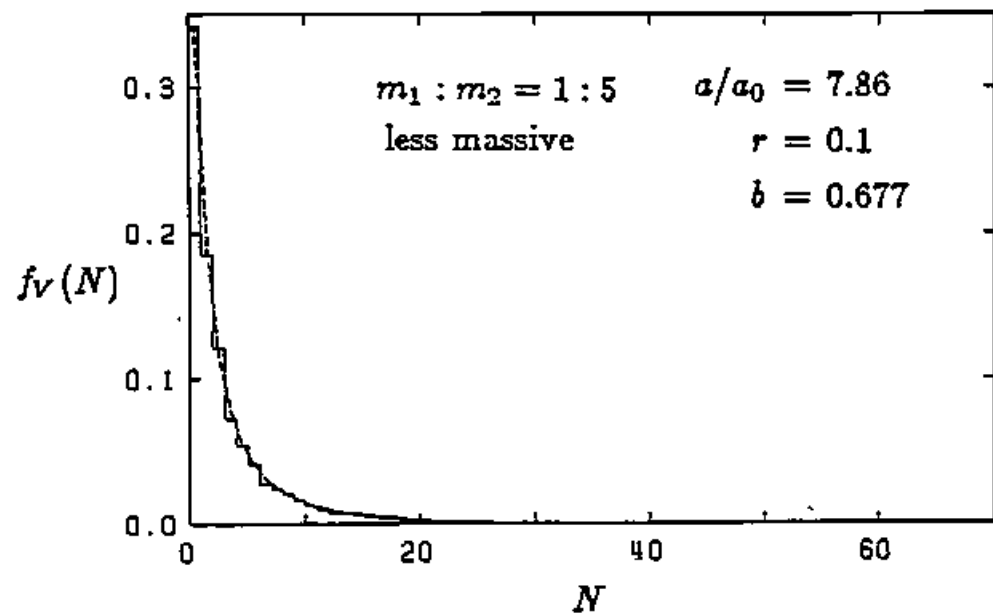
Figure 9(b)
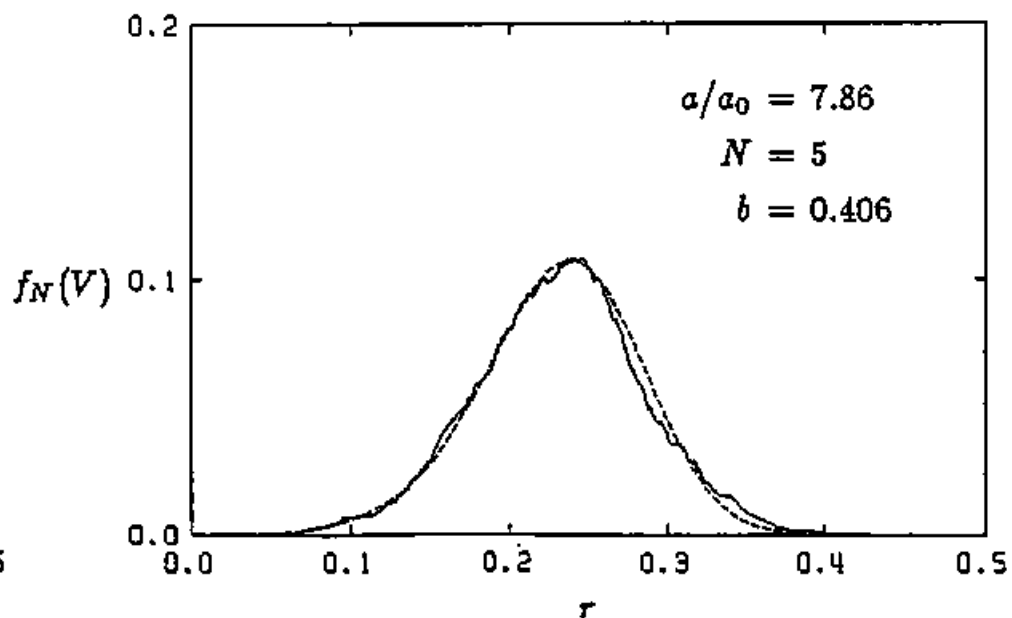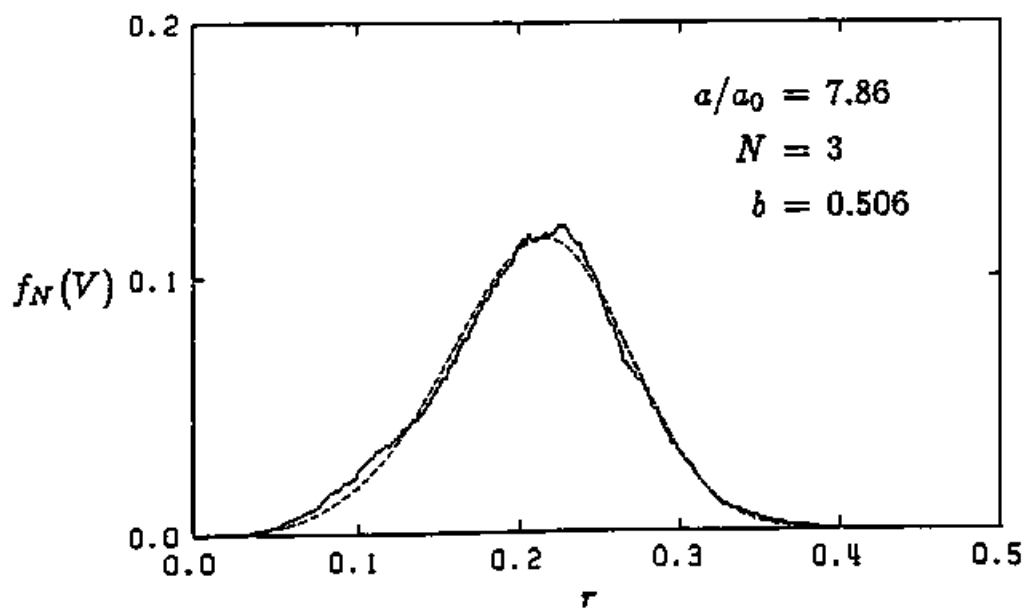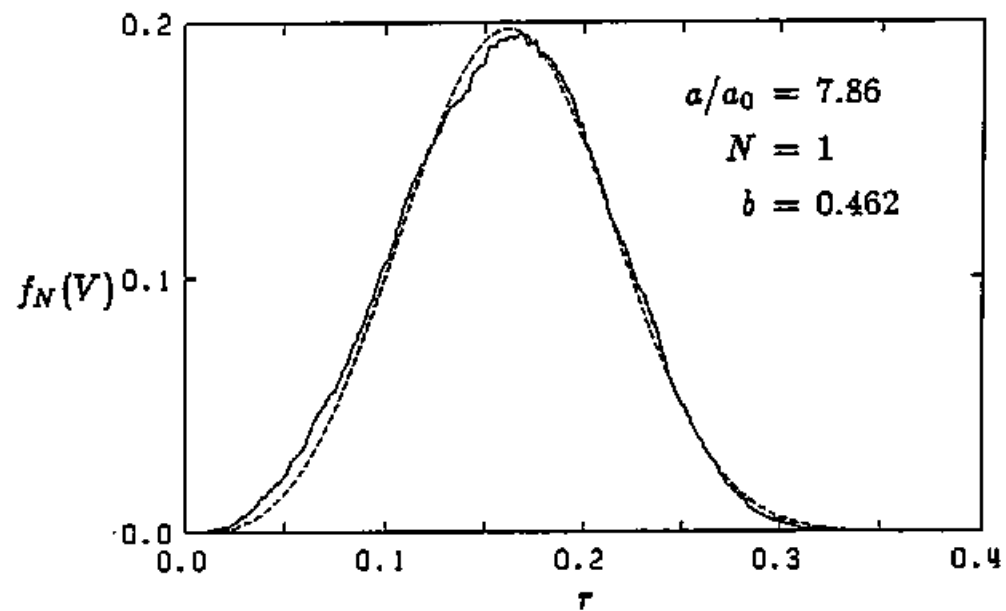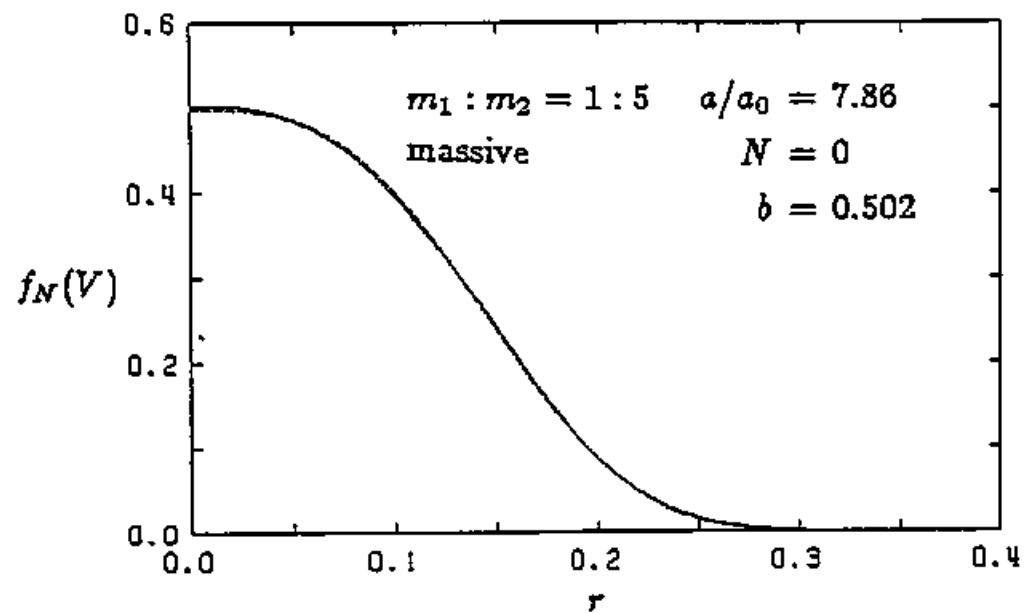
Figure 10(a)
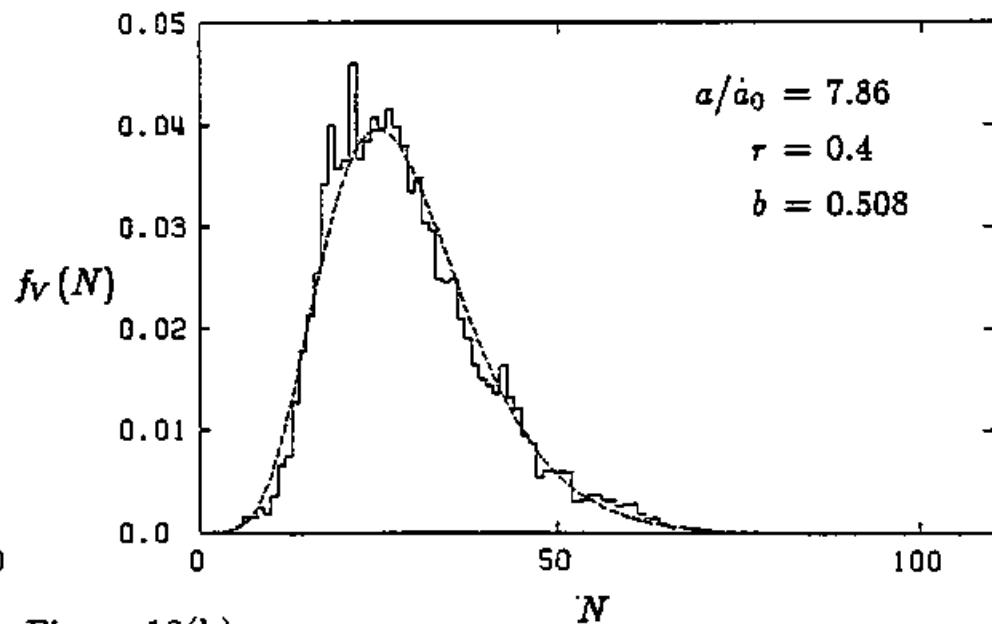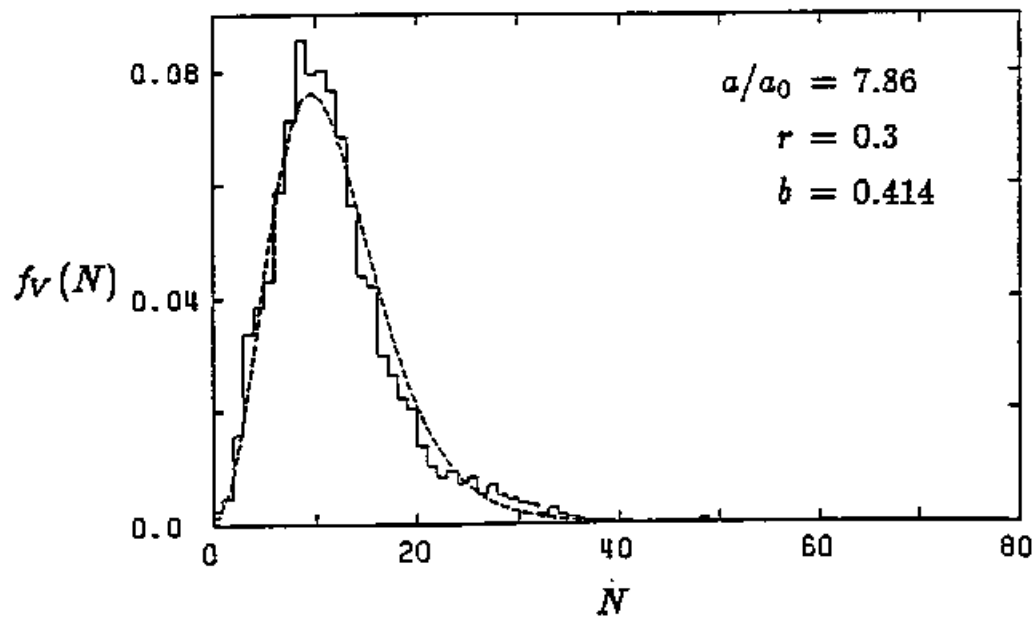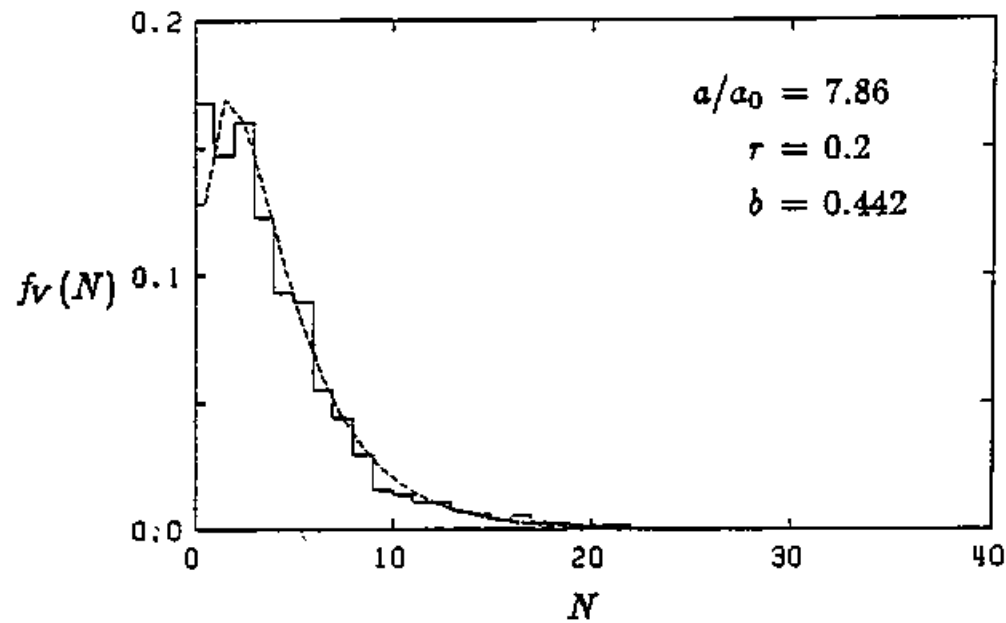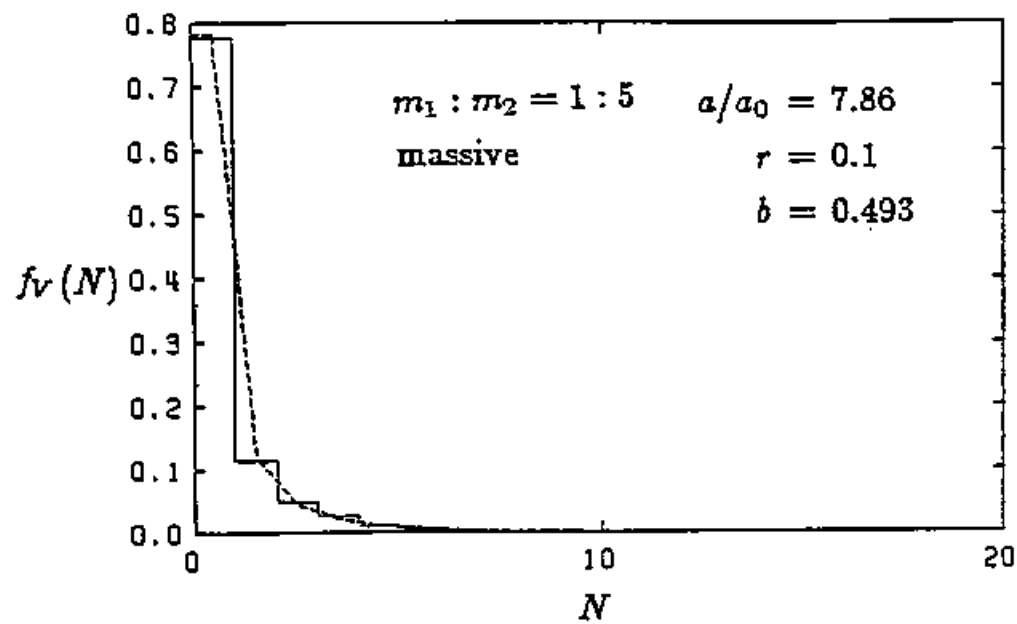
Figure 10(b)
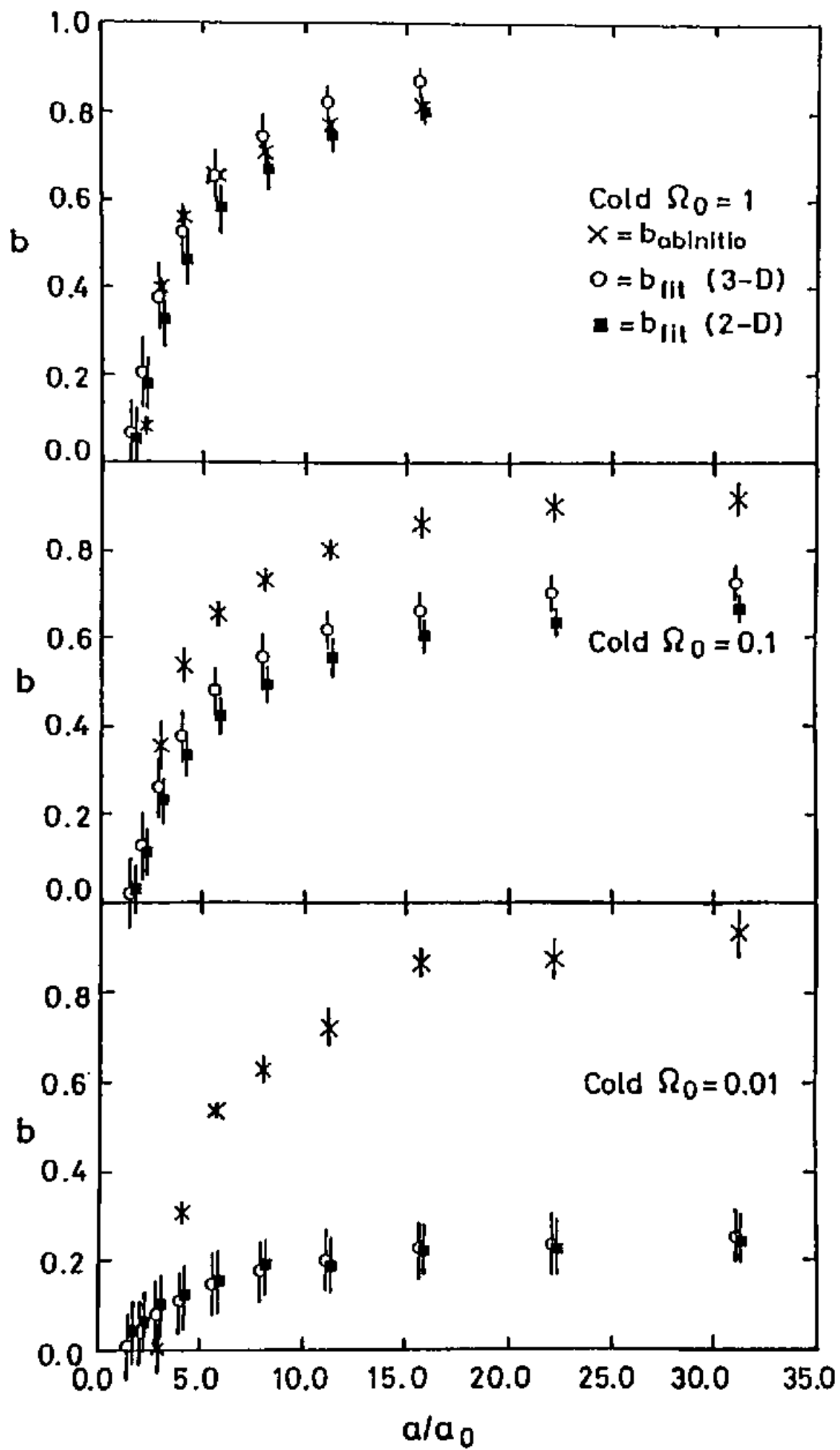
Figure 11
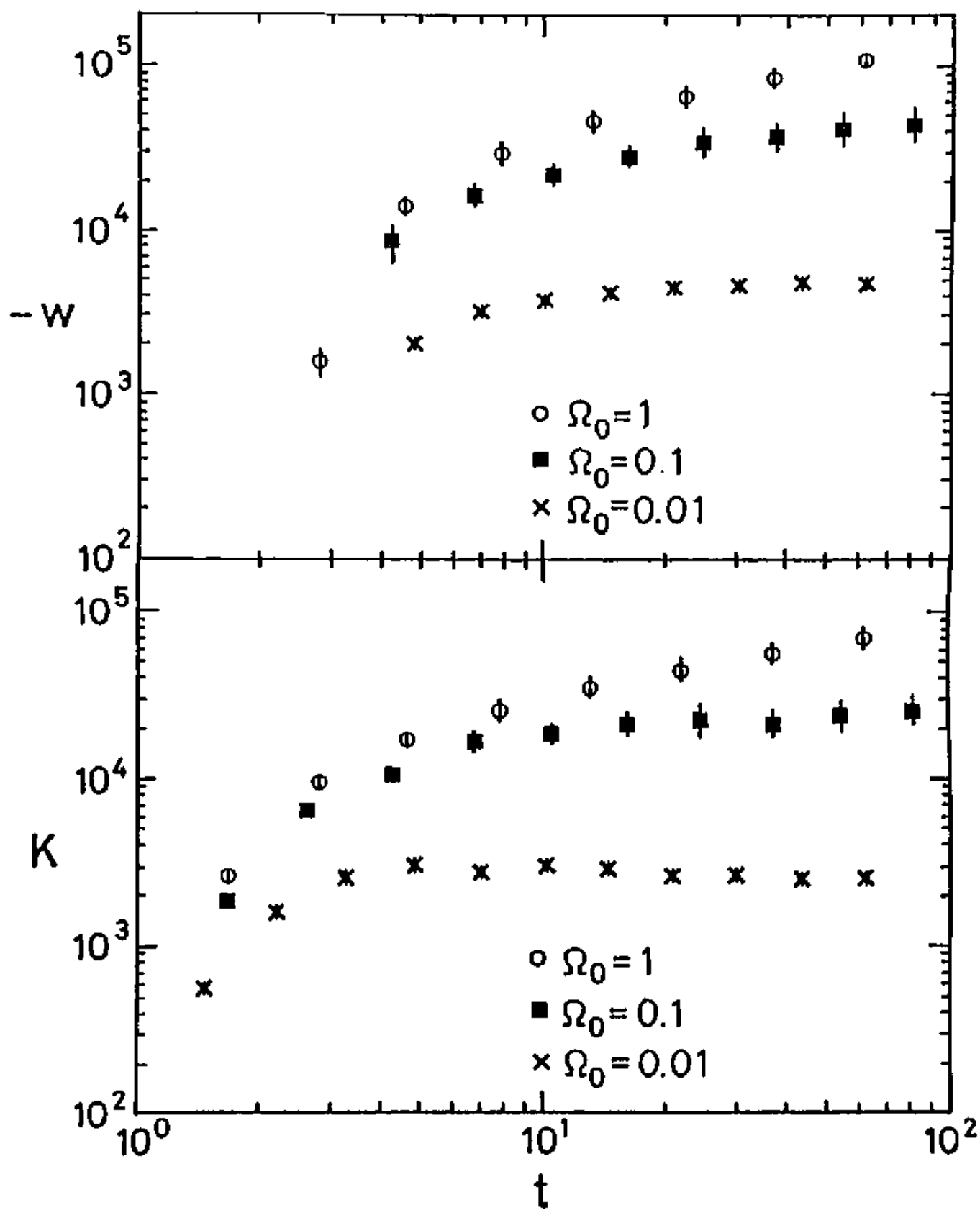
Figure 12
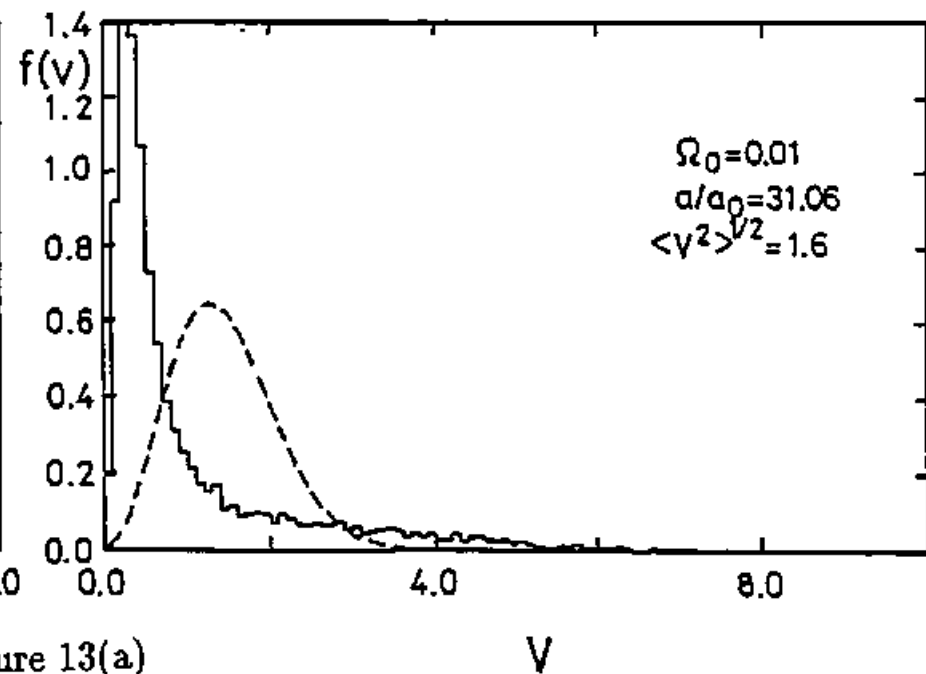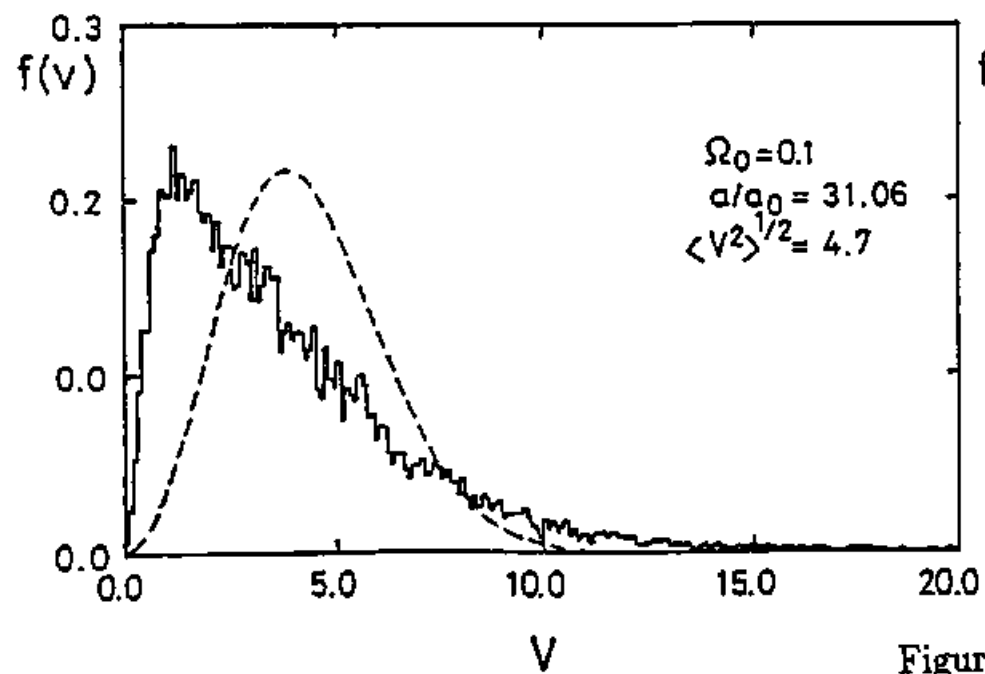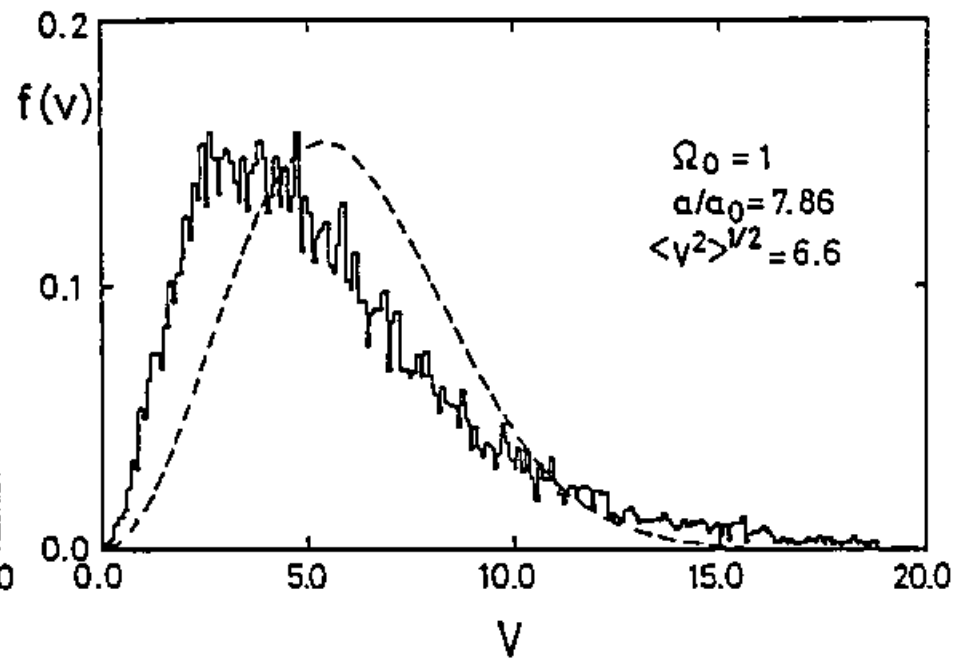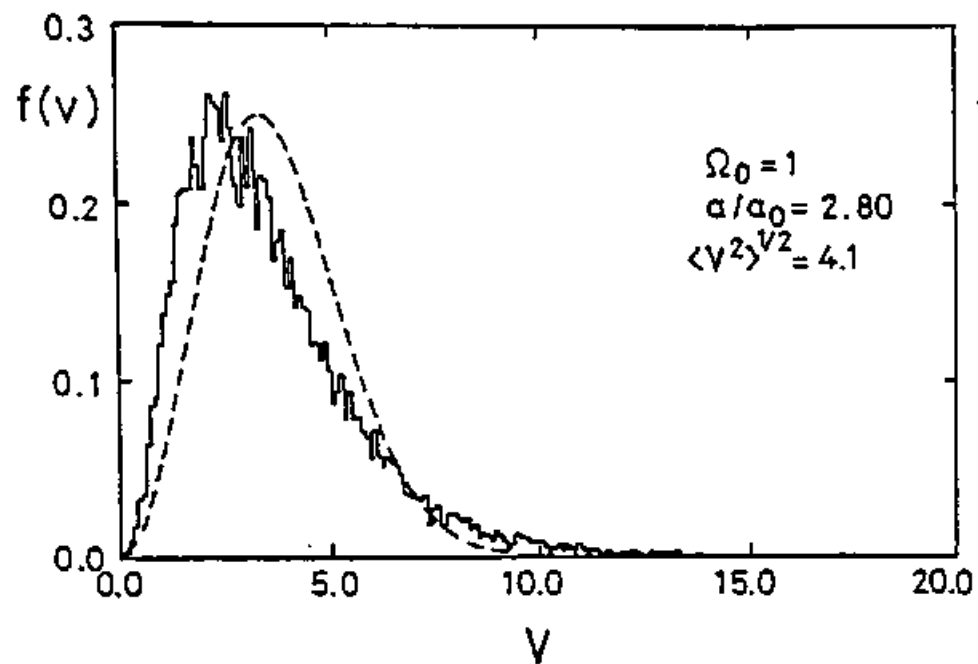
Figure 13(a)
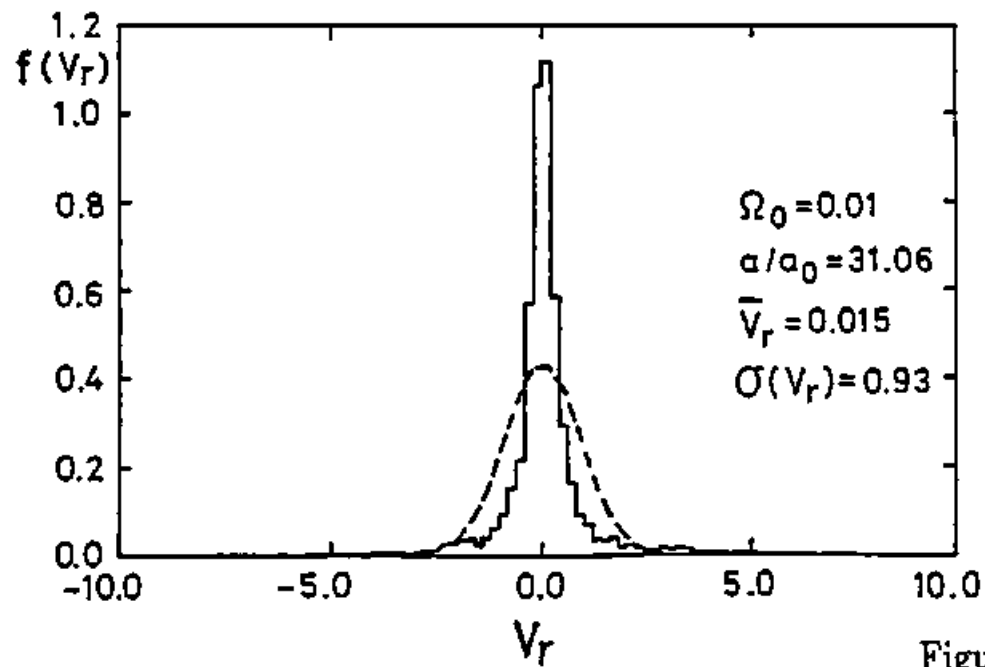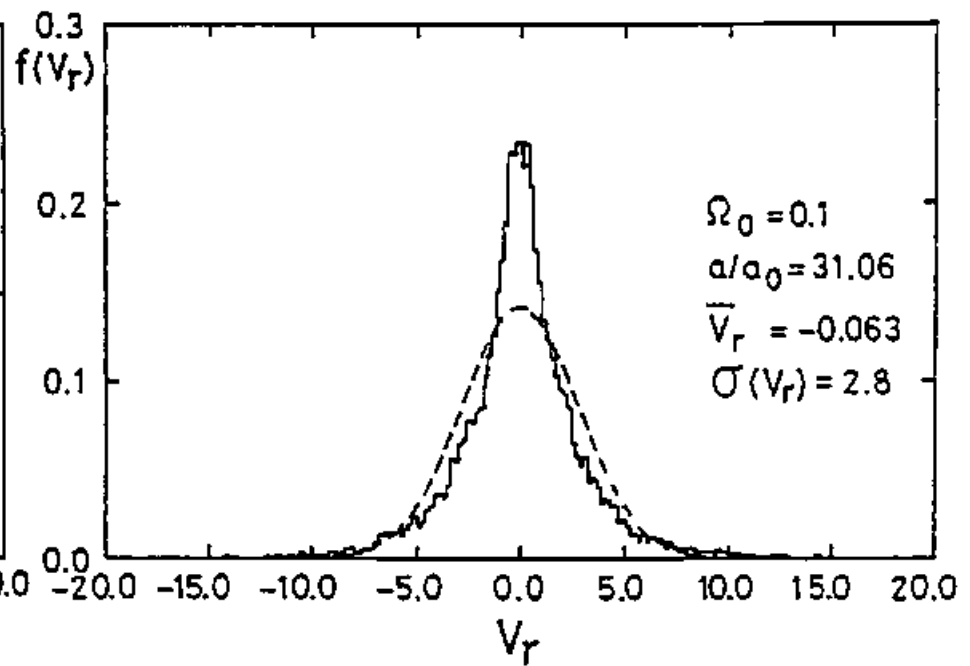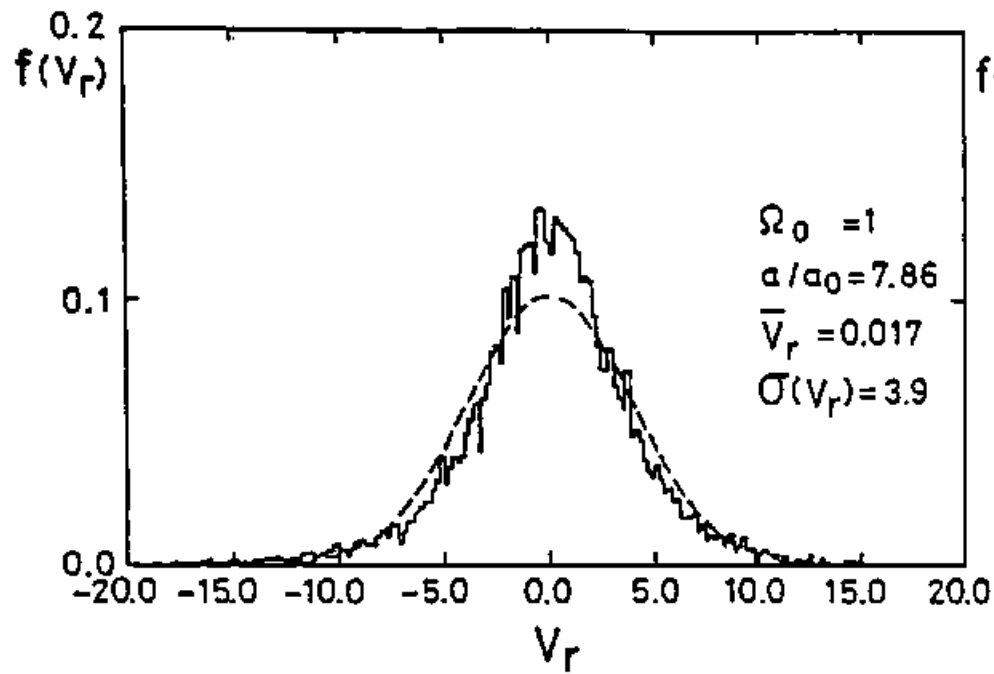
Figure 13(b)
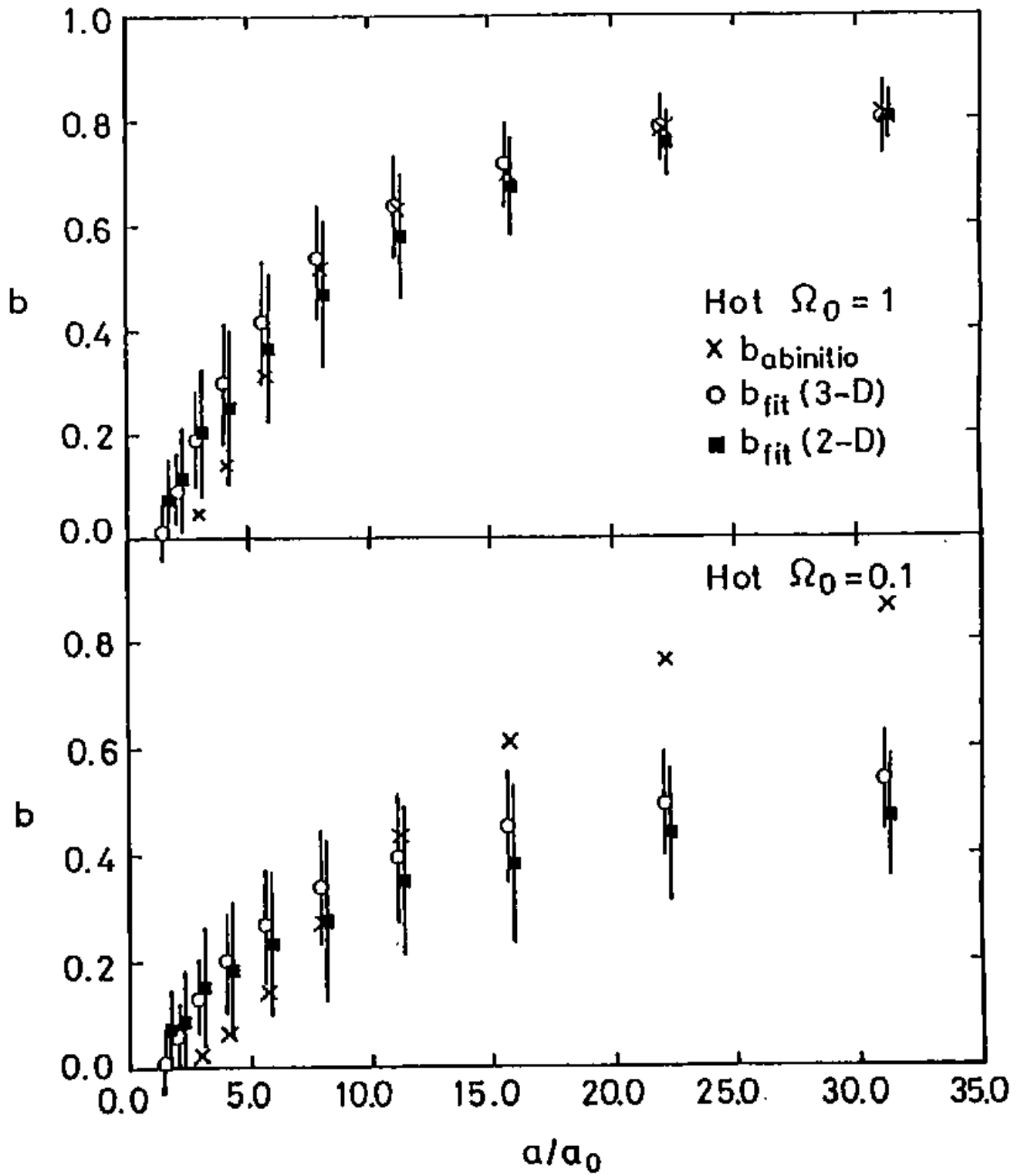
Figure 14
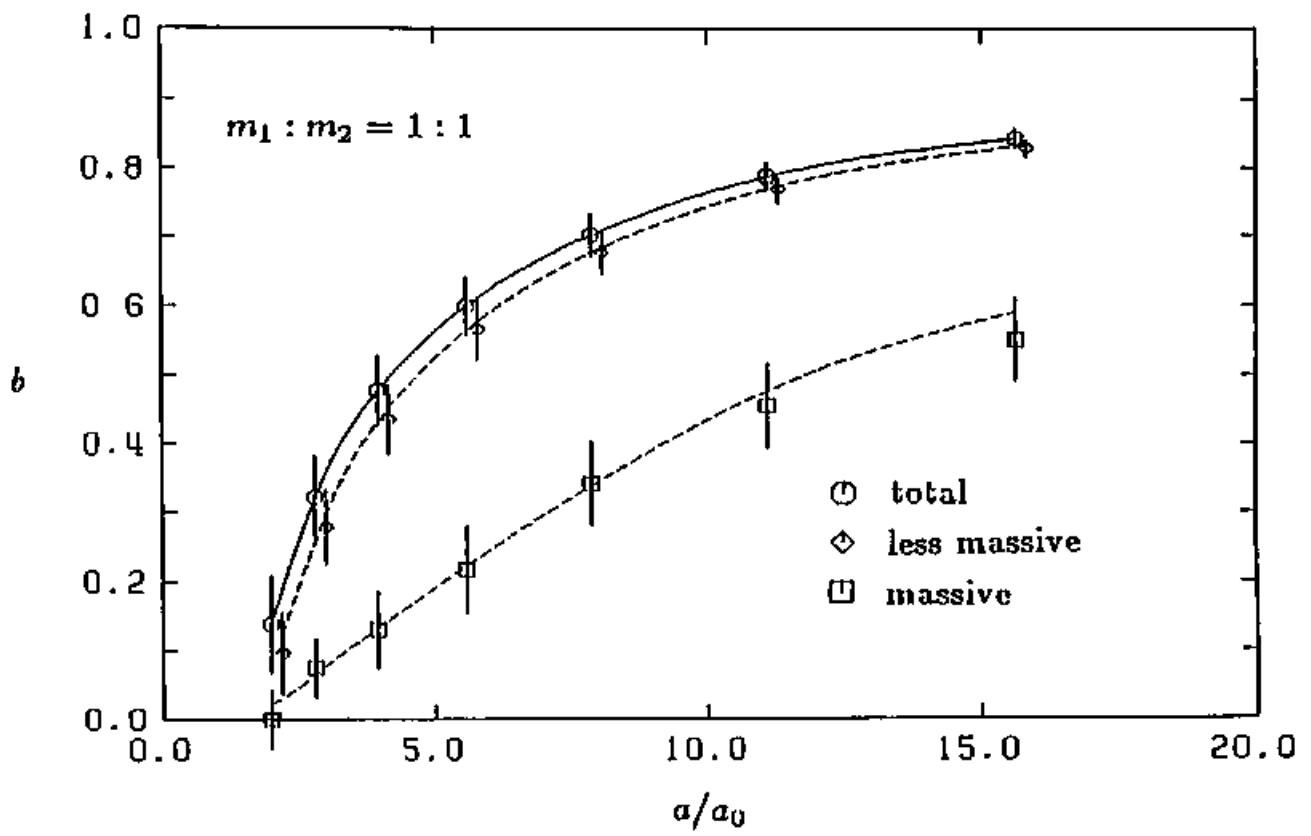
Figure 15(a)
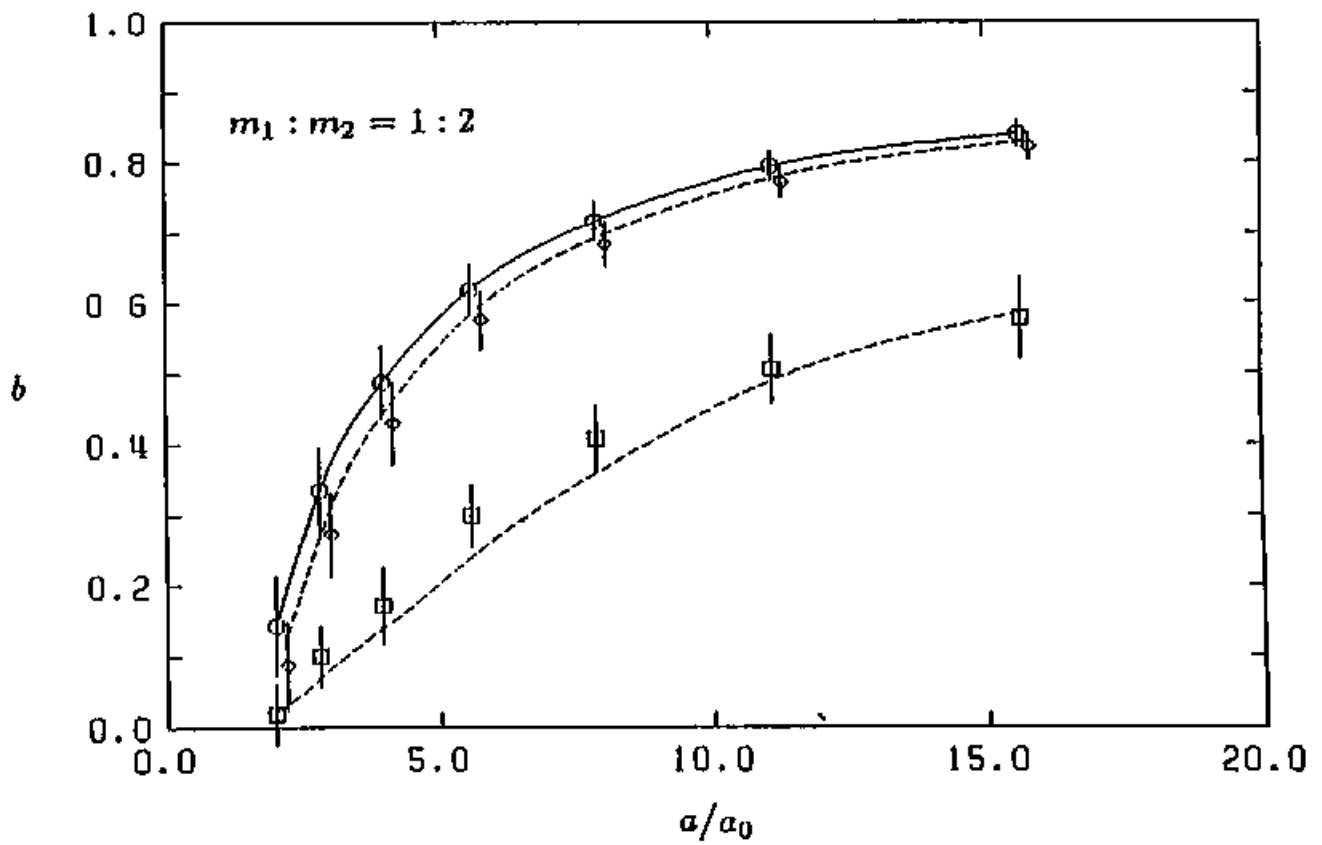
Figure 15(b)
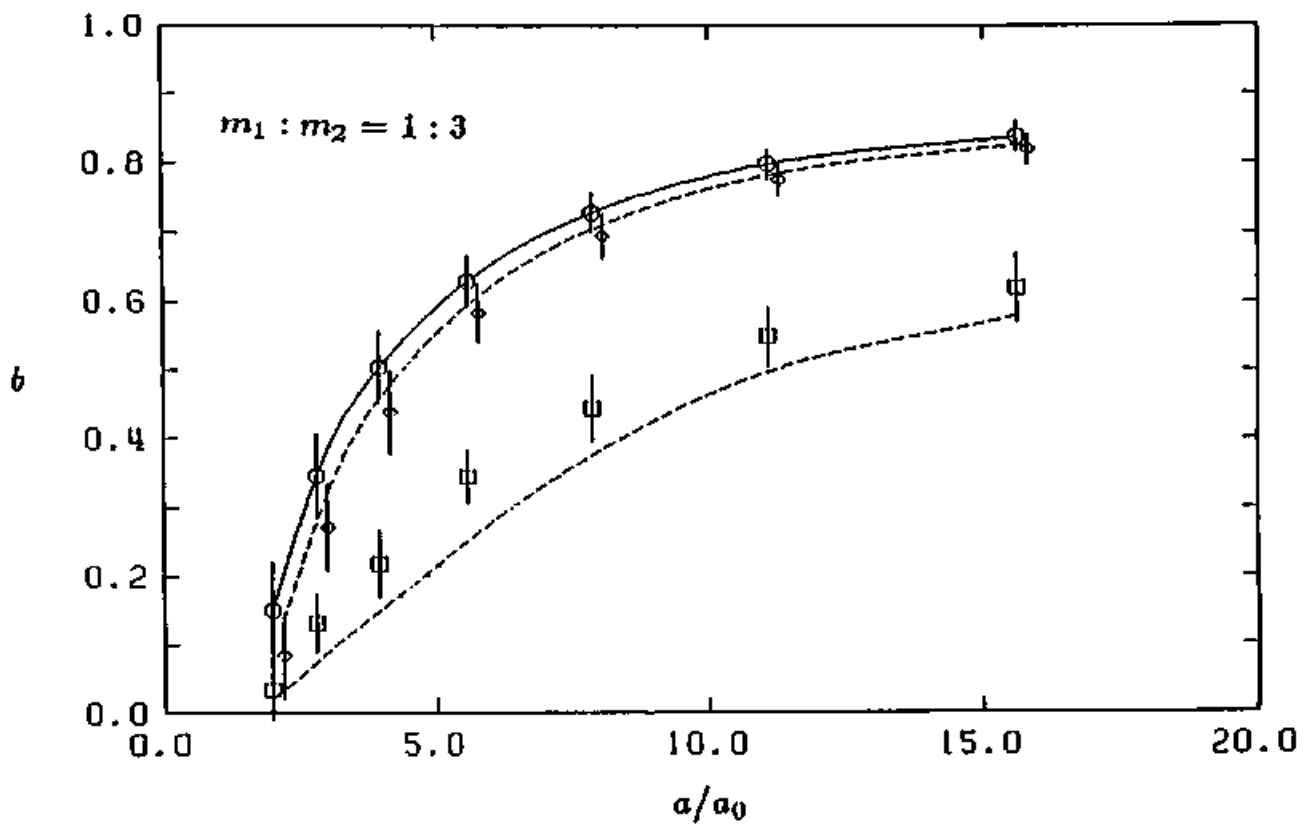
Figure 15(c)
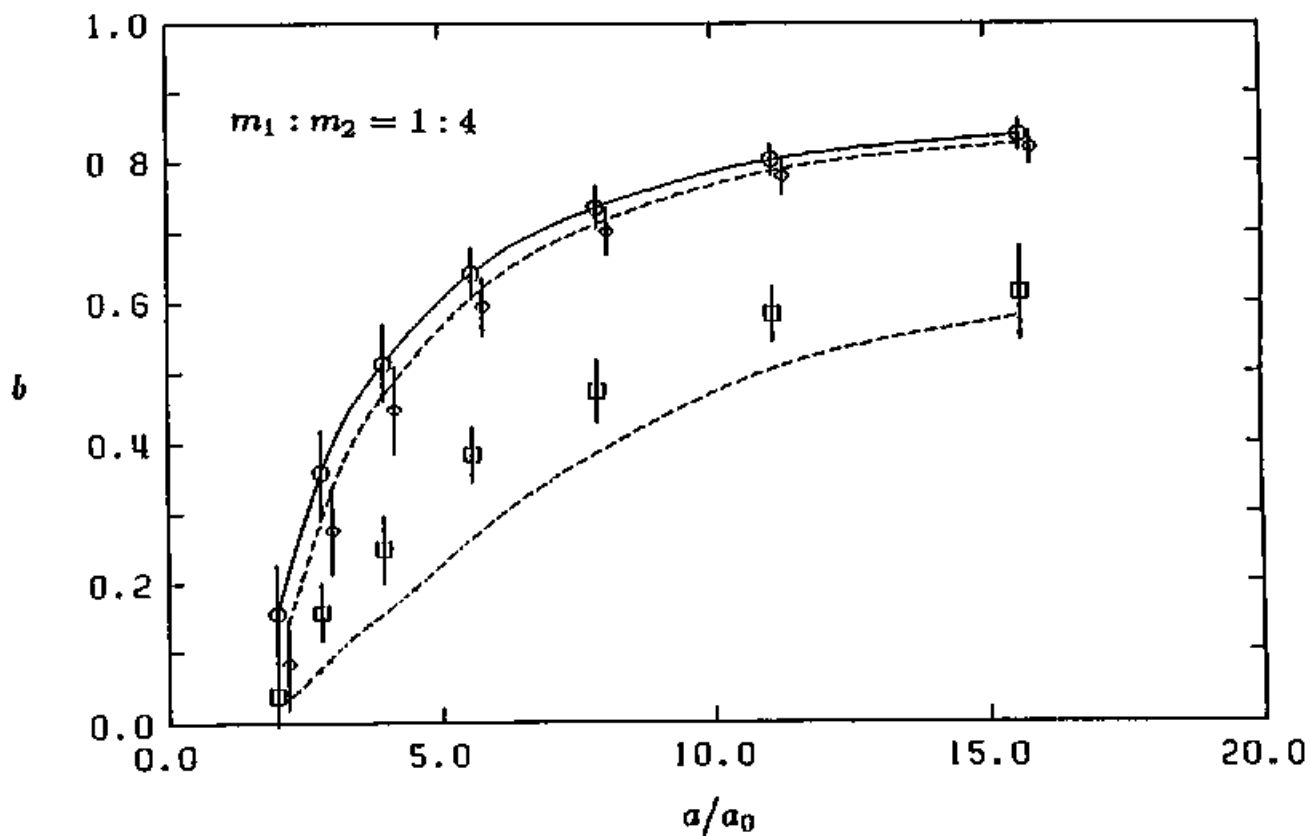
Figure 15(d)
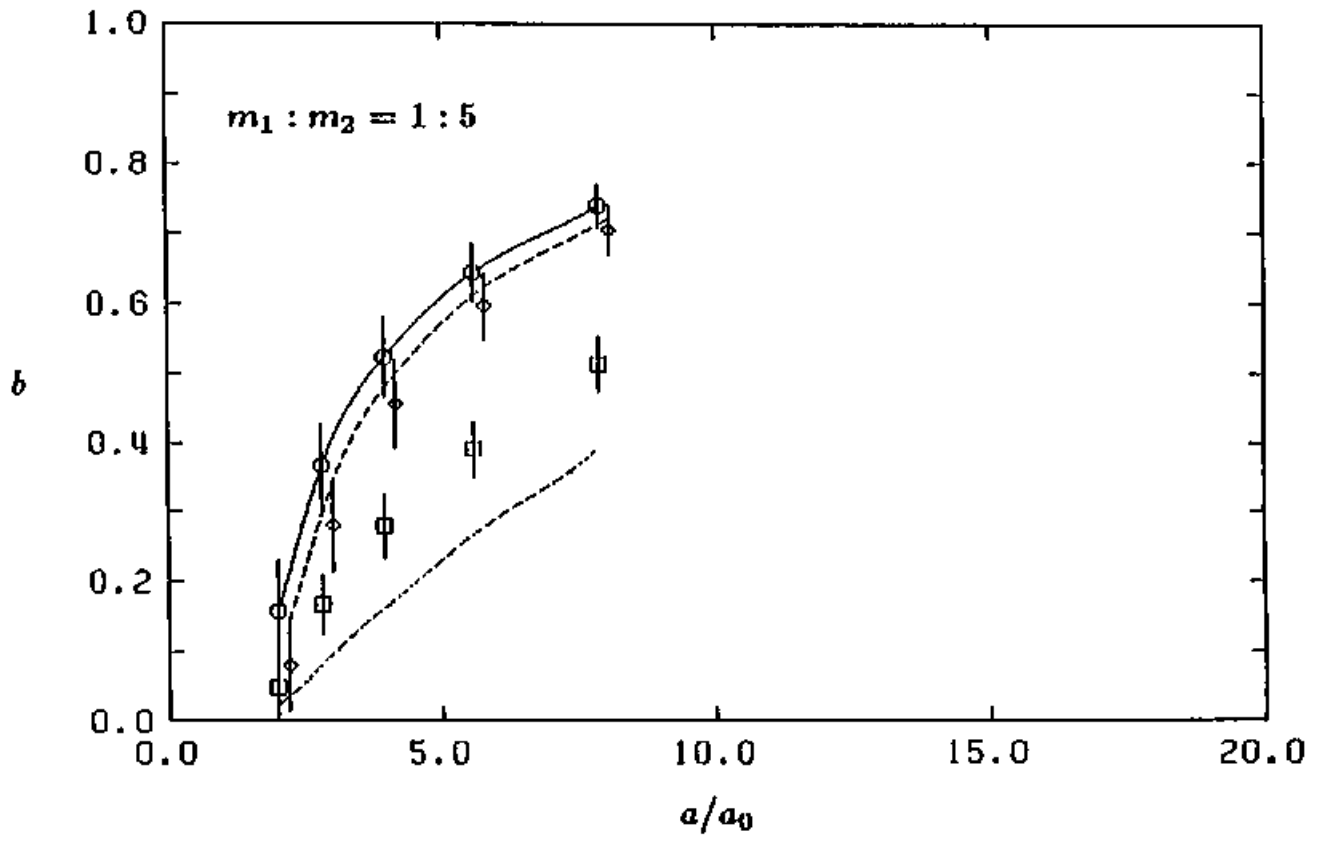
Figure 15(e)
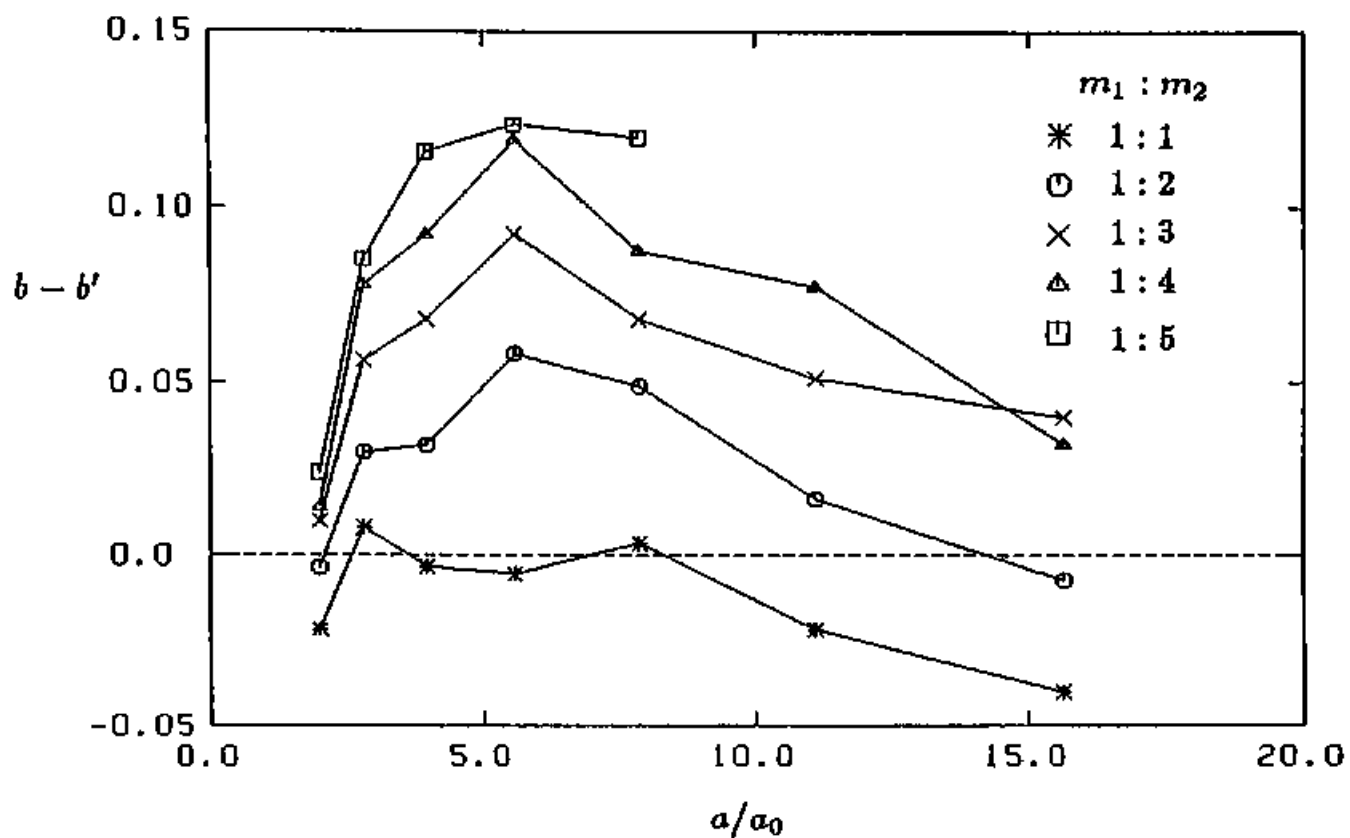
Figure 16(a)
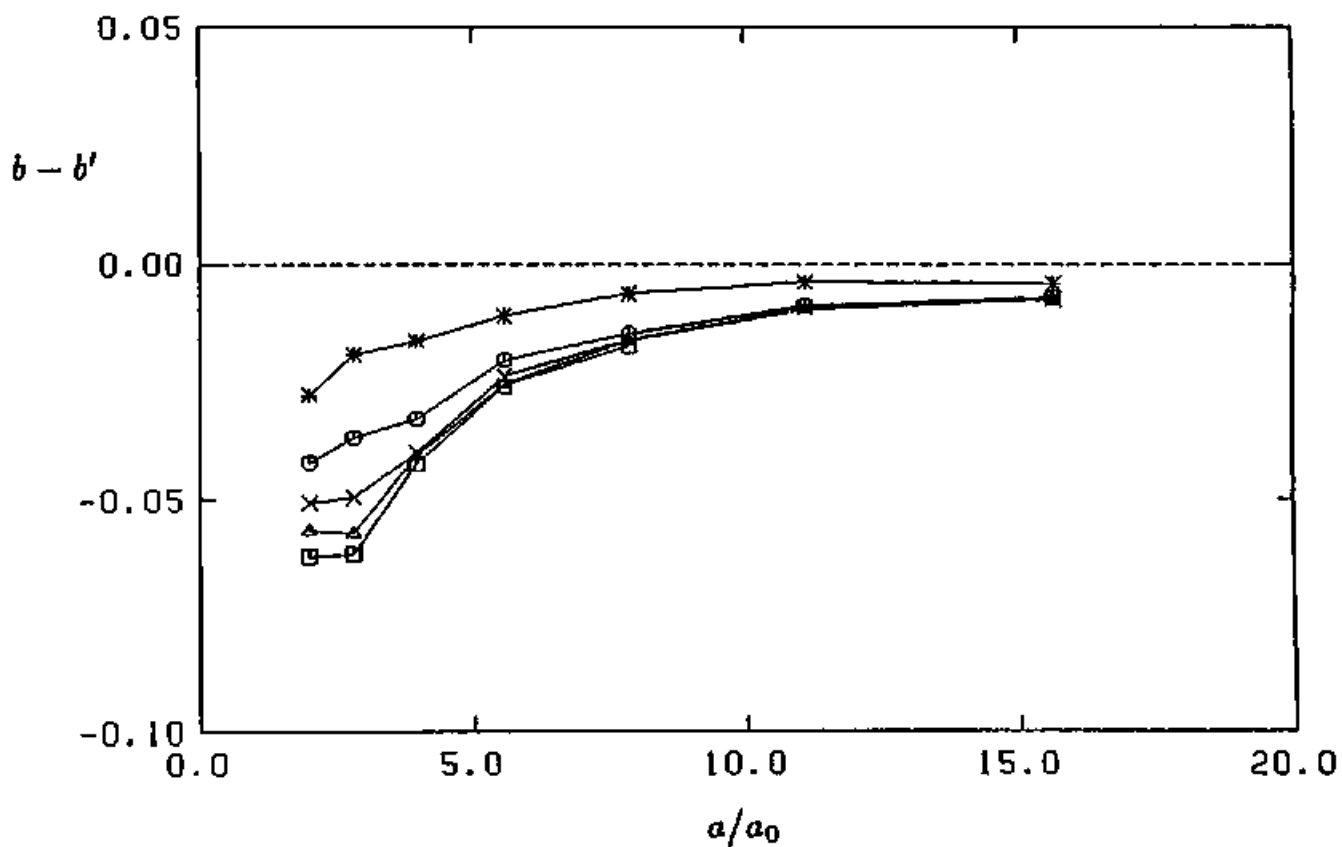
Figure 16(b)
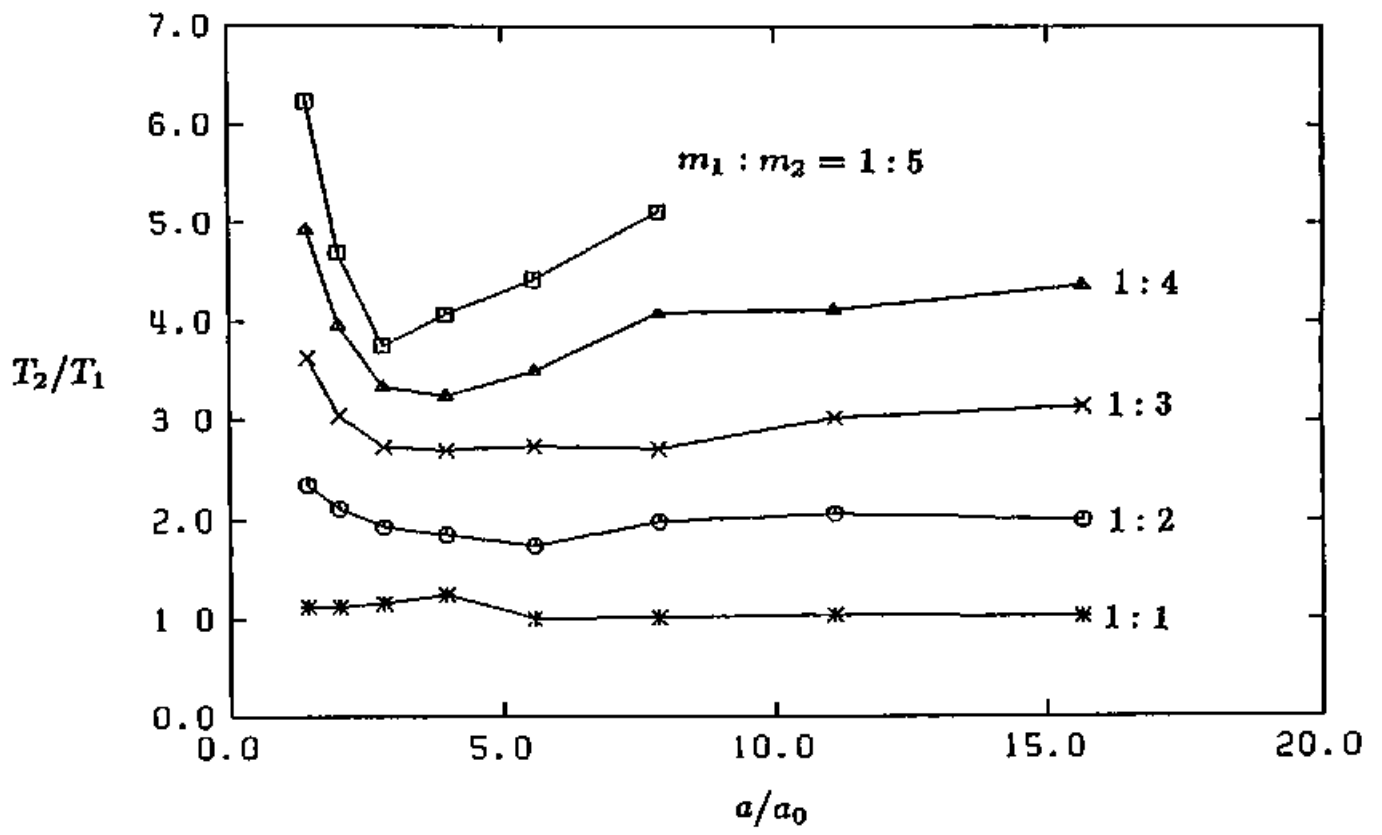
Figure 17
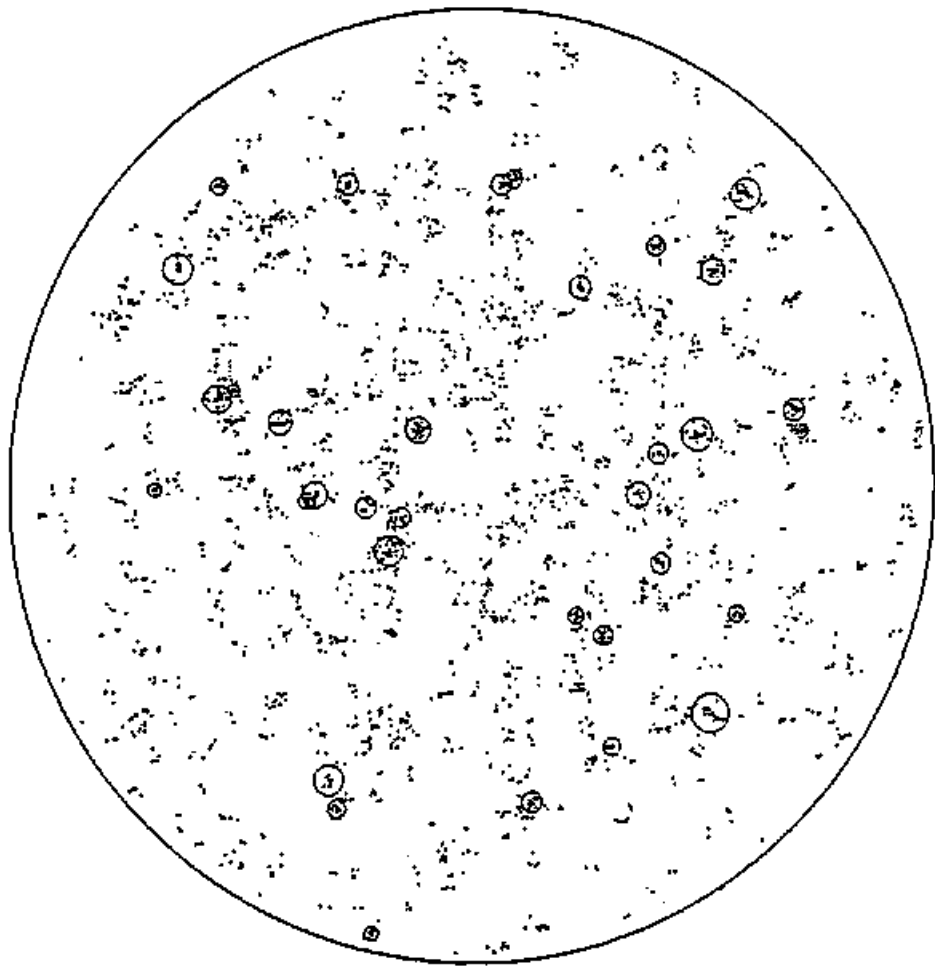
Figure 18
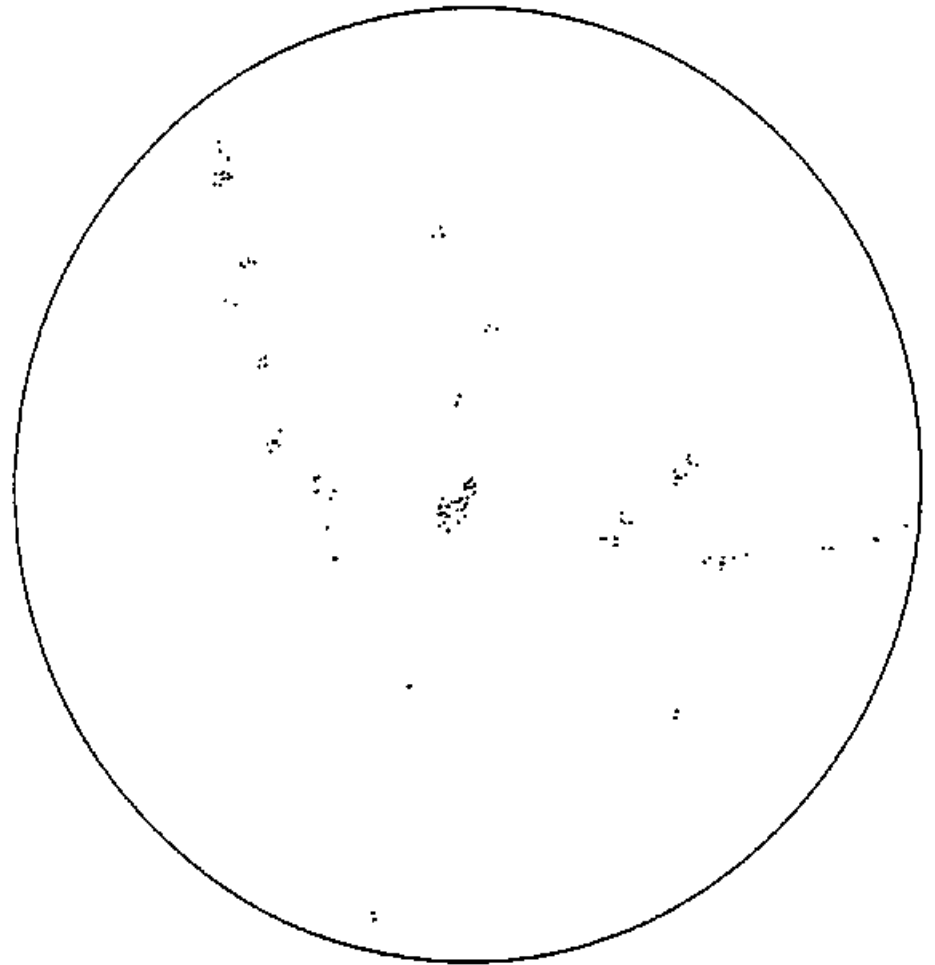
Figure 19
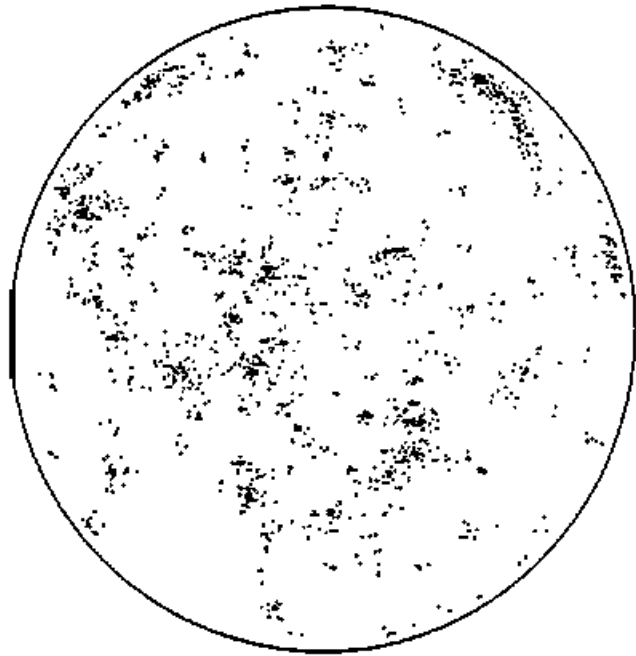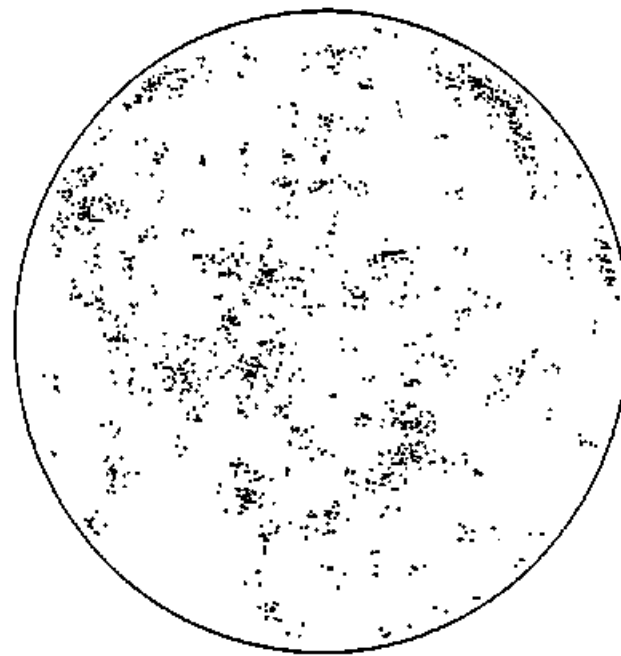
Figure 20(a)   Figure 20(b)   Figure 20(c)
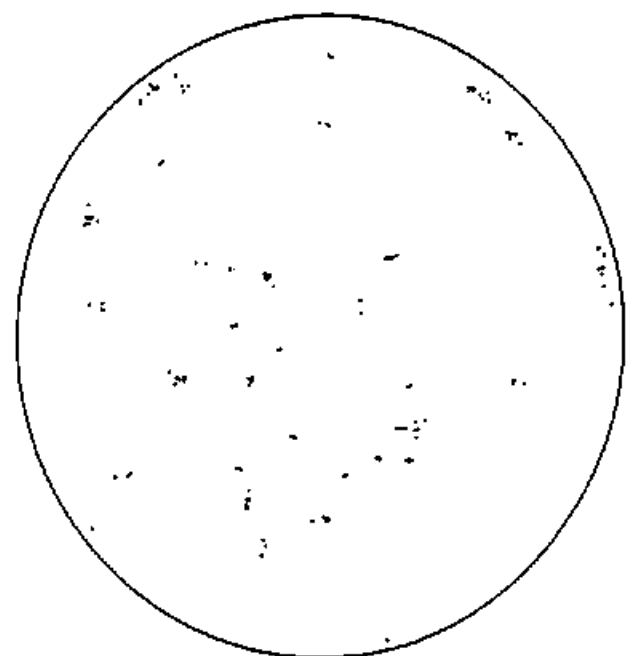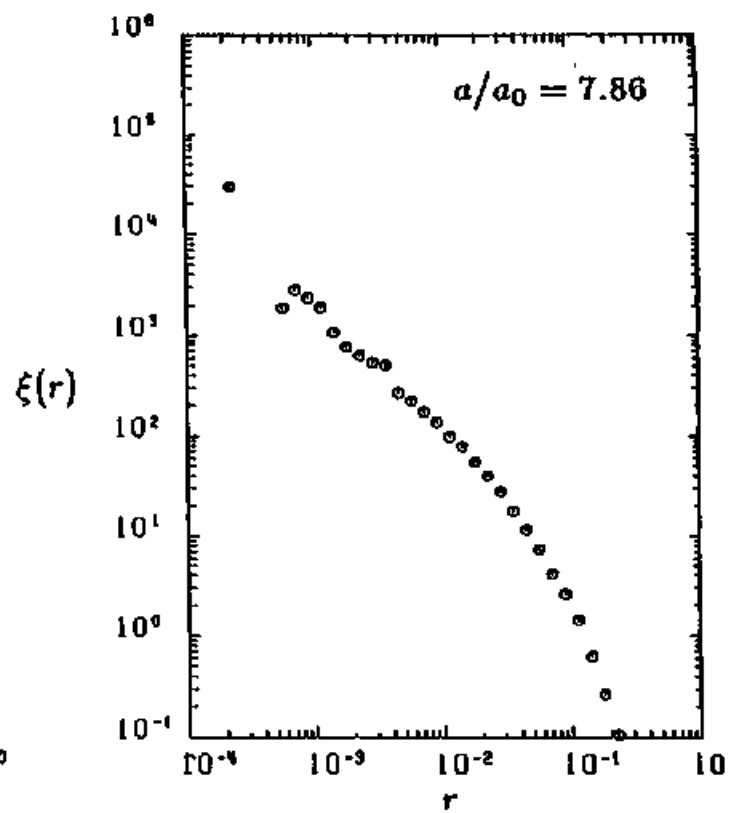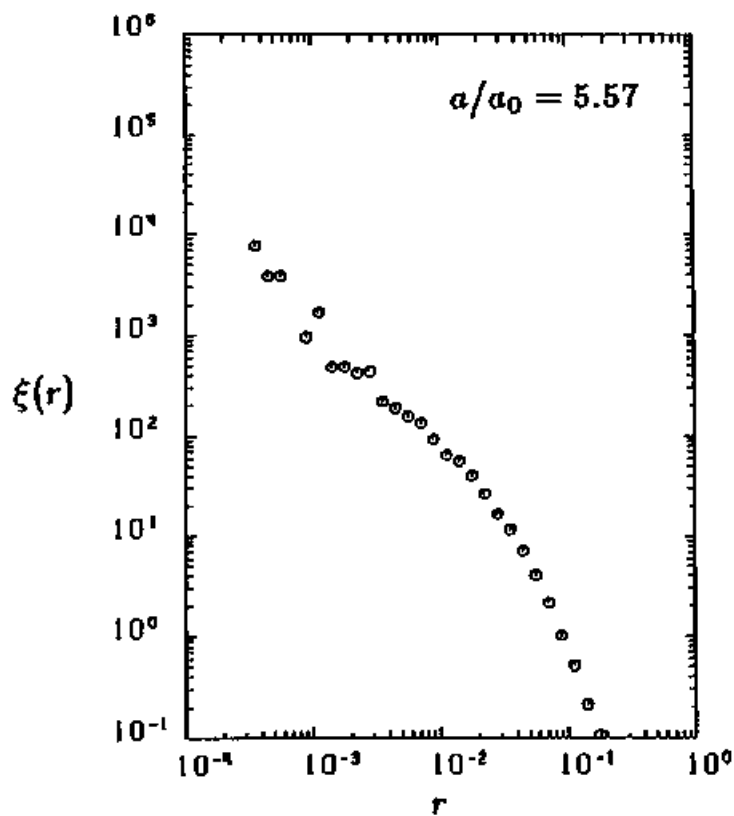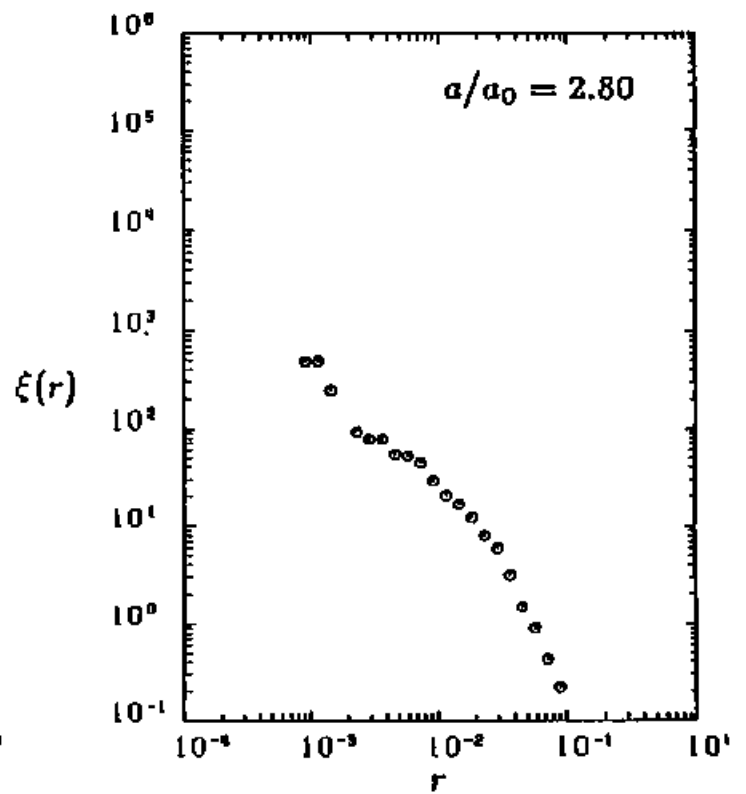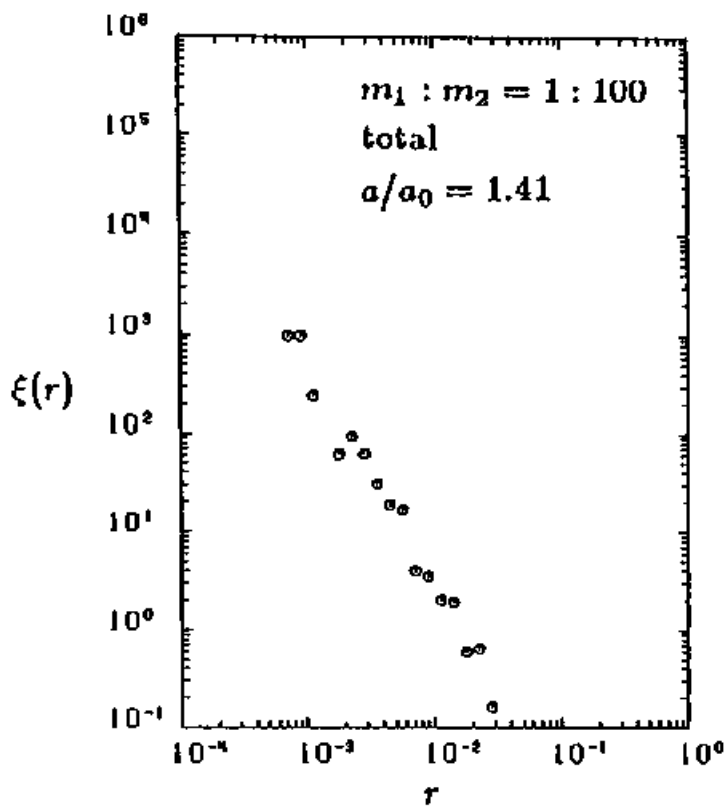
Figure 21(a)
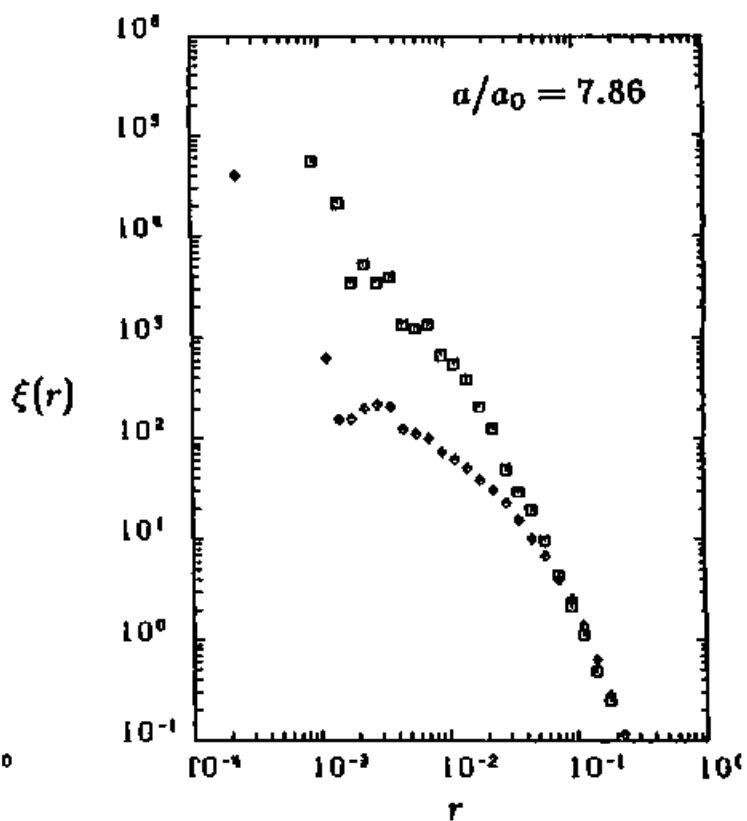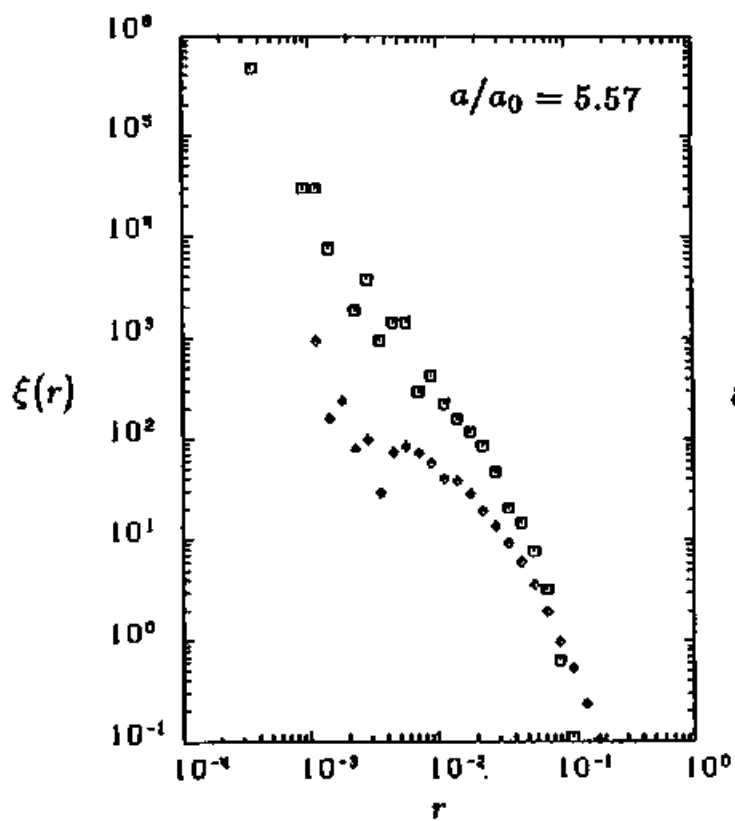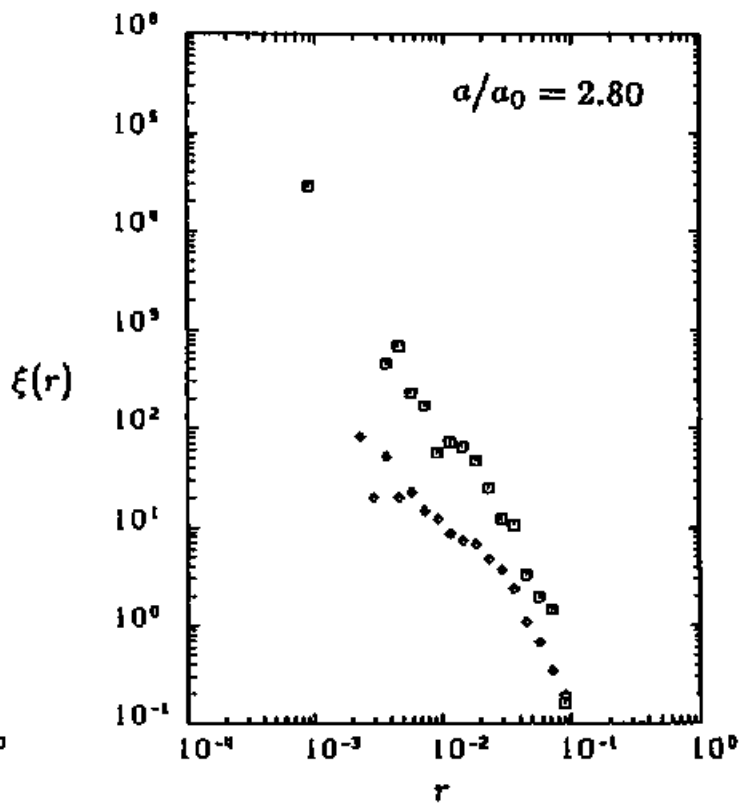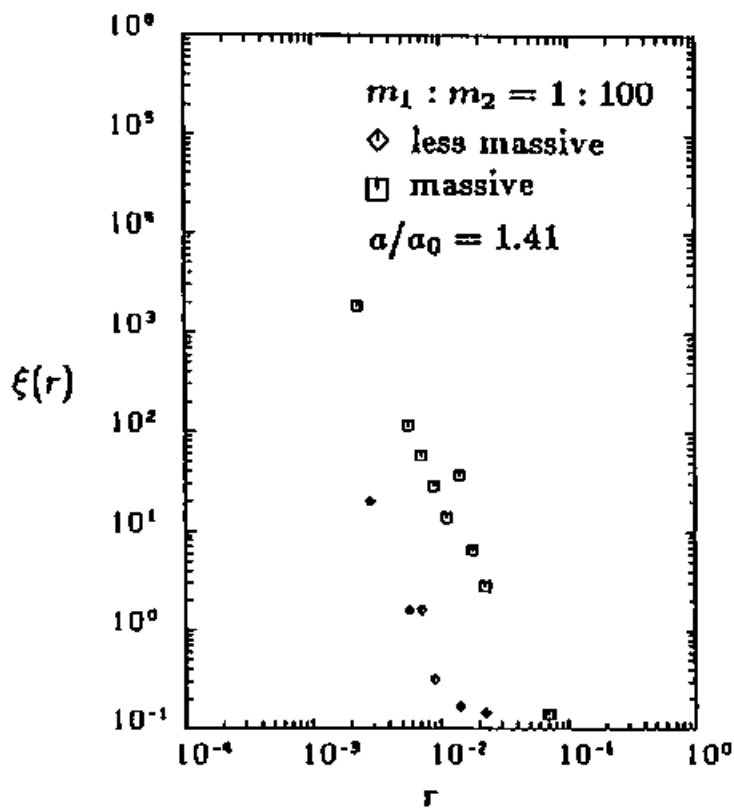
Figure 21(b)
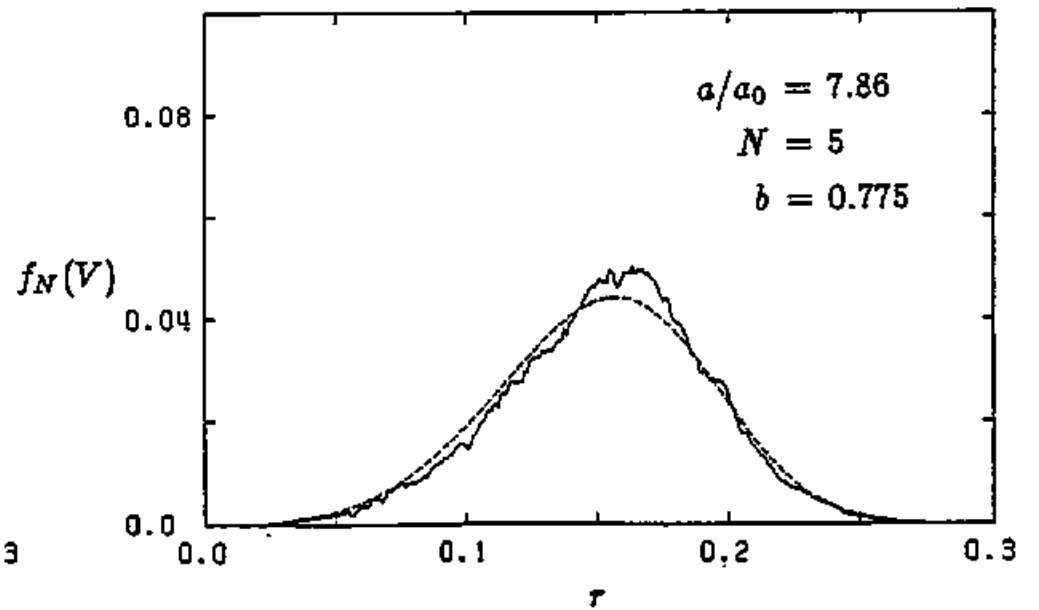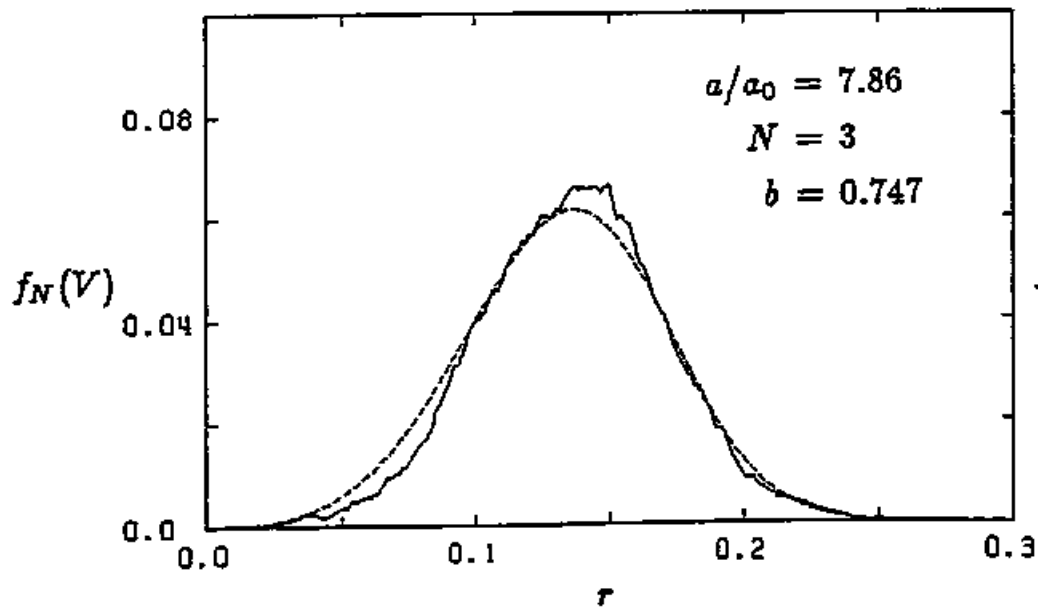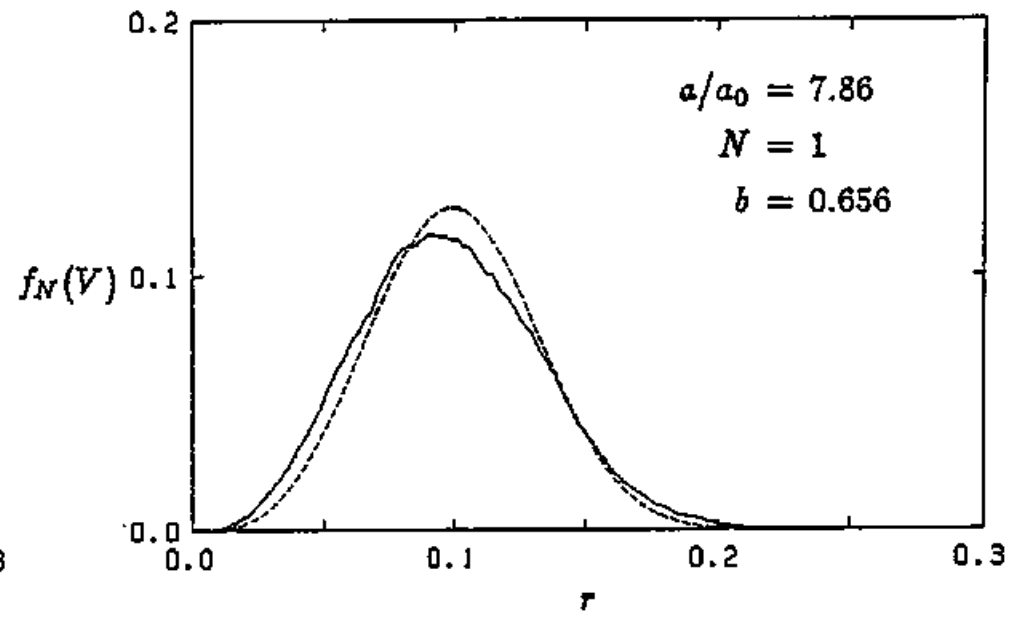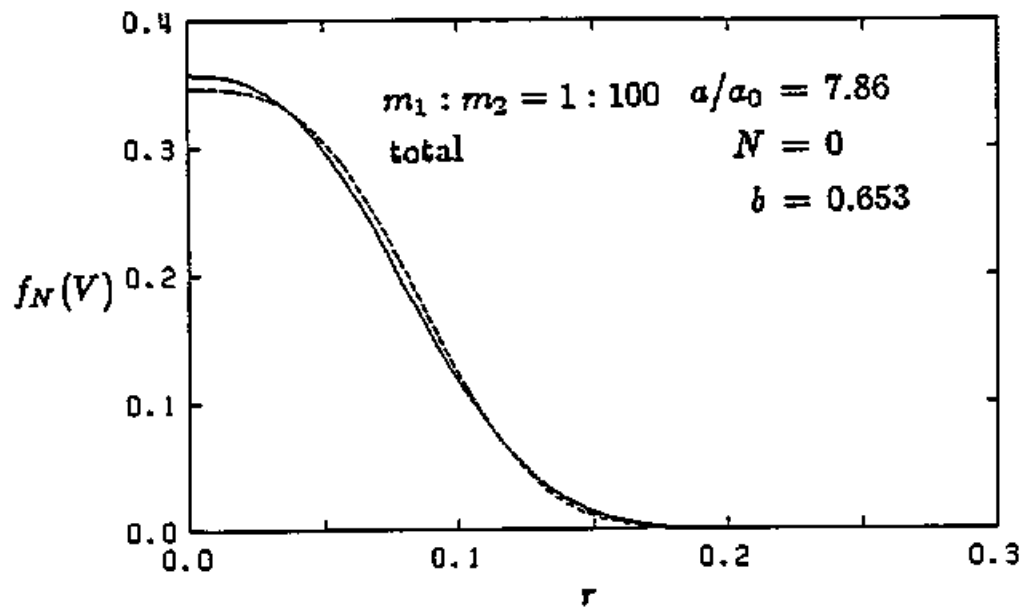
Figure 22(a)
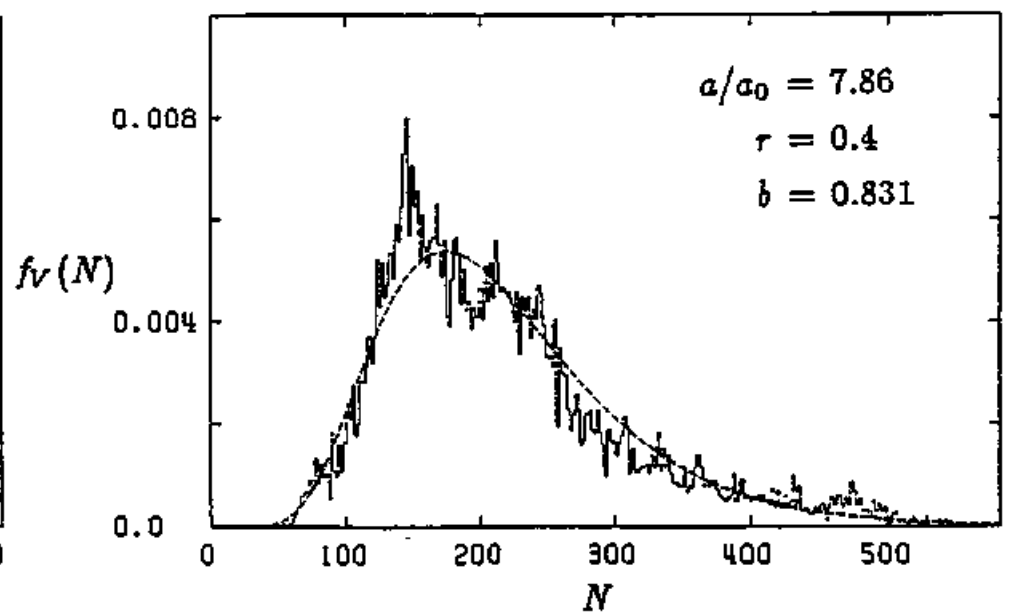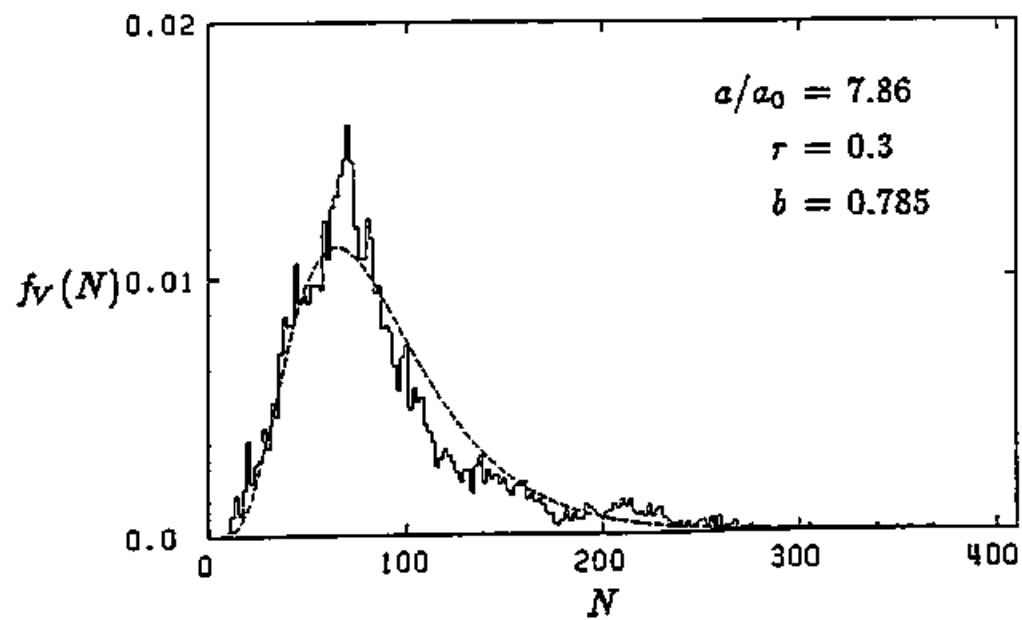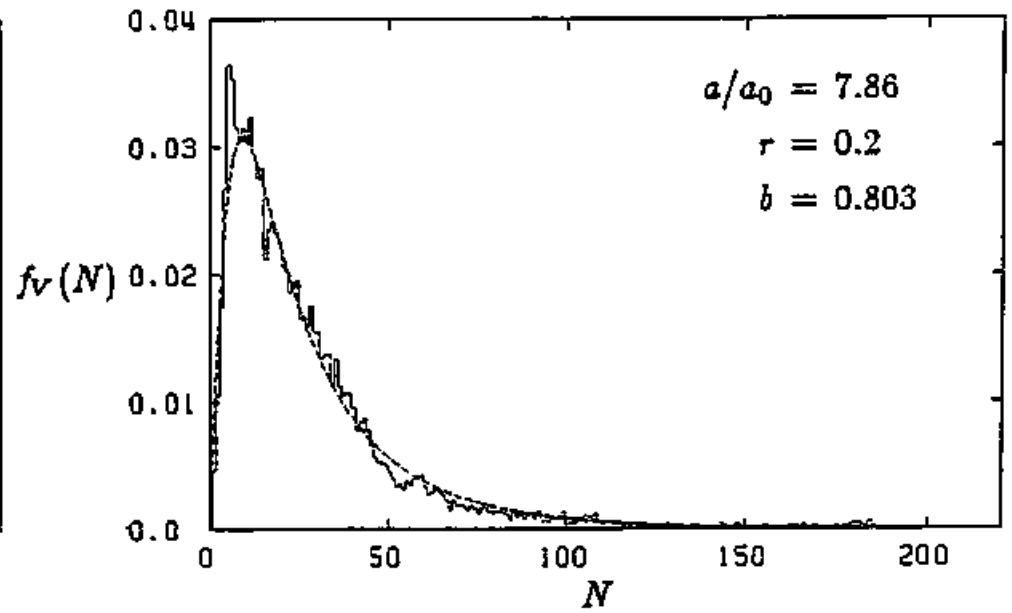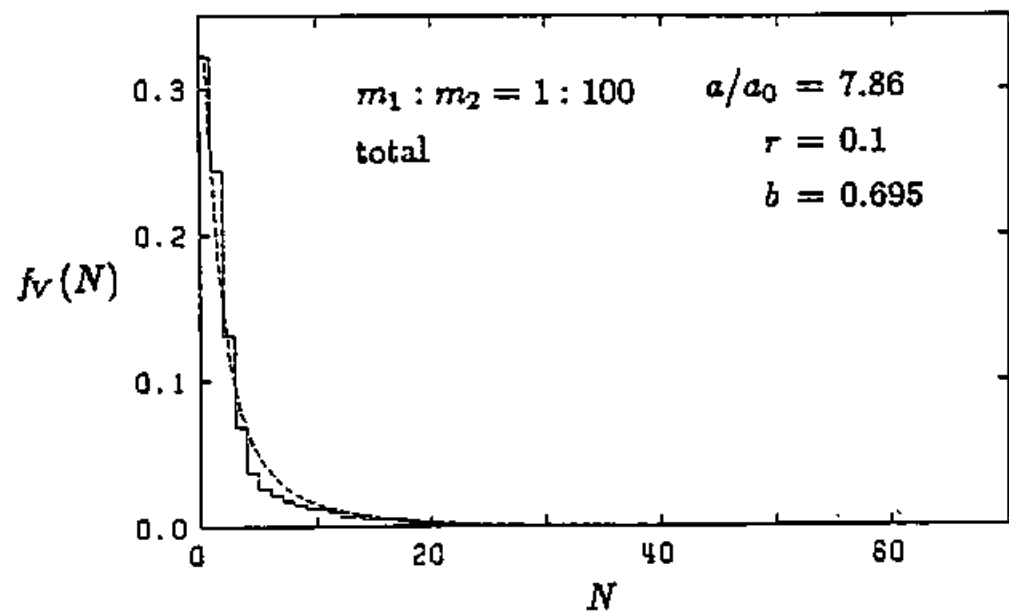
Figure 22(b)
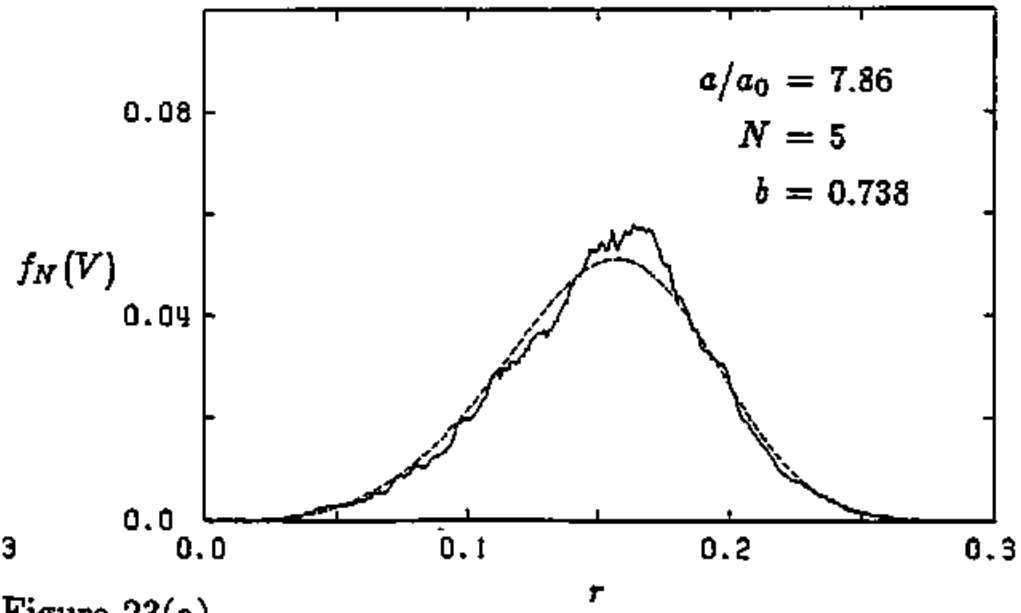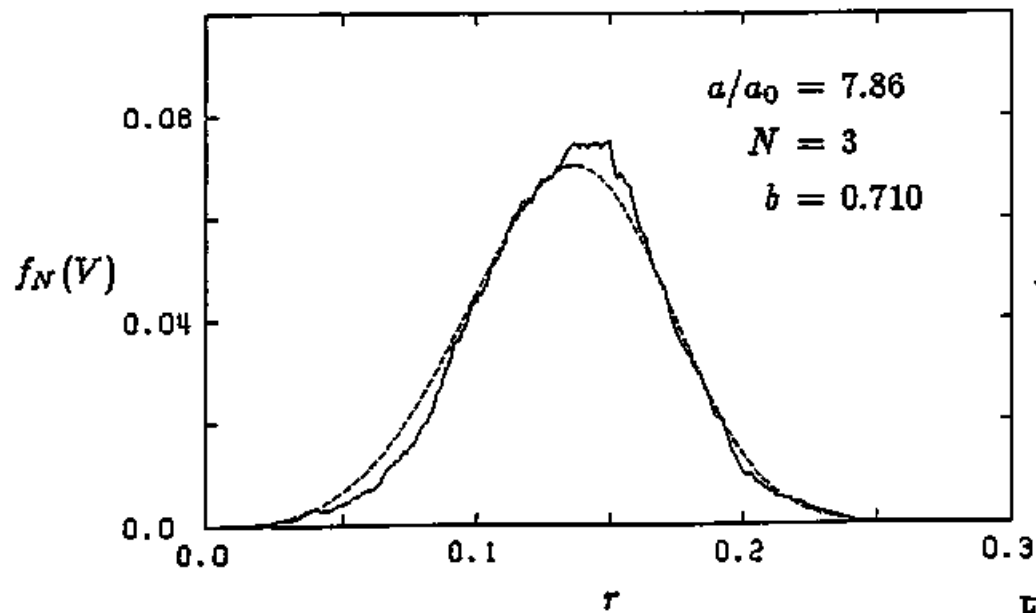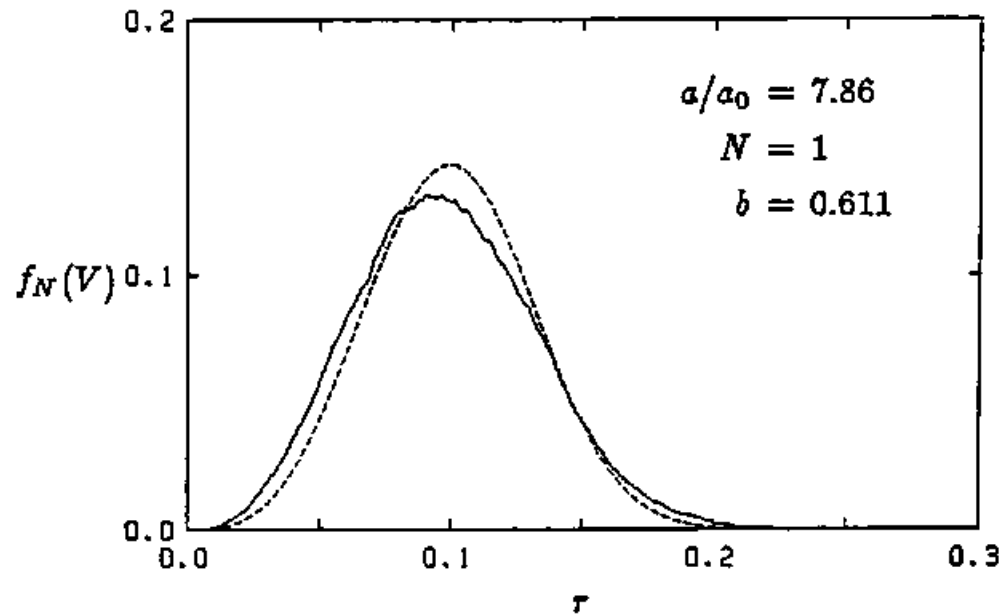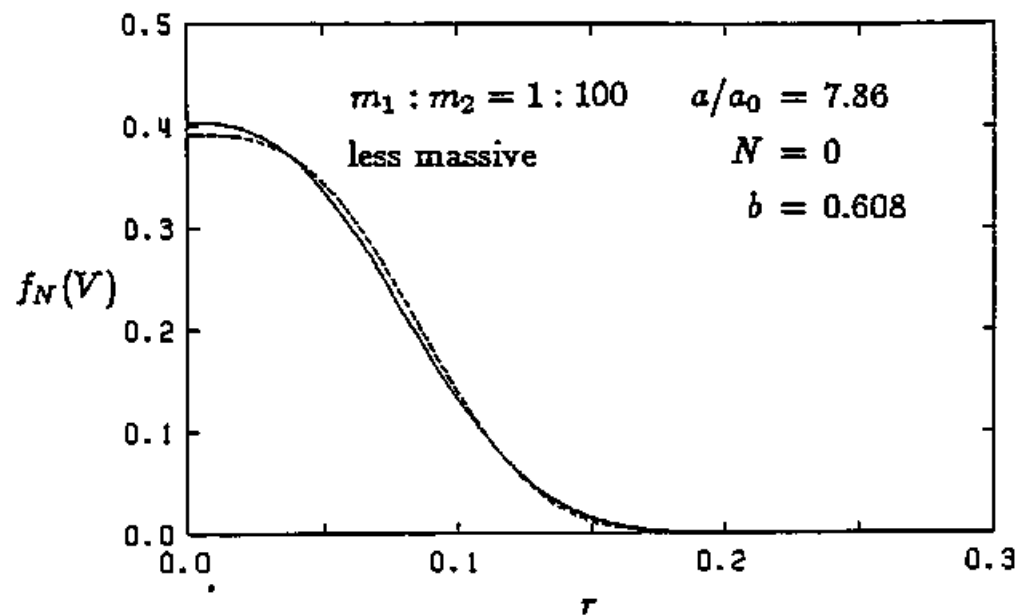
Figure 23(a)
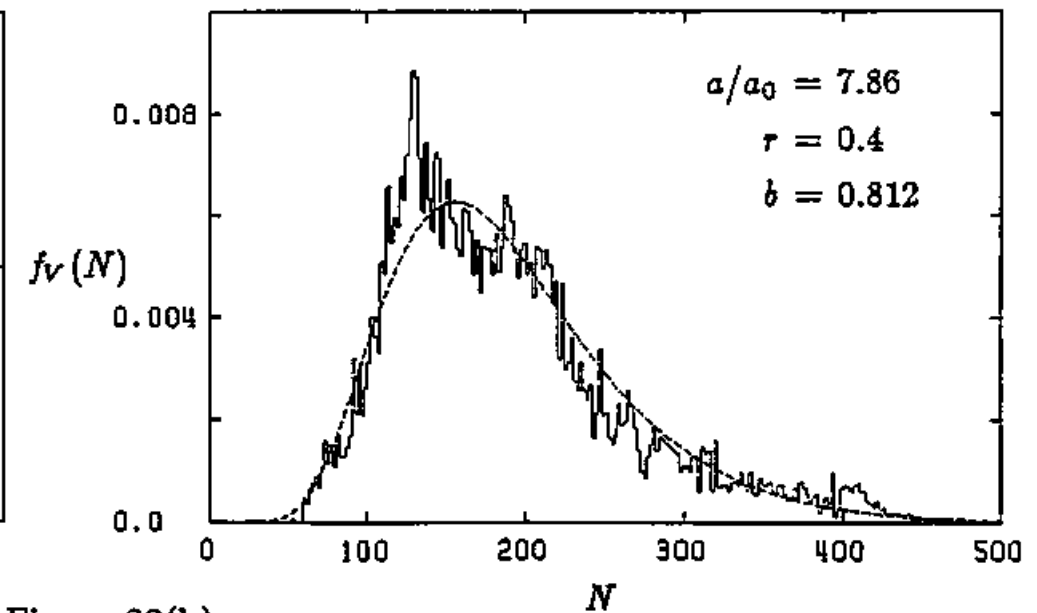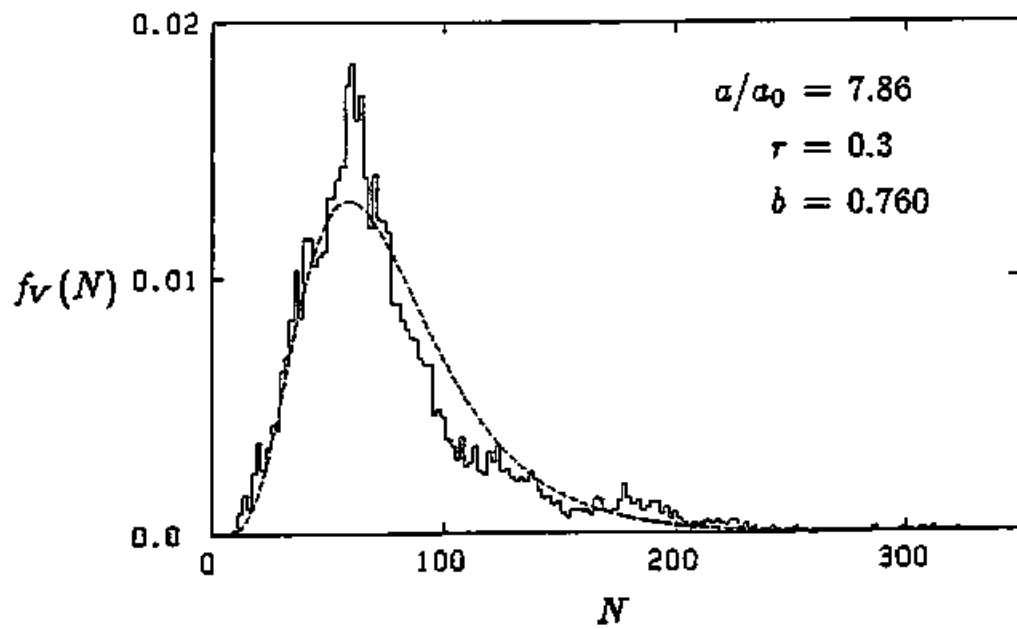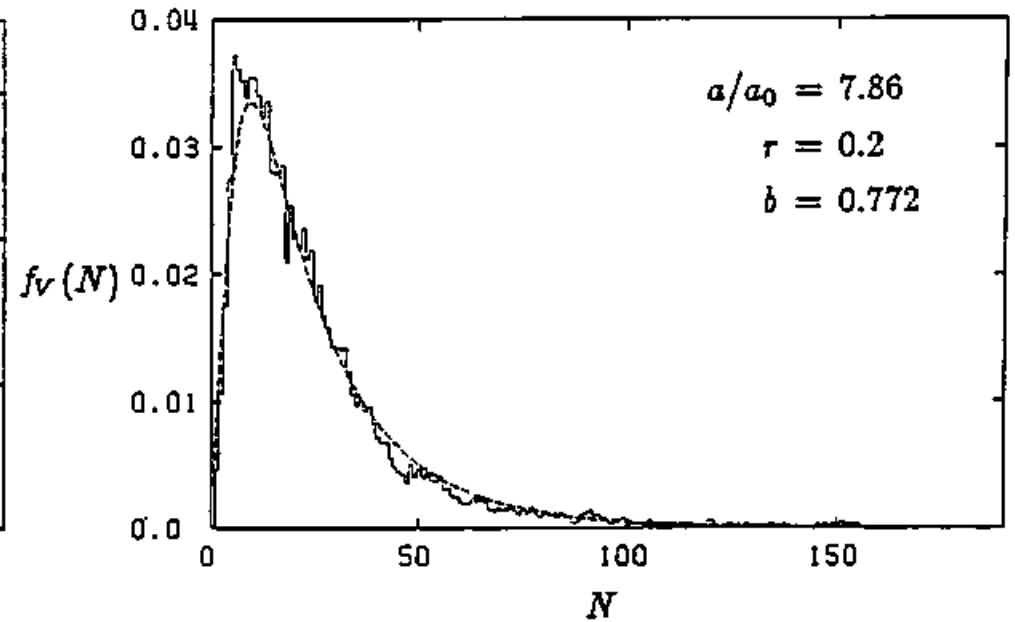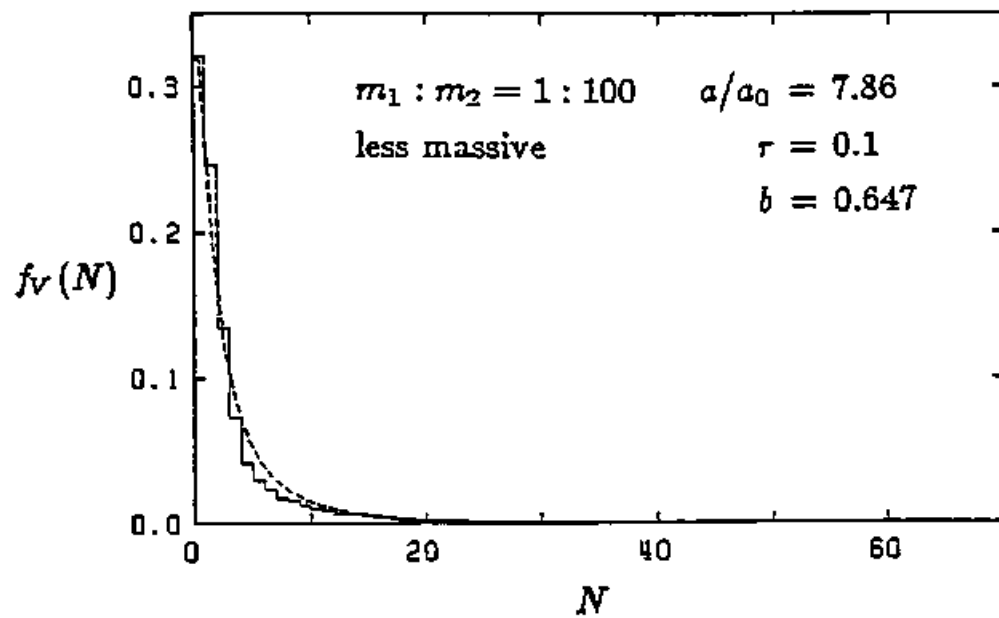
Figure 23(b)
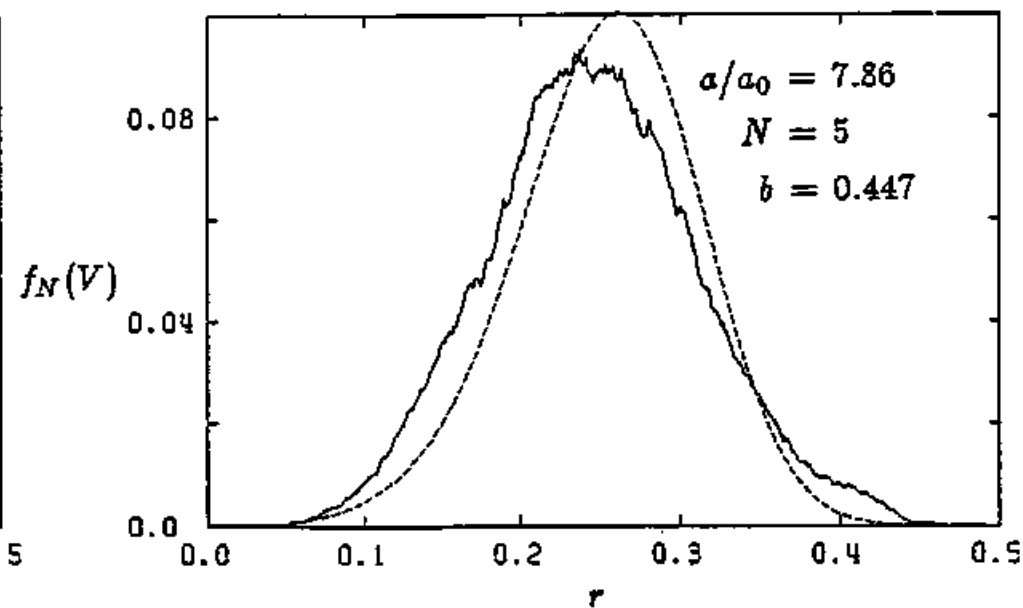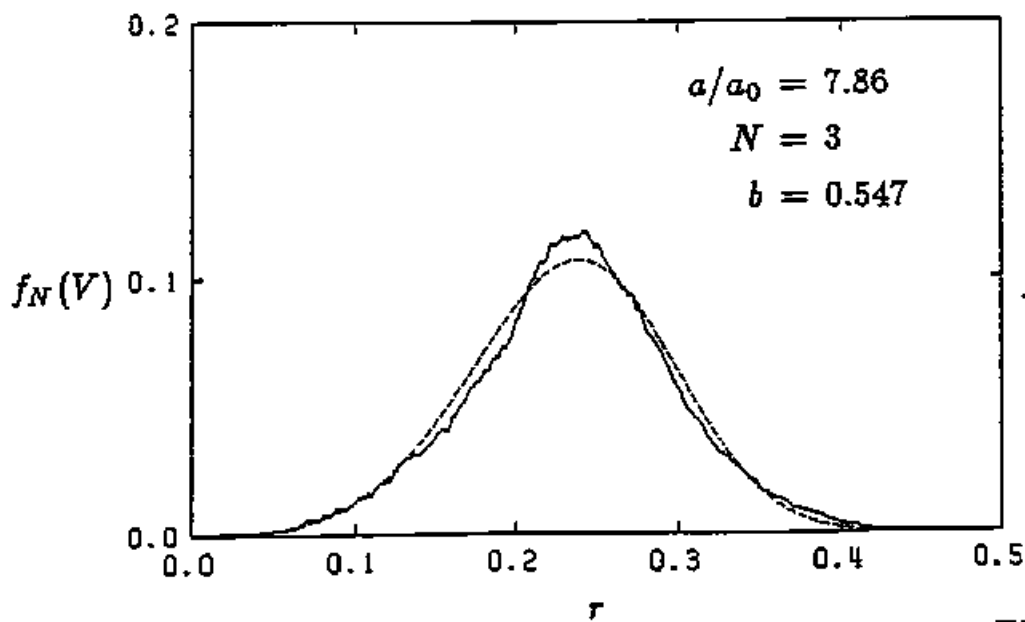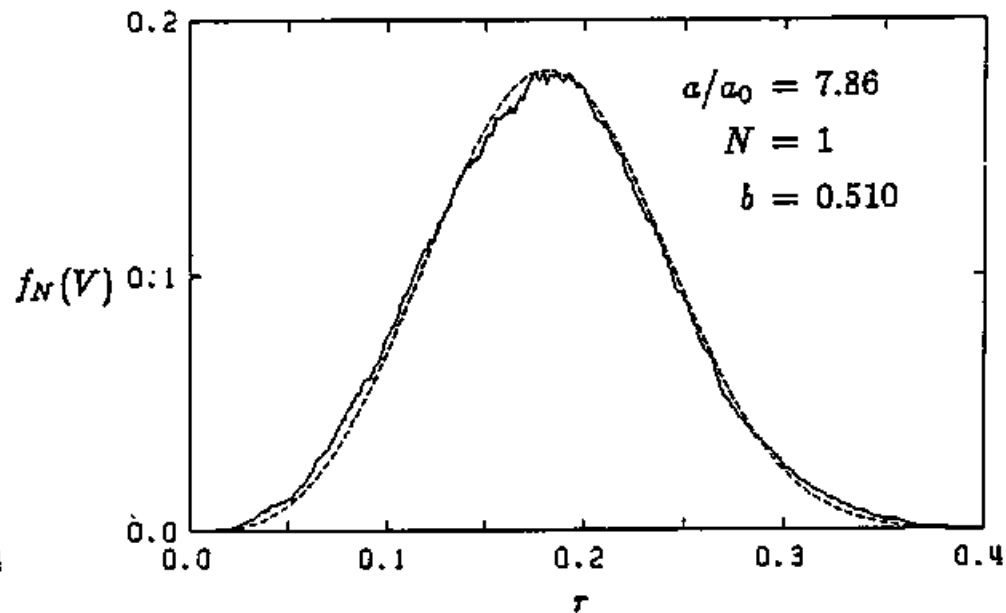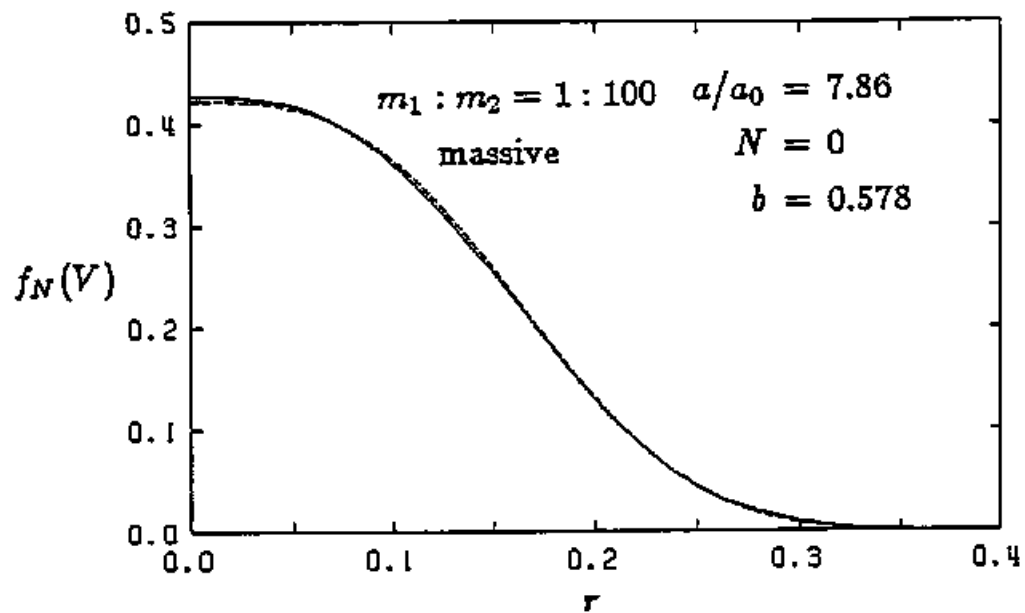
Figure 24(a)
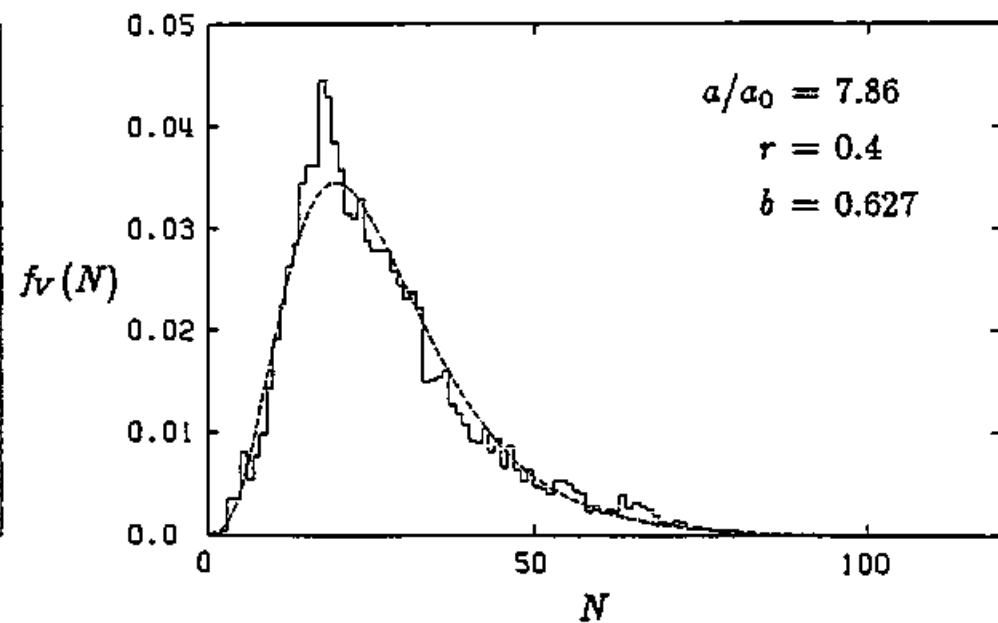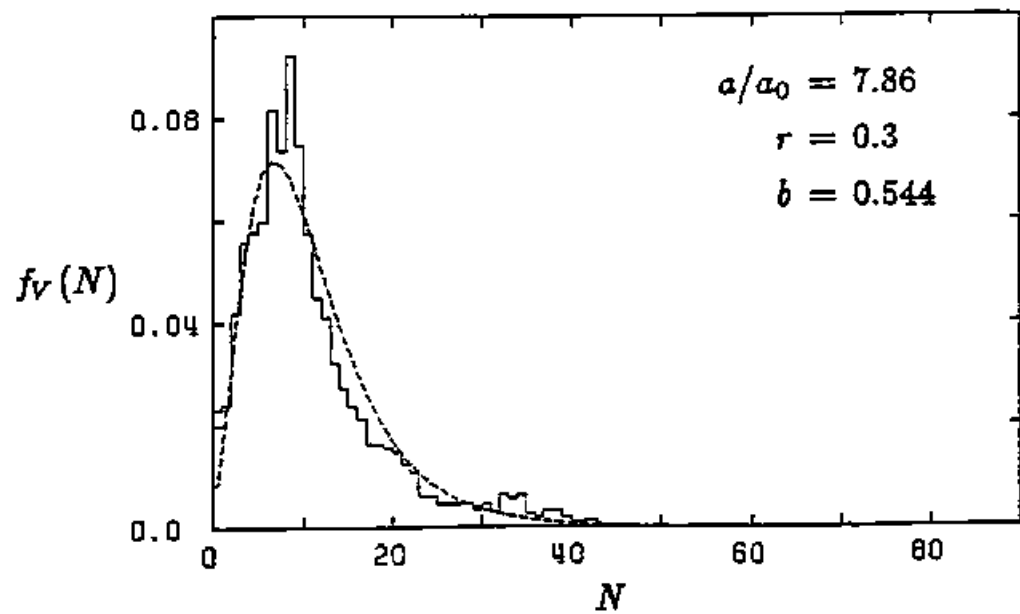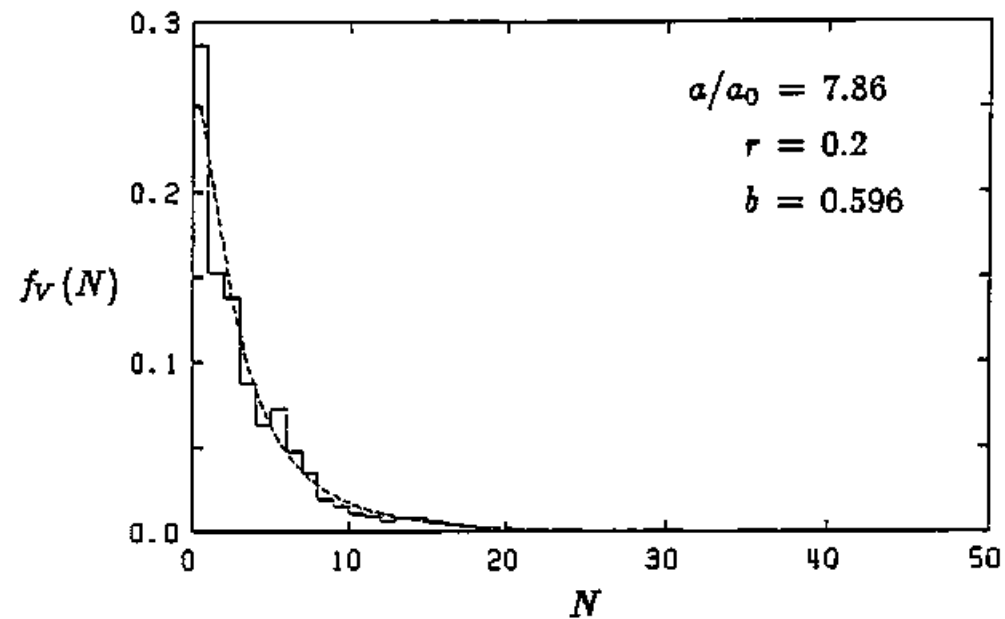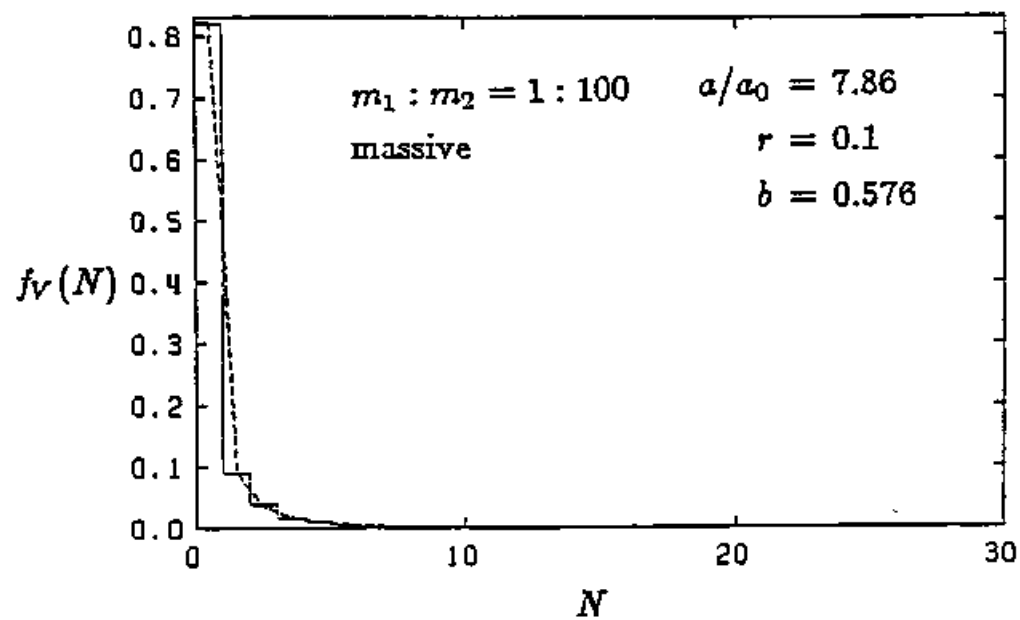
Figure 24(b)
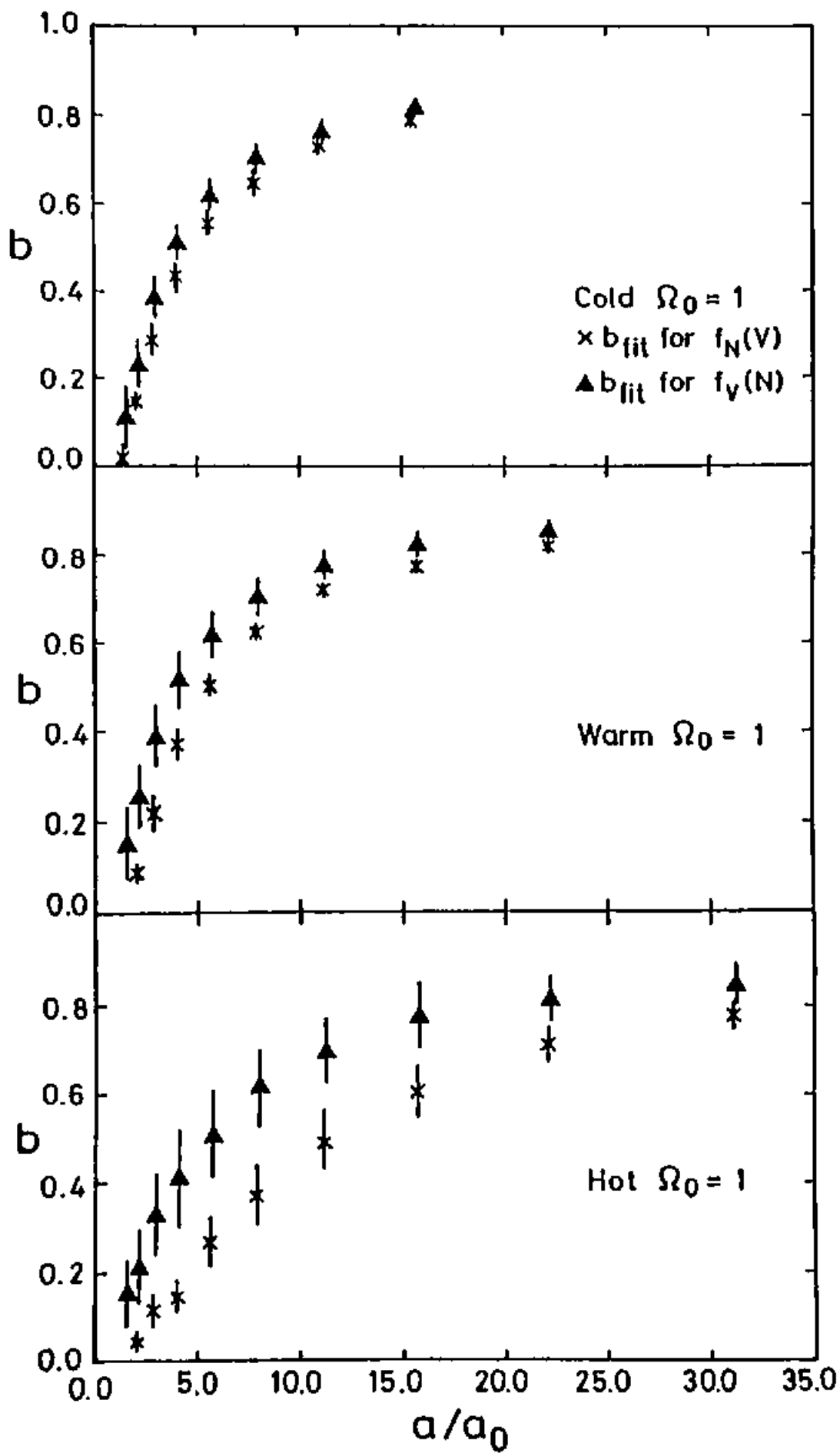
Figure 25

Figure 26(a)

Figure 26(b)